1-1-2014

Investigation Of Ion Current Signal In A Modern Automotive Diesel Engine

Rojan Mathew George
Wayne State University,

Recommended Citation

George, Rojan Mathew, "Investigation Of Ion Current Signal In A Modern Automotive Diesel Engine" (2014). *Wayne State University Theses.* Paper 298.

INVESTIGATION OF ION CURRENT SIGNAL IN A MODERN AUTOMOTIVE DIESEL ENGINE

by

ROJAN MATHEW GEORGE

THESIS

Submitted to the Graduate School

of Wayne State University,

Detroit, Michigan

in partial fulfillment of the requirements

for the degree of

MASTER OF SCIENCE

2014

MAJOR: Mechanical Engineering

Approved by

Advisor Date

DEDICATION

This thesis is dedicated to Almighty God, who has guided me through the whole period of my studies.

Also, this thesis is dedicated to my parents and brother for their endless love, support and encouragement to work hard for the things that I aspire to achieve.

Finally, this thesis is dedicated to my fiancée who has been a great source of motivation and inspiration.

ACKNOWLEDGEMENTS

I would like to express the deepest appreciation and gratitude to my adviser Prof. Dr. Naeim A. Henein, for his guidance and wealth of knowledge, which has contributed immensely towards my research work. His spirit of adventure in regard to research and an excitement in regard to teaching was a constant source of motivation during my time at Wayne State University.

My sincere thanks to, Dr. Walter Bryzik, Dr. Trilochan Singh, Dr. Marcis Jansons, and Dr. Dinu Taraza, for being my thesis committee members' and providing me their support and valuable feedback during the course of my research. I acknowledge the help of Eugene and Marvin from the machine shop for their support in machining engine parts as well as the sensors required for the research.

I would like to thank Tamer Badawy for helping me out in every possible way and for sharing the knowledge and expertise from time to time. I would also like to thank all my other fellow members of Center for Automotive Research particularly Sanket Gurathi, Amit Shrestha, Ziliang Zheng and Sahil Sane for their co-operation, support, and encouragement.

TABLE OF CONTENTS

LIST OF FIGURES

LIST OF TABLES

CHAPTER 1

INTRODUCTION

With the rapid advances in the field of internal combustion engines, automobile industry is considering different approaches for the efficient utilization of the fuels and reduced engine-out emissions. The ever increasing demand for better fuel economy and reduced emissions resulted in the production of down sized boosted engines. With the use of the technological advances, the new trend is to produce smaller engines with turbocharging so to attain the benefit of higher fuel economy and reduced power requirement of the engine. Even though compression ignition engines produce relatively high NO and soot emissions, they are known for a variety of characteristics such as low fuel consumption, high power density, high durability and reliability and low unburned hydrocarbons and carbon monoxide emissions. Diesel engines have undergone vast technological improvement over the years. In order to improve the performance and reduce the emissions, the essential factor is to understand the complex nature of diesel engine combustion. It has always been a constant challenge to outline the course of combustion due to its heterogeneous nature of the mixture and the complex auto ignition process. In order to have an efficient combustion control, ECU should be able to constantly re-adjust based on the in cylinder characteristics in a real-time manner. Although the new technology used for the development of the ECU tries to consider the variations in the physical and chemical properties of diesel fuels (and the diesel like fuels), creating a map for the engine considering the changes in Cetane number, fuel volatility, heating value, H/C ratio, viscosity under different engine operating conditions would be time consuming as well as less accurate. A feasible solution is to use a closed loop engine control system based on the feedback signal, which is indicative of the in cylinder combustion process.

Ions current technology has been under development for many decades, and has been successfully implemented in some gasoline engines for knock and misfire detection. A complete understanding of ionization during combustion of the heterogeneous charge in diesel engines has not yet been achieved. Also, the implementation of ion current technology in diesel engines, during all operating conditions needs further research and development.

This thesis includes an investigation of ion current signal characteristics as well as combustion, auto-ignition and engine out emission characteristics in a modern high speed diesel engine. The thesis also includes an investigation of the effect of using alternate fuels like JP-8 and Sasol IPK on the ion current, combustion, performance and emissions. ULSD is considered as the baseline fuel.

CHAPTER 2

LITERATURE REVIEW

2.1 *Introduction*

Internal combustion engines are continually optimized for better performance and fuel economy while meeting stringent emission regulations. This requires a feedback signal to the ECU which is indicative of the in-cylinder combustion process. Although there are many techniques to sense the combustion process in IC engines, most promising ones are the cylinder gas pressure transducer and ion current sensor. Comparison between these two sensors is explained in detail in Ref [1]. The pressure transducer does have the high degree of accuracy and reliability in the production of an in-cylinder gas pressure trace. But its major drawbacks include the high cost of the sensor and the modification needed for the installation of the pressure sensor on the cylinder head. Alternate approaches to determine the cylinder gas pressure include the extraction of pressure signal from the dynamic torque of the flywheel, load cells on the head gasket, transducer mounting on the spark plugs in gasoline engines or the glow plug in diesel engines. Of the available techniques ion current technique stands out due to its low production cost and good durability.

Ion current sensors have been used in both spark ignition engines as well compression ignition engines. The ion current signal in spark ignition engines is measured using spark plug and the ionization process is very well understood in SI engines. Unlike SI engines, the ion current signal produced during diesel engine combustion needs further research. The ion current signal characteristics depend on the combustion process as well as the products of combustion in each engine type. The combustion process in SI engines takes place in a homogenous mixture with an equivalence ratio close to unity. The heterogeneous nature and complexity of diesel engine combustion are the main reasons for the limited research on ionization in diesel engines.

2.2 *Ionization in hydrocarbon flames*

Ion current produced from hydrocarbon flames are formed from chemi-ionization and thermal ionization processes. Ion current signal production depends on the air fuel ratio of the mixture and the combustion temperature. Researchers have proven that the ion technique can be successfully used to monitor the combustion process in gasoline engines. In SI engines the combustion process starts from the flame kernel and propagates in the chamber with a flame front thereby dividing the chamber into burned gases zone and unburned charge zone. The charge in SI engine is maintained to be homogenous where the air fuel ratio is very close to stoichiometric conditions. It has been concluded that the ion current in gasoline engine operation produces separate peaks for chemi ionization, which is produced from the flame front propagation, and thermal ionization of the hot gases mainly NO ionization, in the post flame zone. The main developments of the ion current techniques in the field of the SI engine combustion are discussed below.

Ion current technique has been widely used for several applications in SI engines. Major applications are the use of ion current as the feedback signal for optimizing the combustion control and development of closed loop controller, detection of the engine knock, misfire and location of peak combustion pressure [2] [3]. Correlations between ion current signal and air fuel ratio have also been established [4].

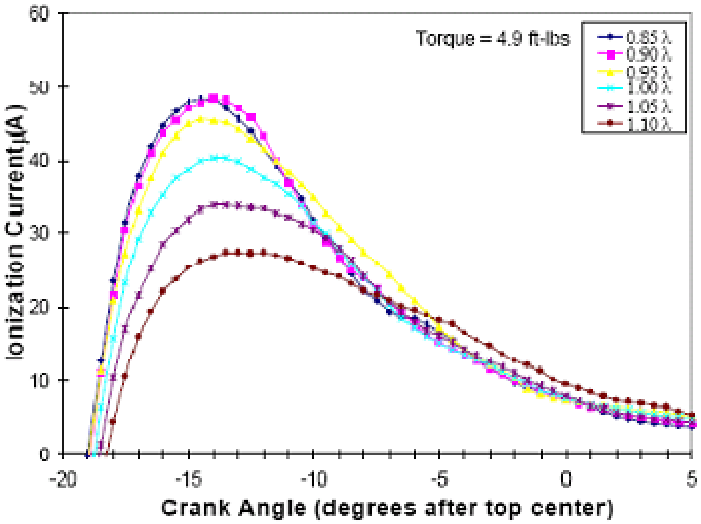

Figure 2-1. Ion current signal as a function of Air fuel ratio [4]

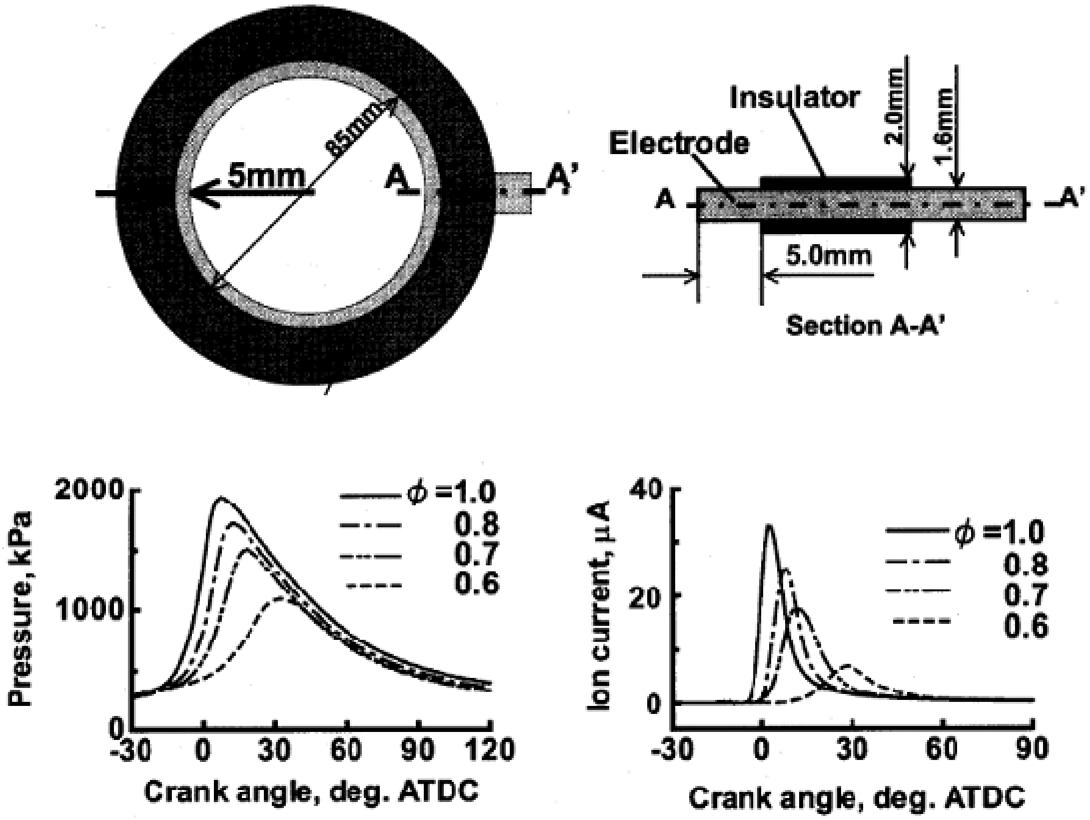

Figure 2-2. Design of gasket ion sensor and pressure and ion signal for different equivalence ratios in a SI engine [2].

Figure 2-1 shows the ion current in a SI engine for different equivalence ratios. Kenneth et al. [2] developed a correlation of the air fuel ratio and ion current signal. The cylinder charge air fuel ratio approximation was done using the spark gap ionization signal. This work identified the air fuel ratio range in which the ion current peaked [4]. The ion current signal has been captured by using various parts of the engine as the electrode. Yoshiyama et al. used a gasket ion sensor for combustion diagnostics and they extended the work by using the spark plug, piston and exhaust ion sensor [5]. The finding from the latter research was focused on the signal from the exhaust and this was useful when analyzing the late burn cycles under idle operation for the ignition retard management. Figure 2-2 shows the design of gasket ion sensor and the signal obtained from it for different equivalence ratios [2] [5].

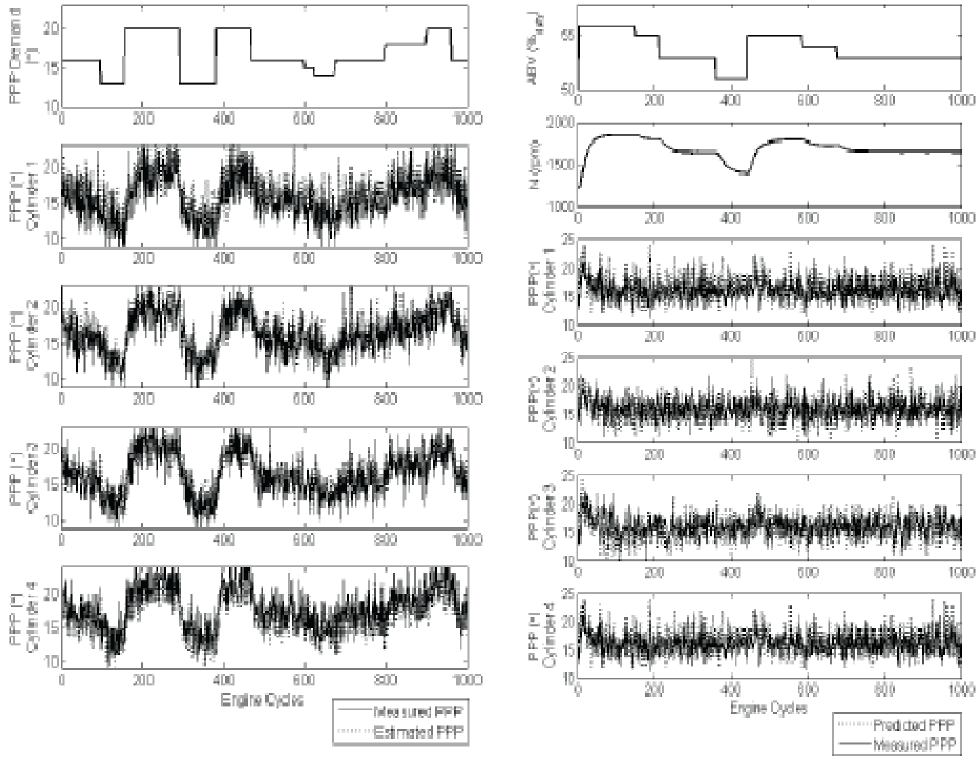

Figure 2-3. Peak position control using ion current in 4 cylinders SI engine [3]

The peak position of combustion pressure in each cylinder can be controlled using the feedback from ion current signal as shown in Figure 2-3. The location of peak pressure in each cylinder was estimated from the ion current signal using a neural network algorithm which was trained in a range of conditions [3]. Ion current signal has been used as a closed loop feedback control in the ignition control to obtain the MBT as well as to avoid knocking. The spark timing is controlled depending on the feedback from the ion control, thereby operating the engine in the true MBT timing when the operation is not limited by knock and operate within the limits when the operation is limited by knock [6].

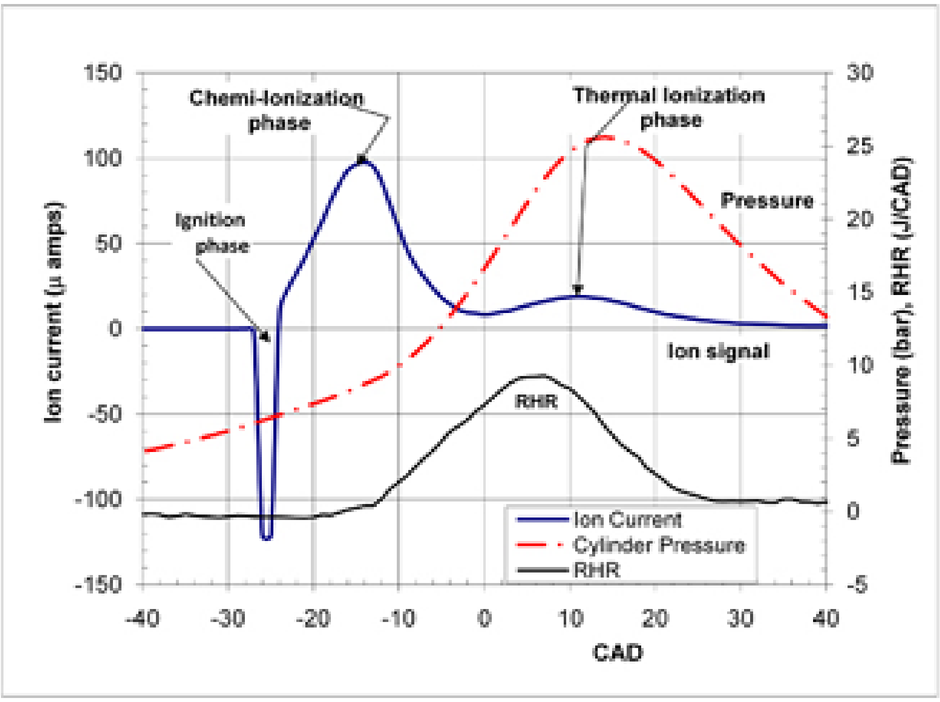

Figure 2-4.Typical ion current signal in a SI engine (Speed = 1300rpm, Torque = 20Nm) [1] [7].

Figure 2-4 shows a typical ion current signal in a gasoline engine along with the in cylinder pressure and RHR trace. Two ion current peaks in SI engines as seen in this figure have been reported by many investigators. The ion current started to rise at 24°bTDC after the electric spark discharge and reached first peak at 14° bTDC followed by the second peak at 12° aTDC. The general agreement is that the first ion peak is caused due to chemi-ionization produced in the local reaction zone of the flame kernel and the second peak is formed from the thermal ionization caused due to the increase in temperature of gases. The amplitude of the peaks of ion current depends on the equivalence ratio, combustion gas temperature and EGR rates [7] [1] [8].

In gasoline engines, the mixture being homogenous and ignition initiated by an electric spark, the combustion occurs by a high temperature flame which propagates through the chamber. The combustion process in compression ignition engines are complex unlike the spark assisted gasoline engines. The charge in CI engines is heterogeneous and auto ignition process depends mainly on the local equivalence ratio, pressure and temperature. Due to the complex process involved in the diesel engine combustion such the fuel atomization, evaporation, mixing process which then leads to the conditions favorable for auto-ignition process, the theories or mechanisms used to explain the ion current signal in gasoline engines cannot be used here. Unfortunately, only a limited number of investigations have been done in the field of ion current in diesel engines. The main developments of the ion current techniques in the field of the compression ignition engine combustion are discussed below.

Magnus Glavmo et al. investigated the effect of EGR and soot contamination on ion current in a diesel engine and tried to use ion current signal as a feedback signal to control the start of combustion where they modified the glow plug to measure the in cylinder ion signal for the first time. Henein, N.A. et al. conducted a series of investigation on a single cylinder and multi cylinder automotive diesel engines to explain the characteristics of ion current signal in diesel engines. They reported that the ion current signal in diesel engine during single injection strategy can have one, two or more peaks depending on the engine operating parameters like load, speed , injection pressure, and injection timing [9] [10]. The design of the ion sensor, its location in the combustion chamber and the combustion chamber design have an effect on the shape of the signal [11]. Badawy et al. investigated the ion signal characteristics over a wide range of operating parameters including EGR rates and injection events and developed correlations between the ion current signal and different combustion parameters and the engine out emissions [12].

Ion current signal has also been used for closed loop control in diesel engine by Badawy et al. wherein a correlation was developed between the start of ion current and the location of peak of the rate of heat release due to premixed combustion which was utilized to control the combustion phasing [13]. The combustion phasing controller was successfully implemented for both steady state as well as transient engine conditions. Figure 2-5 shows the correlation between SIC and LPPC for a range of loads and injection pressures at constant SOI. Figure 2-6 shows the utilization of this correlation in maintain the same combustion phasing while changing the speed from 1800 RPM to 1300 RPM at a constant IMEP of 5 bar. Other correlations between ion current parameters and engine speed, in cylinder temperature and ignition delay were also established [11].

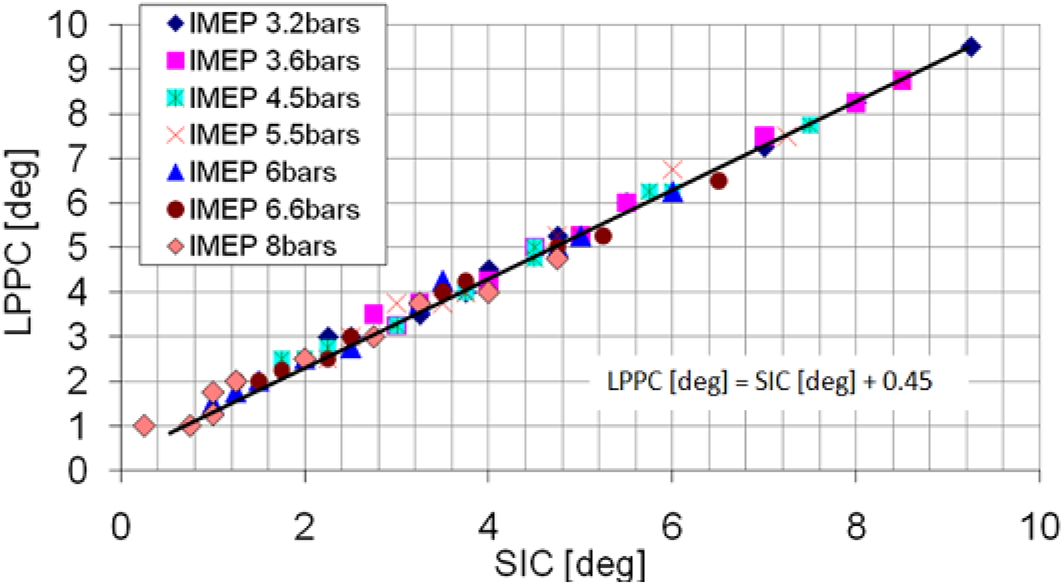

Figure 2-5. Correlation between SIC and LPPC at Sweep loads and injection pressures [IMEP= 3.3 - 8 bar, Speed= 1800RPM, Inj. Press. = 250 to 1100 bar, SOI= 10°bTDC] [13]

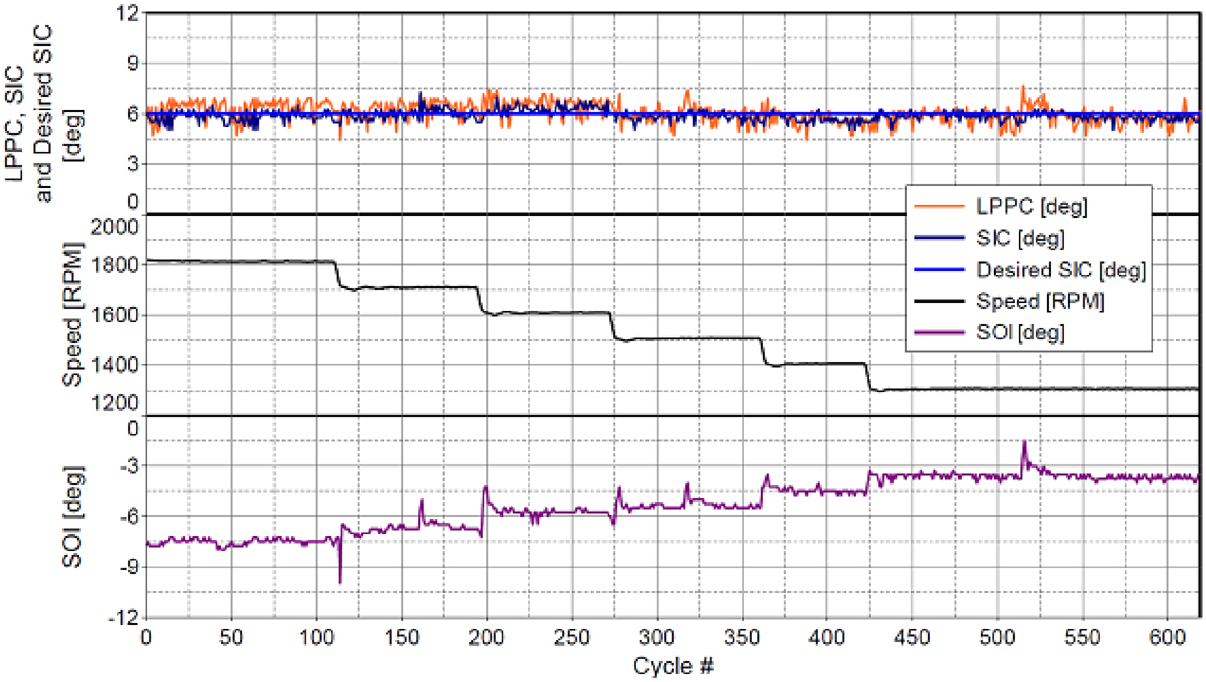

Figure 2-6. Change of engine speed from 1800 to 1300 RPM, at Const. SIC 6° aTDC [IMEP= 5 bar, Const. Speed= 1800 to 1300 RPM, SOI=Var.] [13]

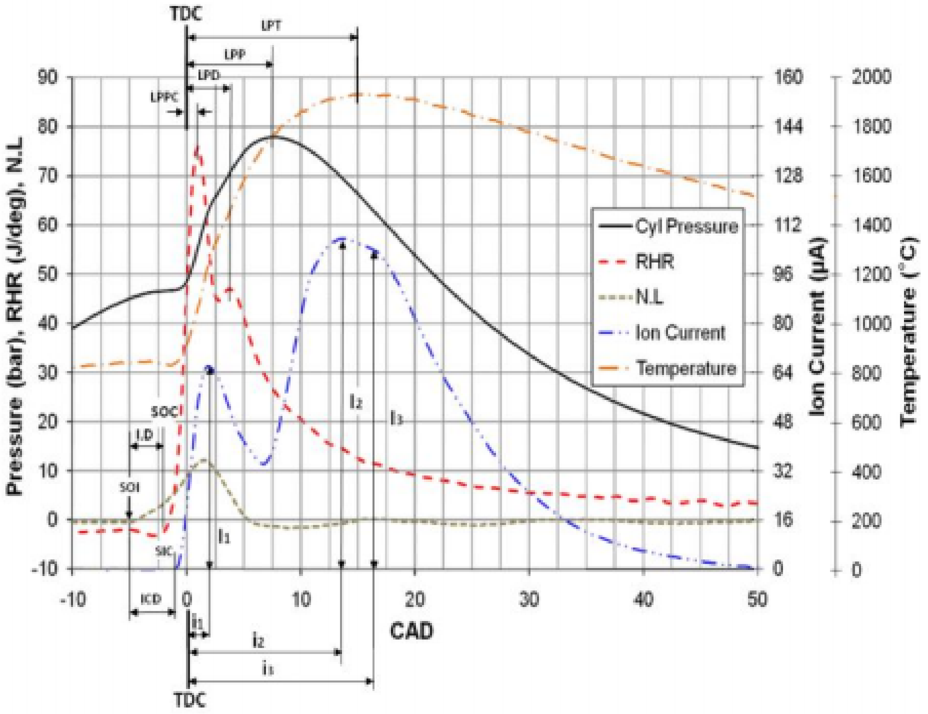

Figure 2-7. Typical ion current signal along with pressure, RHR, temperature and needle lift, for a diesel engine operating on single injection strategy [11]

Figure 2-7 shows a typical ion current signal along with cylinder pressure, RHR, temperature and needle lift traces for a diesel engine operating on the single injection strategy. Three peaks in the ion current signal can be seen which are represented as I1, I2 and I3 respectively. The first peak of ion current can be correlated to the peak of premixed combustion of the heat release whereas the second peak of ion signal occurs in the peak temperature region. The third peak is highly dependent on the engine load and I3 becomes clearer at higher loads, where more amounts of fuel burns and flame reaches the sensor after bouncing back from the piston, characterized by soot formation and oxidation [11].

While above investigations dealt mainly with the operation during single injection strategy of diesel engines, Kubach et al. studied the effect of sensor location and design on the ion current formation using pilot injection wherein he investigated the sources of ionization in various stages of combustion [14].

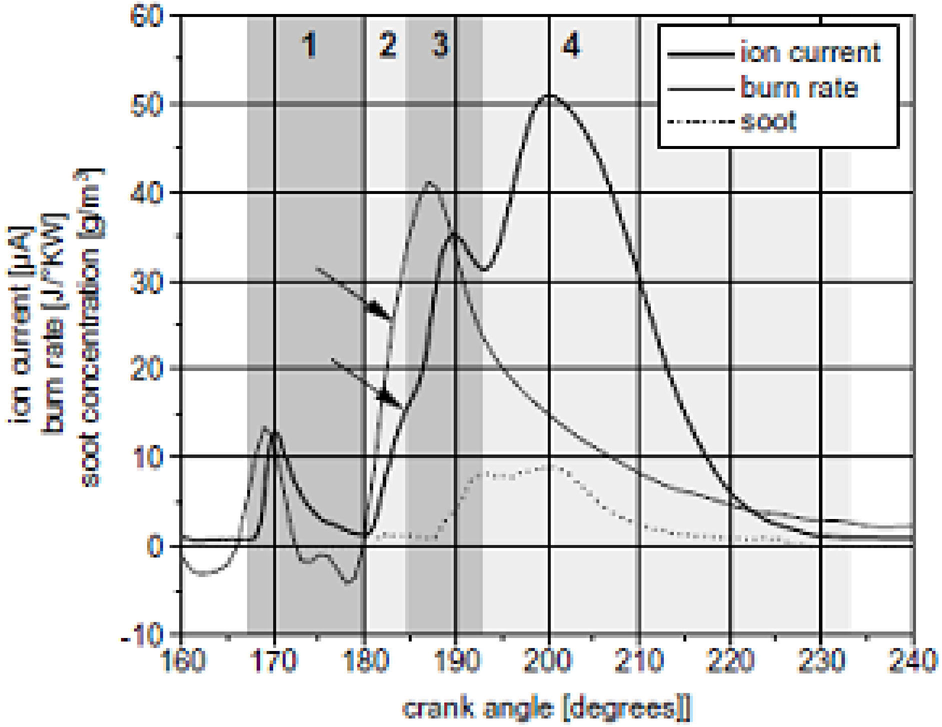

Figure 2-8.Typical ion current signal from diesel engine operating with pilot injection [14]

Figure 2-8 shows the typical ion current signal from a diesel engine operated with pilot injection along with burn rate and soot concentration traces. A separate ion peak for pilot mass of fuel burned can be observed along with three peaks from the main injection event. The ion current signal has been divided into four zones. The zone 1 is the result of the burning of the fuel from the pilot injection event. Premixed combustion fraction burns in the region 2 whereas area 3 and 4 occurs as a result of diffusion controlled combustion. The separation of distinctive peaks in the third and fourth regions might not be always possible as the number of peaks in the signal depends on the engine operating conditions. It was also observed that the soot formation was predominant in zone 3 whereas in zone 4, soot oxidation is seen to be dominating [14].

MECHANISMS OF IONIZATION IN DIESEL ENGINES

The main mechanisms reported in the literature for the chemi-ionization and thermal ionization are [11]:

Chemi-Ionization

Under this mechanism, the following five different reactions contribute in ion formation:

$CH + O \rightarrow CHO^+ + e^-$ (1)

$CH + C_2H_2 \rightarrow C_3H_3^+ + e^-$ (2)

Charge Transfer

$CHO^+ + CH_2 \rightarrow CH_3^+ + CO$ (3)

$CHO^+ + H_2O \rightarrow H_3O^+ + CO$ (4)

Recombination

$H_3O^+ + e^- \rightarrow H_2O + H$ (5)

Thermal-Ionization

$M + E_{ion} \rightarrow M^+ + e^-$ (6)

Reaction (1) and (2) shows initiation of ion formation by the CH radical whereas the reaction (3) & (4) shows the charge transfer reactions. Reaction (5) shows the recombination reactions.

Under thermal ionization mechanism, reaction (6) shows the formation of ions from combustion products (mainly NO molecule) at high temperatures in close to stoichiometric hydrocarbon air flames.

2.3 *Conclusion*

The literature review shows that the ion current signal contains useful information about the in-cylinder combustion process for both SI and CI engines. Ion current technology has the potential to replace the in cylinder pressure sensor or other combustion sensors. It was seen that most of the research on the ion current signal has been conducted on spark ignited gasoline engines identifying the possible sources and mechanisms of ionization. The ion current technique was utilized for various combustion control parameters such as spark timing control, peak pressure and knock control etc. The limited research work of ion current in the field of diesel engines can be attributed to the complexity in the heterogeneous diesel combustion and cyclic variations.

The ion current signal characteristics during the operation of diesel engines on single injection strategy have been explained in various engines. Ion signal correlates with various combustion parameters and it is mainly dependent on cylinder gas temperatures and the equivalence ratio. The characteristics of the signal under various operating conditions with single injection have been studied and a closed loop feedback control using ion signal was successfully implemented in both steady and transient conditions. However more investigations are needed to explain the ion current characteristics during diesel engine operation with pilot injection or multiple injection strategies. A detailed investigation is also needed to determine the effect of fuel properties on the ion current signal.

CHAPTER 3

ENGINE SET UP AND INSTRUMENTATION

3.1 *Engine set up*

The engine used in this research work is a 2.0L Volkswagen Industrial Engine which is water cooled four-cylinder inline diesel engine with direct fuel injection, exhaust gas recirculation, a turbocharger and a charge air intercooler. It does have four valves per cylinder, driven by overhead belt-driven camshafts. The electronically controlled Bosch common rail injection system supplies the high pressure fuel into the cylinder using piezo operated injectors. Forced oil lubrication is attained by an oil pump driven by a toothed belt and the oil cooled using an oil/water heat exchanger. Even though the engine had exhaust gas recirculation system, it was isolated in order to simply the engine operation as well as to reduce the cylinder to cylinder variations. The engine being equipped with diesel particular filter (DPF), meets the EU 5 emissions standards. However DPF was removed from the current investigation in order measure the emissions without any after treatment systems.

The engine was mounted on a docking cart and coupled to a water brake dynamometer to apply load on the engine. A radiator/ intercooler were also mounted on to the mobile cart which provided the cooling for the turbocharged intake air. No modification was done to the engine. The in cylinder pressure measurements were taken from the gas pressure transducer fitted in the glow plug opening of cylinder # 1. Ion current signal is measured using a modified glow plug ion current sensor in cylinder #4. The engine was operated using the original/ OEM ECU and hence all the engine operating parameters such as injection timing and events, fuel injection pressure, boost pressure were controlled by the OEM ECU. The only user defined parameters in this research were the engine load and speed. A detailed description of instrumentation on the engine along with DAQ system, emission analyzers and other sensors used for the research are explained in detail in the following sections. Figure 3-1 shows the experimental engine set up and instrumentation.

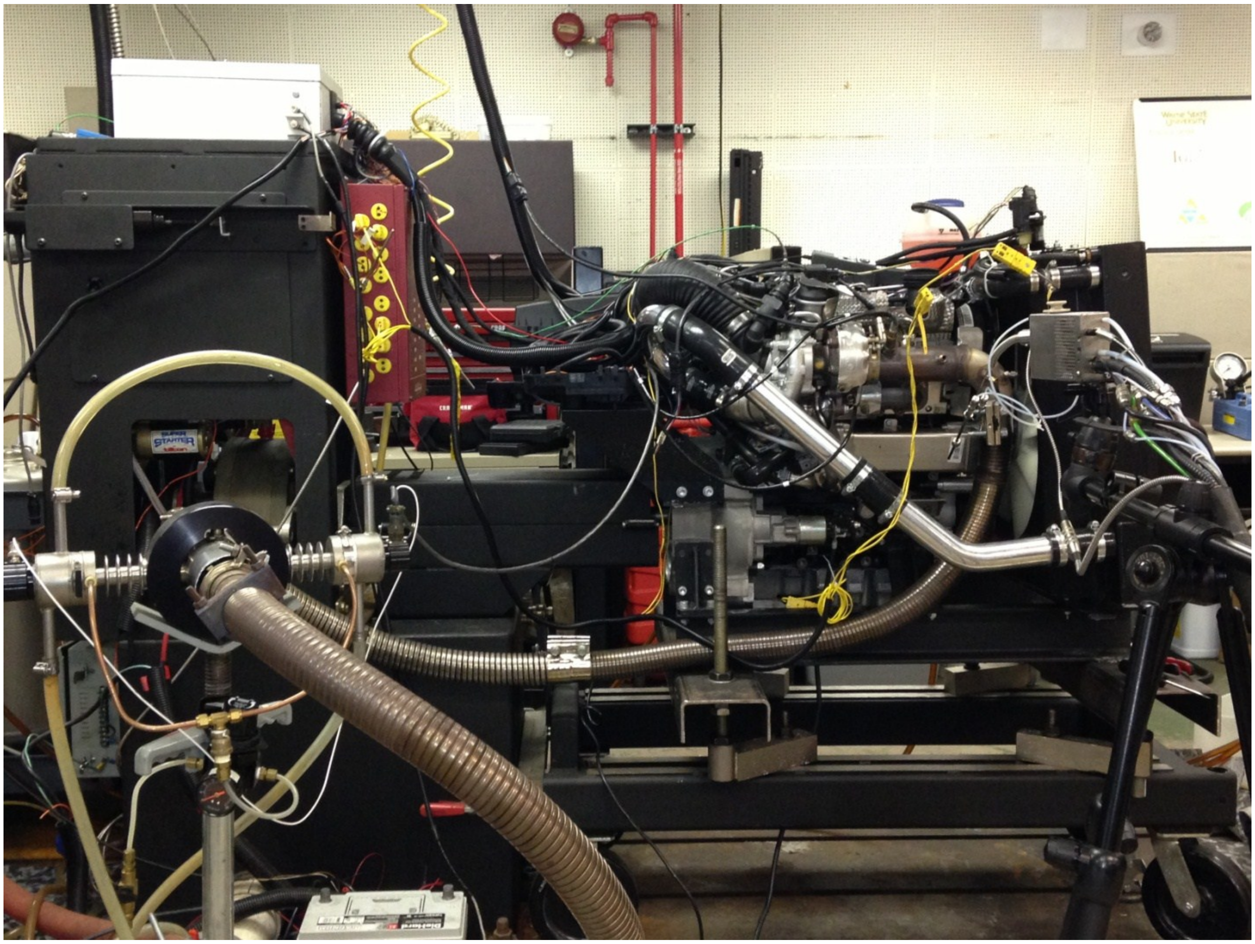

Figure 3-1. Experimental set up – Exhaust side

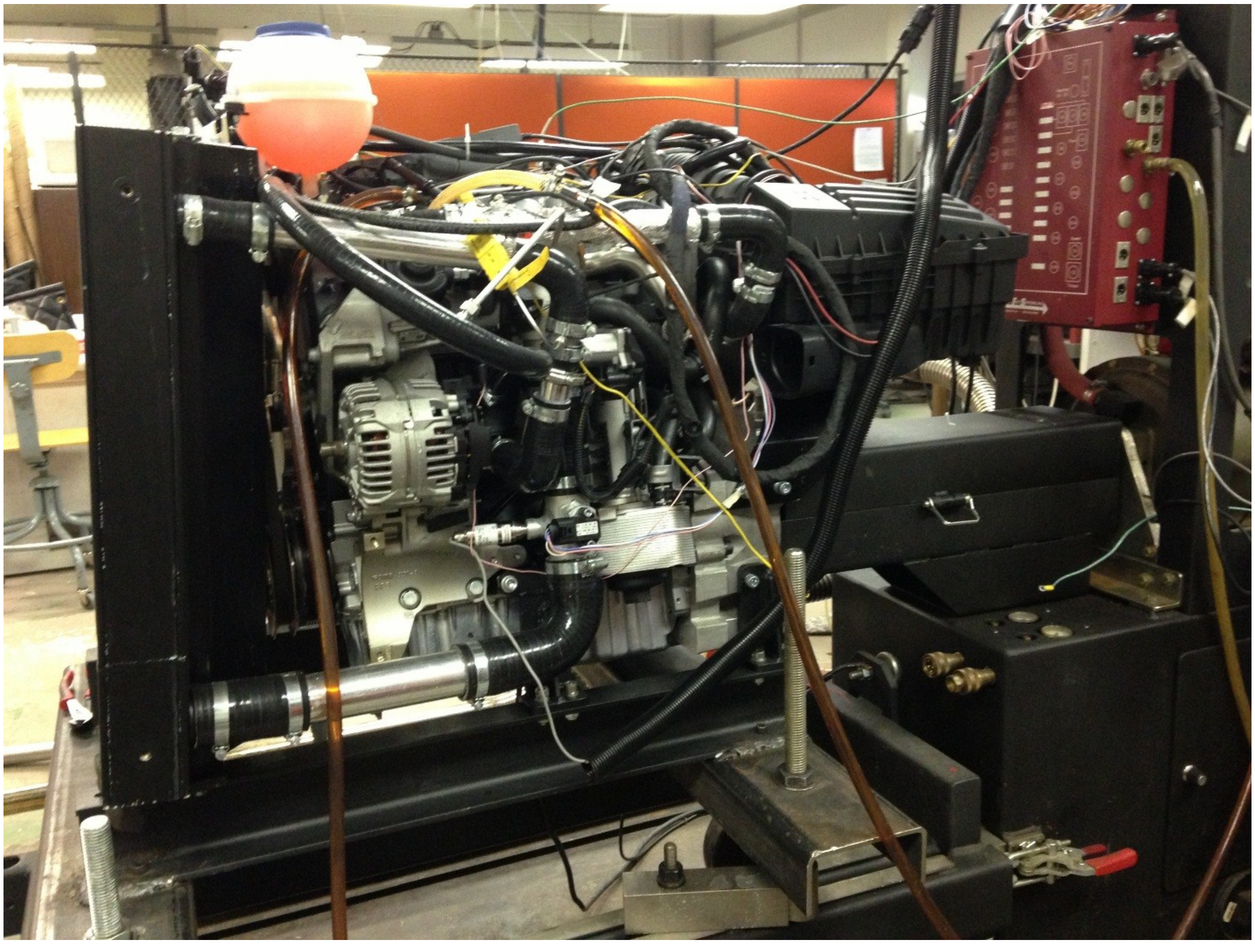

Figure 3-2 Experimental set up - Intake side

3.2 *Engine specifications*

The specifications and technical details of the engine are provided in Table 3-1 and Figure 3-3 shows the permissible operating angles.

Table 3-1. Specification and technical data of 2.0L VW TDI [15]

Engine type	Diesel 4-stroke
Number of cylinders	4 - Inline
Bore / stroke (mm)	81 / 95.5
Connecting Rod (mm)	144
Displacement (cm^3)	1986
Compression ratio	16.5 : 1
Max. Torque @ 1750 rpm	285 Nm
Max. Power @ 3000 rpm	75 kW
Engine weight, dry (kg)	150
Lower idling speed (rpm)	830 + 50/-25
upper idling speed (rpm)	3400
Lubrication oil capacity (lt)	4.5
Maximum tilting (°)	12

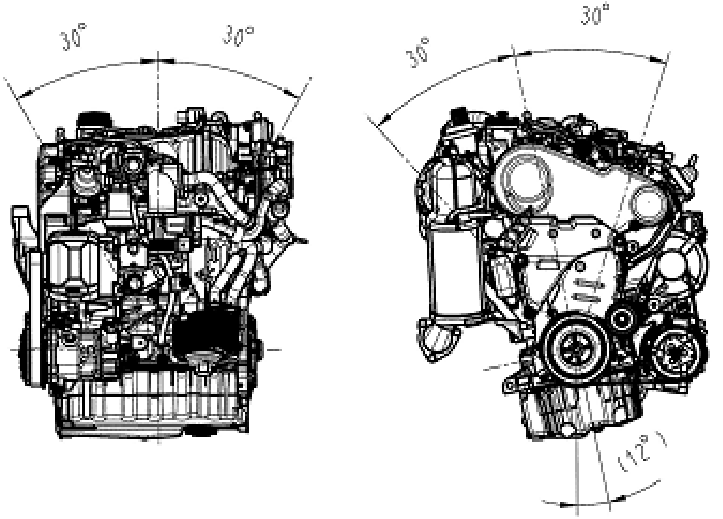

Figure 3-3. The permissible operating angles of the engine [15]

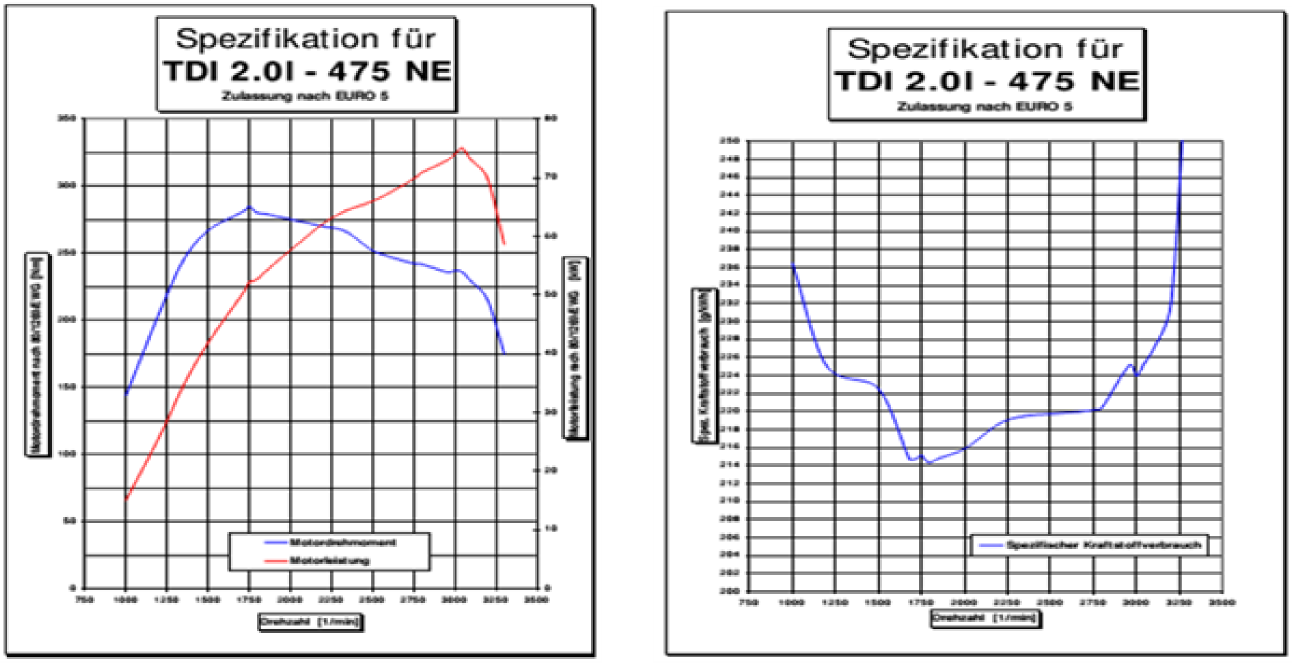

Figure 3-4. Engine output curves and specific fuel consumption curves for the engine [16]

The engine has a maximum torque output of 285Nm at 1750 rpm and max power output of 75 kW at 3000rpm. The engine output curves and specific fuel consumption curves are shown in Figure 3-4.

3.3 *Cylinder head and piston geometry*

The cylinder head of the 2.0 L TDI engine is a cross flow aluminum cylinder head with two intake and exhaust values per cylinder and the valves being arranged vertically overhead. The two overhead camshafts are connected and driven by the exhaust camshaft which is connected to the crankshaft by a belt drive.

The pistons of this engine come with no valve pockets contrary to the old designs. This reduces the clearance volume of the cylinder and enhances the formation of swirl inside the cylinder. The piezo operated injectors are vertically positioned and centrally located over the more flat, wider and shallow piston bowl chamber [16].

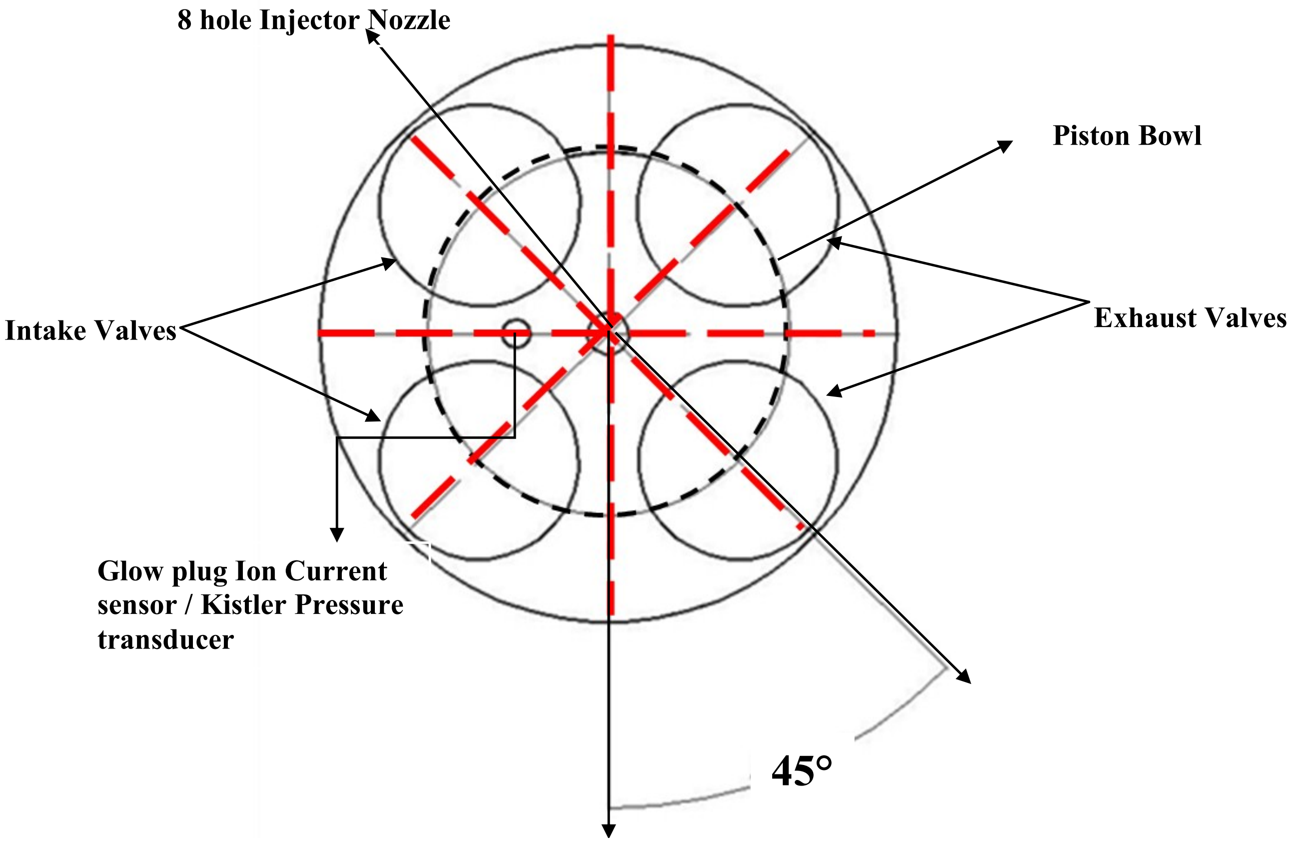

Figure 3-5. Top view of the combustion chamber showing locations of the sprays, Ion sensor, piston bowl and the valves

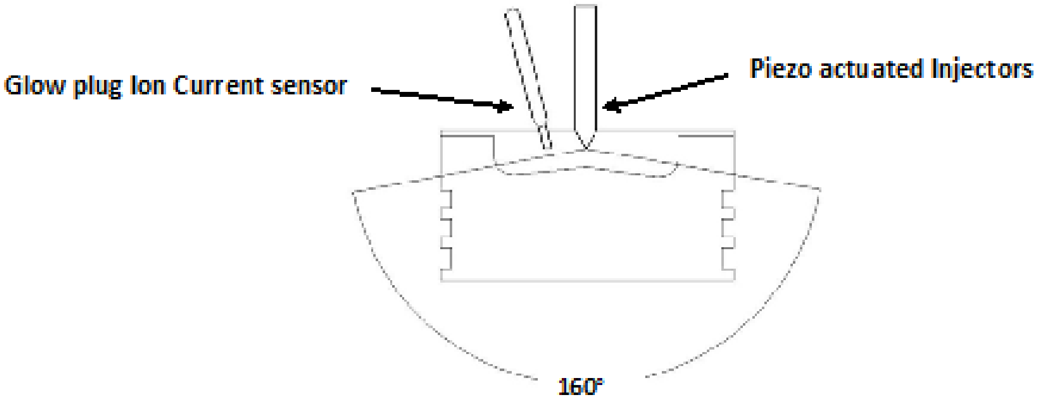

Figure 3-6. Front view of the combustion chamber

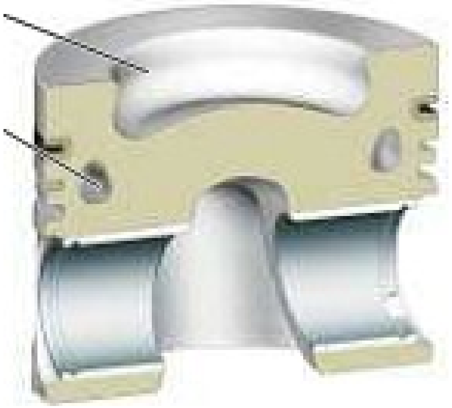

Figure 3-7. Cross sectional view of the piston [16]

3.4 *Piezo common rail system*

VW 2.0 L engine is equipped with a common rail fuel injection system which consists of a separate high pressure pump which generates the pressurized fuel for injection. The high pressure fuel is accumulated in the high common rail and supplied to the injectors. The injection pressure varies from 230 bar to 1800 bar depending on the engine operating conditions. The common rail system uses injectors which are controlled using a piezo actuator stacks. The introduction of piezo injectors in the engine comes with certain advantages. It approximately has

4 times faster switching speeds and 75% less moving mass at the injector needle, when compared to solenoid injectors. Also it can deliver up to five injection events per working cycles. Due to the very short switching times of the piezo injectors, injection quantities and phases can be precisely controlled [17] [18]. A detailed working of the piezo operated injectors and driver signal details is provided in ref. [18] [19].

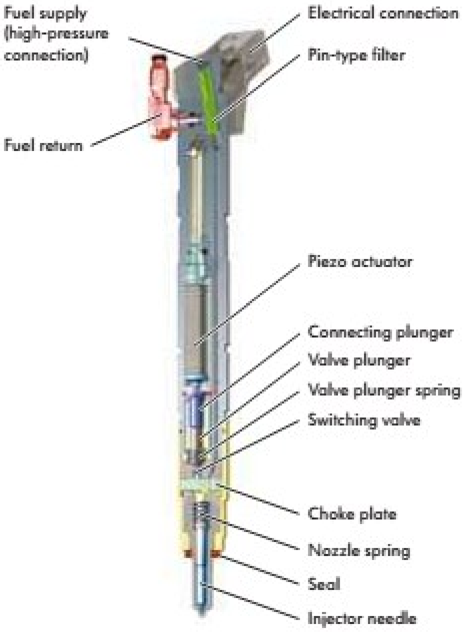

Figure 3-8. Cross sectional view of the piezo operated injectors [17]

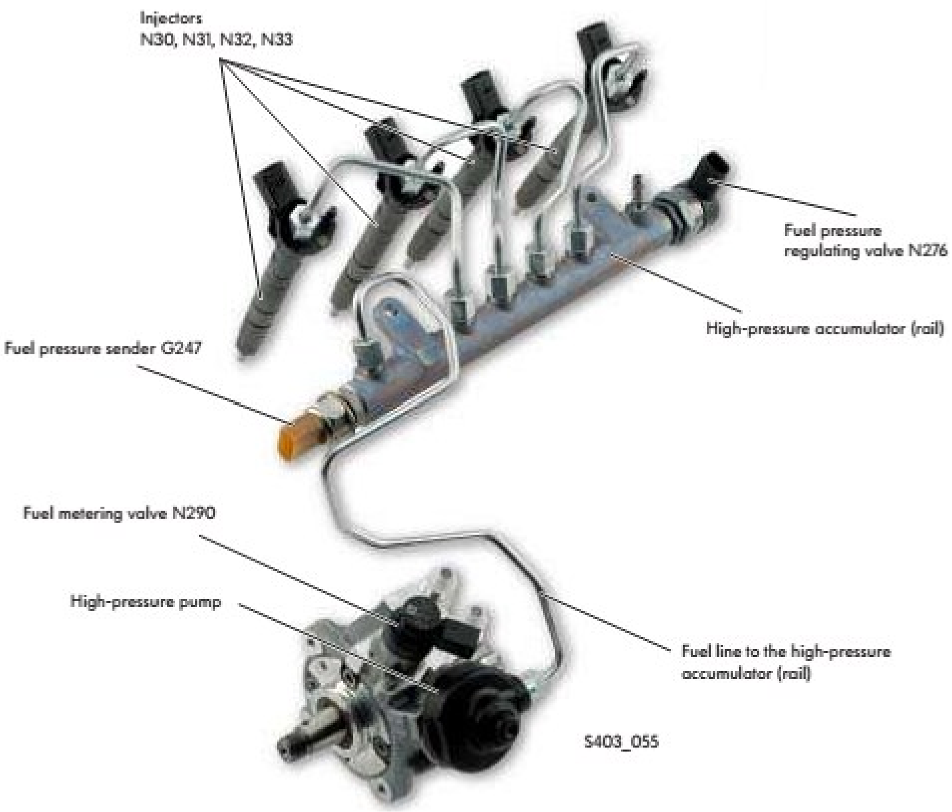

Figure 3-9. Common rail injection system showing different components [16]

3.5 *Engine instrumentation*

The engine has been instrumented with various sensors, measurement and control devices in order to operate as well as to monitor the combustion, performance, emissions and ion current parameters. Various instrumentation on the engine are described in the following subsections.

3.5.1 Dynamometer control set-up

The engine is coupled to a water brake hydraulic dynamometer from Dynamic Test System (DTS). A splined shaft and a constant velocity (CV) coupling were used for coupling since it allows the smooth engine running even in the case of slight misalignment. The dyno system consists of a built in control system as well as a time based slow speed data acquisition system. The engine load is controlled by means of an electric stepper motor where the user defined load can be applied on the engine. It is equipped with a speed sensor, a load cell, a slow response thermocouples and pressure sensors. The control software of the dynamometer calculates the speed, engine torque, brake power, various thermocouple readings such as cooling water temperature, intake and exhaust temperatures, oil pan temperature, room temperature and relative humidity. The water pressure for the dynamometer operation is controlled using a pressure regulator valve where the water pressure is maintained at 5 bar pressure. Figure 3-10 and Figure 3-11 show the dynamometer control interface as well as the display and the block diagram of the dynamometer set up along with its various parts respectively.

Figure 3-10. Dynamometer control unit display

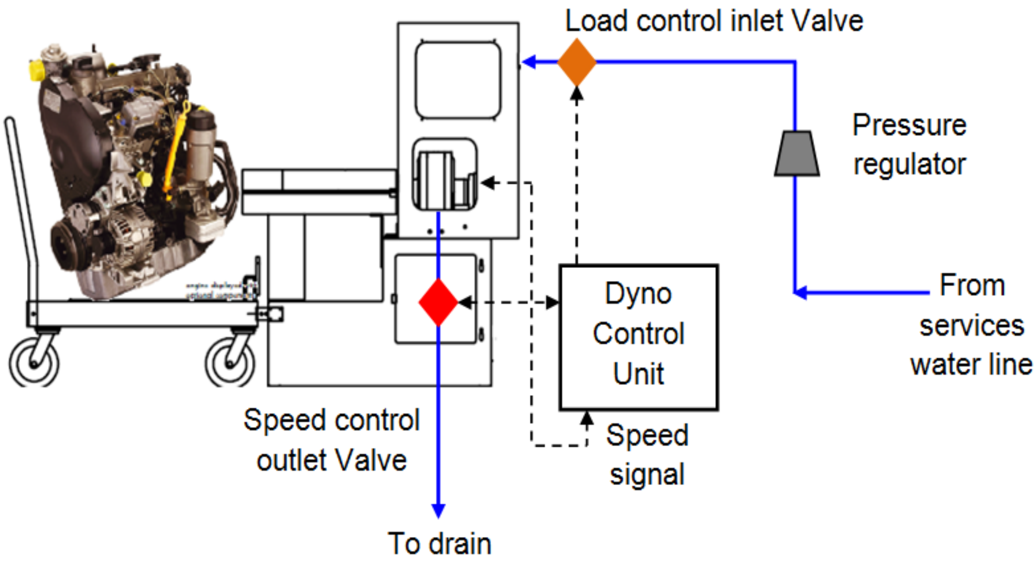

Figure 3-11. Dynamometer setup

3.5.2 Optical encoder

An optical encoder is installed on the camshaft to measure the instantaneous crank angle degree. The encoder mounted on the cam shaft was supported by a bracket to take into account any vibration or misalignment that could come between the encoder shaft and camshaft. This optical shaft encode has the resolution of 0.25 pulses/degree. A resolution of 0.25 CAD was selected since any higher resolution would induce more noise and lesser resolution would result in the loss of combustion data. It sends the TDC pulses as well as the crank angle pulses to the high speed data acquisition system. The TDC of the engine was matched with the TDC of the encoder in order to eliminate any offset.

3.5.3 Pressure transducer

A Kistler Pressure Transducer - Type 6052 A is installed on Cylinder #1. The pressure transducer was integrated on the glow body to gain access in to the combustion chamber and thereby capturing the in cylinder combustion pressure without any modification to the cylinder head. The sensor is connected to a charge amplifier - Type 5010 which converts the electrical charge produced by the piezoelectric sensors into a voltage signal. The high speed data acquisition system records and converts this voltage signal as the in cylinder combustion pressure. Figure 3-12 shows the Kistler pressure transducer, Type 6052-A, assembly set up.

The pressure in the common rail fuel system is monitored using a Kistler high pressure piezo resistive sensor - Type 4067A2000 installed on the high pressure fuel line. The pressure sensor was installed on the high pressure fuel line of cylinder #4 using a special mounting clamp. The location of the sensor was selected such that is it should be as close as possible to the fuel injector such it can capture the drop in fuel line pressure when the injection events start. A charge amplifier, Type 4618 A, was used to convert the electrical charge produced by the piezo resistive sensor into a voltage signal. The high speed data acquisition converts and records this voltage signal as the fuel rail pressure.

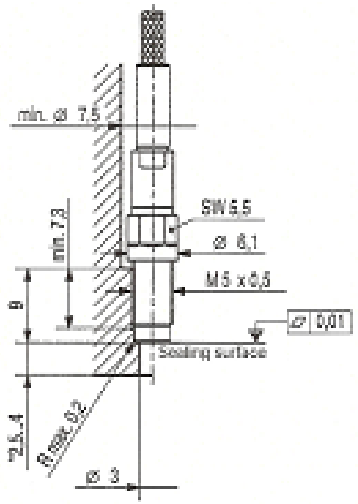

Figure 3-12. Pressure transducer Assembly [20]

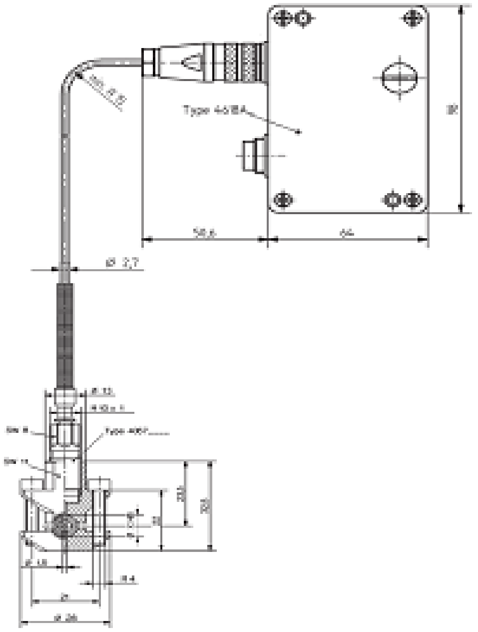

Figure 3-13. Rail pressure sensor assembly [21]

3.5.4 Intake temperature and pressure

In order to monitor the intake pressure, an Omega Pressure transducer (PX209 30 - V85G5V) was used. The intake manifold was machined to accommodate the pressure sensor. The intake air pressure is monitored to provide pegging to the in cylinder pressure trace, as the intake pressure variable due to the boosting provided by the turbocharger. The calibration chart for the manifold absolute pressure sensor is plotted as shown here.

The intake air temperature is monitored using a K Type thermocouple installed on the intake manifold. The variation in the intake air temperature occurs as result of the turbo charging and the exhaust gas recirculation (EGR) which needs to be monitored.

3.5.5 Fuel supply and measuring circuit

The fuel is delivered, using a low pressure pump, from the fuel tank to the engine. The fuel passes through a fuel filter and a flow meter, from Max Machinery Inc (Model 710), before reaching the intake of the engine driven high pressure common rail pump. The fuel from the return line of the high pressure pump comes back to the fuel circuit through a heat exchanger, which is water cooled. The cooled fuel is then goes back to the reservoir fuel tank and again circulated. The flow meter measures the rate of fuel consumption in centimeters cubes per minute (ccm). A detailed diagram showing the flow supply and fuel flow metering circuit is shown in Figure 3-14.

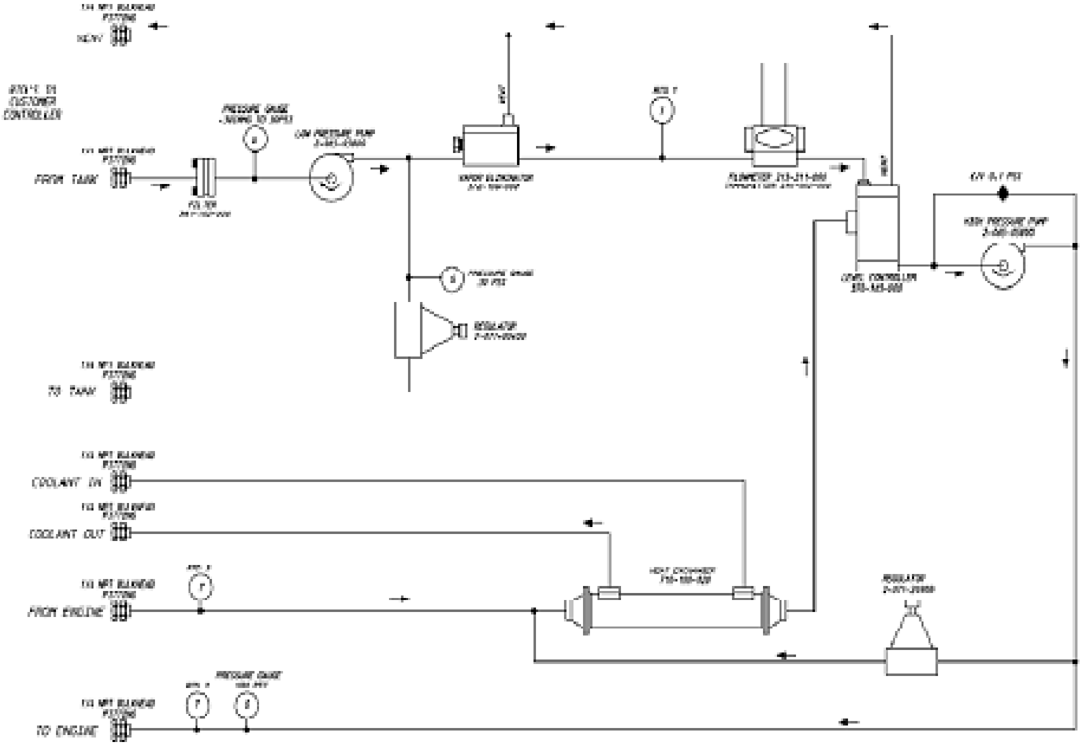

Figure 3-14. Fuel flow and measuring circuit [22]

3.5.6 Current probe sensor

A current probe is attached to the electrical connection of the injector of Cylinder #1 in order to capture the start of the injection, injection duration and number of injection events. The current probe captures the current signal waveform passing to the injector.

The sample piezo injector signal is explained in the Figure 3-15.

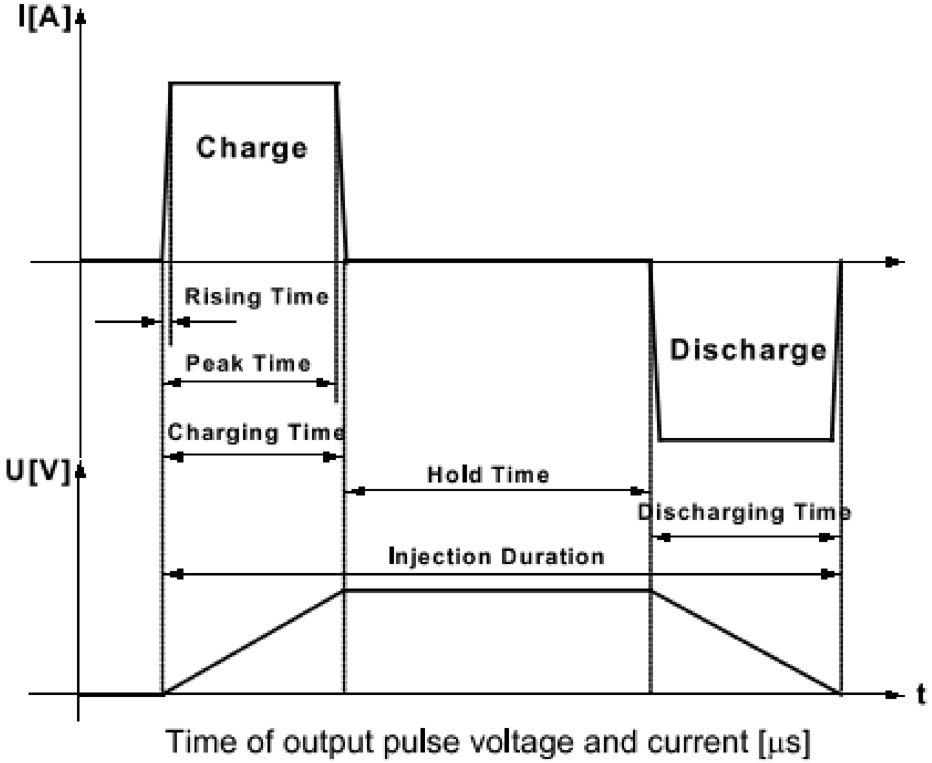

Figure 3-15. Current and voltage waveform which drives the piezo injector [19]

3.5.7 Lambda Sensor

The engine was instrumented with a lambda sensor in the exhaust manifold. The lambda in the exhaust gas can be obtained in a real time manner and is connected to the DAQ. Lambda sensors, also referred to as oxygen probes is used to the measure the oxygen contained in the exhaust emissions. The working principle of lambda sensor is based on the oxygen ion conductance of zirconium oxide at high temperature. The sensor measures the difference between the amount of oxygen in the exhaust gas and amount of oxygen in air. The fuel – air equivalence ratio can be obtained by taking the reciprocal of the value provided by the lambda sensor.

3.5.8 Temperature measurements

The temperature at various engine locations has been monitored and recorded. It is necessary to keep track of the engine conditions in order to make sure that engine maintains the steady state of operation. Slow response K-Type thermocouple are used to monitor the temperatures from the following locations.

1. Cooling water temperature
2. Oil temperature in the sump
3. Compressed air temperature in the intake manifold
4. Exhaust temperature
5. Room temperature

The thermocouples connections from various engine parts are plugged into the dyno control system which contains the built in time based data acquisition system.

3.6 *Data acquisition system and engine combustion analyzer*

The engine data was recorded either time based or crank angle based depending on the type of the signal. The crank angle based high speed data acquisition was attained through the data acquisition system from Electro Mechanical Associates (EMA) which recorded in cylinder combustion pressure, intake manifold pressure, fuel rail pressure, ion current signal, and current probe injection signal, NO in the exhaust and Opacity %. The time based data acquisition, as described in the previous sections, is used for recording various slow speed temperature measurements.

The signal from the shaft encoder is fed into the high speed DAQ to record data on a crank angle basis. The software of the DAQ allows the user to define the calibration constants for the sensor such as the offset, slope and the coefficients. The data acquired by the DAQ can be displayed in real time or as an average of many cycles. In order to reduce cycle to cycle variation, all the recorded data was based on an average of 100 cycles. Smoothening is applied to signals in order to reduce the noise during capturing the signals.

The system includes engine combustion analyzer software which calculates many engine parameters and displays them in real time. The different engine parameters calculated by the engine are, but not limited to, IMEP, peak cylinder pressure and location, indicated torque, mean engine speed, mass burnt fraction and coefficient of variation of different parameters.

3.7 *Emission measurements*

Of all the diesel combustion produced exhaust emissions, soot and oxides of Nitrogen (NOx) are of utmost importance.

3.7.1 NO measurement

A CLD 500 Fast NOx analyzer from Cambustion was used to measure the concentration of NO in the engine out emissions. NO analyzer works on the principle of chemiluminescence. The reaction between NO and ozone results in the production of light. The produced light (photons) is detected by a photo multiplier tube (PMT). The voltage from the CLD is proportional to the concentration of NO. The reaction of light production is very fast and hence it reduces the response time of the analyzer. The response time is approximately 2.5 milliseconds. The analyzer gives the concentration of NO in ppm on a crank angle degrees basis and can be connected to the DAQ.

3.7.2 Opacity measurement

A Model 107 in-line opacity meter was installed on the exhaust tail pipe of the engine. It works on the basic principle of attenuation of intensity of light by smoke aerosol absorption and scattering from exhaust gases. This is attained by passing light from an emitter through the exhaust stream from the engine and detecting the loss in the amount of light received at the collector. The loss of light energy can be translated into opacity percentage and smoke density. The values are digitally displayed on the unit as well as obtained on the DAQ. Water cooling is provided for protecting the optical sensors from high temperature exhaust gases.

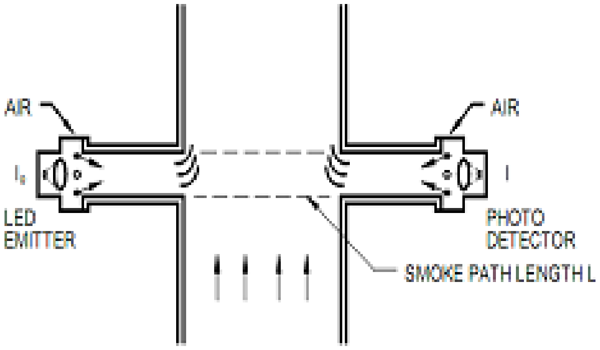

Figure 3-16. Opacity Measurement Principle

3.7.3 CO/CO2 measurements

A NDIR (Non dispersive infra-red) detector from Cambustion is used to measure engine-out CO and CO2 emissions. Although the CO/CO2 emissions are not of much importance during the steady state operation of diesel engines, these measurements are utilized in calculating the EGR percentages. The analyzer can measure the levels of CO and CO2 both at the intake and exhaust simultaneously. The ratio of CO2 in the exhaust to CO2 in the intake can be defined as the EGR%. Special machining was done in the exhaust and intake manifolds to accommodate the sample probes for the measurements of CO/CO2. The analyzer uses two separate sampling heads for measuring CO and CO2. The values from the analyzer can be recorded in the DAQ on a crank angle basis.

3.8 *Ion current measurement circuit*

A glow plug was modified to manufacture glow plug ion current sensor which could perform both the functions of a glow plug as well as an ion current sensor. The heating plug, which was insulated from the engine ground, functioned as one of the electrodes for ion current sensor, whereas the cylinder head / engine ground acts as the other electrode. The heater plug was isolated from the cylinder head by applying high temperature ceramic coating. It uses a positive polarity voltage and heater surface acts as the anode whereas the cylinder head acts as the cathode.

Compared to the previously designed ion current measuring circuits, this circuit uses a 100 Ω resistor instead of 50 Ω and a new signal conditioning module - 8B40 is used. A detailed fabrication procedure for the manufacture of the glow plug ion current sensor is described in Ref. [10].

The ion current amplifier signal box and power supply set up box can be seen in Figure 3-18. The ion current probe used for this research purpose is shown in Figure 3-19. The amplifier/ control box, being designed for a four cylinder engine, can support four ion current sensors. It also has various other controls such the change of polarity, applied voltage across the sensors etc. The ion current signal can be obtained on a crank angle basis from the high speed DAQ.

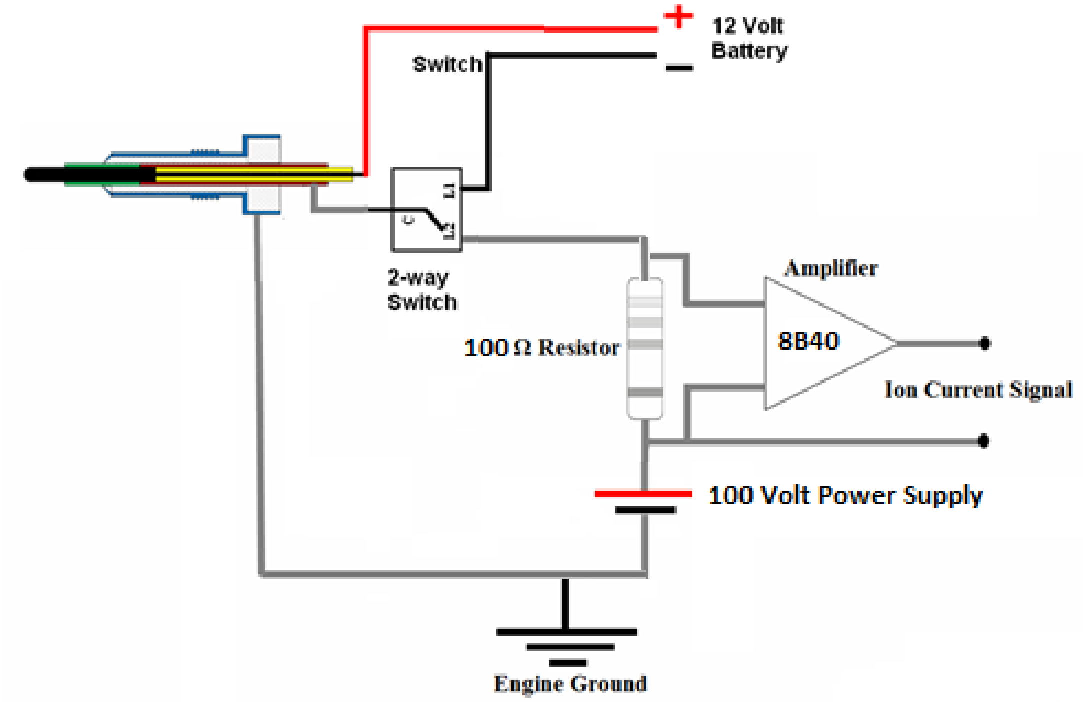

Figure 3-17. Ion current measuring circuit

Figure 3-18. Ion current signal amplifier and power supply box

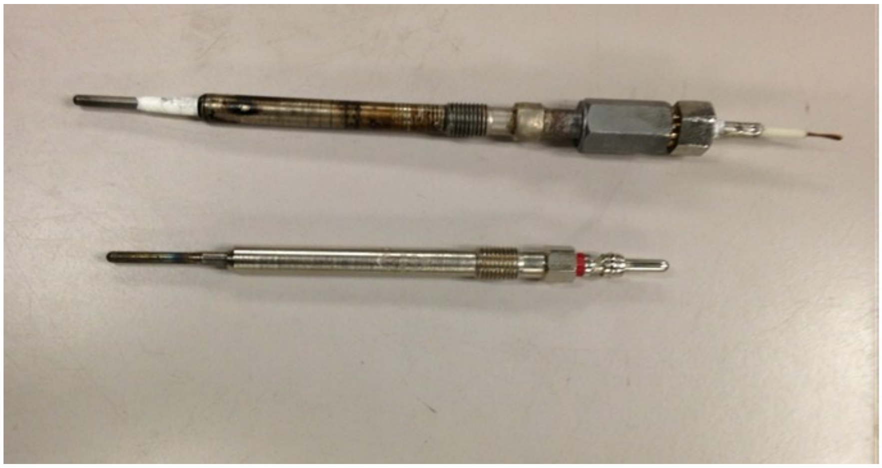

Figure 3-19. Original glow plug and integrated glow plug/ion sensor prototype used for research.

CHAPTER 4

TEST PROCEDURE

The main objective of the current investigation is to understand the various combustion, emission and ion current signal characteristics under different engine operating conditions. The first step in the study was to set up the test cell with 4-cylinder Volkswagen 2.0 L diesel engine and couple it to the water brake dynamometer. The engine was mounted on a docking cart to accomplish the same. Once the engine was set up in the test cell, next step was the instrumentation of the engine with various sensors and thermocouples. All the necessary engine modifications and sensor installations were done at Wayne State University.

After test cell set up and instrumentation, the main objective was to design and manufacture the glow plug ion current sensor. The primary target was to design a reliable sensor and to overcome any design related issues experienced in previous versions of the sensor.

The tests conducted during this research work can be divided into two main sections. First section deals with experiments conducted with ULSD for various loads and speeds. All engine parameters were monitored and recorded to develop an engine mapping. The objective of this part of the investigation is to understand the combustion, auto-ignition, engine out emissions and ion current signal characteristics during the operation with ULSD. The second section deals with the tests designed and conducted to understand the ion current signal characteristics as well as combustion, performance and emission characteristics during the operation with ULSD and jet fuels likeJP-8 and Sasol IPK.

4.1 *Tests with ULSD*

The test matrix was designed and implemented to investigate the effect of load and speed on the various engine operating parameters, combustion characteristics, emission formation and ion current signal. Three different speeds; 1600 rpm, 1800 rpm and 2000 rpm were selected and for each speed, engine load was varied from no load to 150 Nm in steps. Table (4-1) shows the test matrix.

Table 4-1. Test matrix for ULSD

SPEED (RPM)	1600				
IMEP (bars)	1.92	3.38	6.15	9.25	11.7
TORQUE (Nm)	0	20	60	100	150

SPEED (RPM)	1800				
IMEP (bars)	2.31	3.41	6.21	8.97	12.5
TORQUE (Nm)	0	20	60	100	150

SPEED (RPM)	2000				
IMEP (bars)	2.64	3.49	6.36	8.84	13.3
TORQUE (Nm)	0	20	60	100	150

The main objective of this study is to gain a better understanding of the ion current signal under different engine speeds and loads and also to monitor the OEM ECU map strategy for future implementation of open type ECU. In order to reduce the cycle by cycle variation related to combustion, an average of 100 consecutive cycles was used in the detailed analysis. Additionally, all the data set was recorded twice to ensure the reproducibility of the OEM ECU.

4.2 *Comparison of ULSD with jet aviation fuels*

A test matrix was designed and conducted to understand the ion current signal characteristics as well as combustion, performance and emission characteristics during the operation with diesel and jet fuels. A constant speed of 1800 rpm was maintained and the load was increased in steps from no load to 140Nm.Various engine operating parameters as well as engine out emissions were measured and recorded during each steady state operating point.

The test matrix used for comparative investigations between ULSD, JP-8 and Sasol IPK is shown in tables 4-2, 4-3 and 4-4 respectively.

Table 4-2. Test matrix for ULSD

SPEED (RPM)	**1800**						
IMEP (bars)	**2.31**	**3.41**	**4.91**	**6.21**	**7.7**	**8.97**	**12.0**
TORQUE (Nm)	**0**	**20**	**40**	**60**	**80**	**100**	**140**

Table 4-3. Test matrix for JP-8

SPEED (RPM)	**1800**						
IMEP (bars)	**2.26**	**3.16**	**5.35**	**6.30**	**7.18**	**8.56**	**11.1**
TORQUE (Nm)	**0**	**20**	**40**	**60**	**80**	**100**	**140**

Table 4-4. Test matrix for Sasol-IPK

SPEED (RPM)	1800						
IMEP (bars)	1.62	2.8	4.41	5.90	6.86	8.48	10.6
TORQUE (Nm)	0	20	40	60	80	100	140

All the experiments were conducted using the original/OEM ECU. The purpose of this investigation was to study the impact of operating the diesel engine, optimized and calibrated to run on ULSD, when the fuel is changed to jet aviation fuels. The experimental results were analyzed for ULSD, JP-8, and Sasol-IPK and a comparison was made with respect to auto-ignition, combustion, and engine performance and emission characteristics. In order to reduce the errors caused by cycle-to-cycle variations, an average of the 100 consecutive cycles was used for the detailed analysis. Additionally, all the data set was recorded twice to ensure the reproducibility of the OEM ECU.

CHAPTER 5

SAMPLE EXPERIMENTAL RESULTS AND ANALYSIS

The first section in this chapter deals with the discussion of the cylinder to cylinder variation as well as cycle to cycle variation during the combustion process. Sample experimental result and analysis are discussed in section two. To better understand and explain the characteristics of the auto-ignition, combustion, engine out emission and ion current signal, sample results and analysis of a selected test point is presented in this section.

5.1 *Cylinder to cylinder variation and cycle to cycle variation*

This sub section was included to analyze how efficiently the ion current sensor in one cylinder can represent the overall combustion process. As described in the instrumentation section, the cylinder #1 is instrumented with a Kistler 6052A piezo-electric pressure transducer and cylinder #4 with an ion current glow plug sensor. In order to analyze the cylinder to cylinder variation, the instrumentation of cylinder #1 and cylinder #4 are swapped. The results before and after swapping the instrumentation were then compared and analyzed. The cylindrical variation in combustion was compared with respect to in-cylinder pressure and temperature plots, rate of heat release trace, and ion current signal. The coefficient of variation (COV) in the indicated mean effective pressure (imep) was also calculated during the engine operation in each case. However the combustion variation is expected to be small since the tests were conducted without using EGR, which contributes to cylinder-to-cylinder variations [23].

Figure 5-1 shows traces obtained in cylinders #1 and #4 for the cylinder gas pressure, rate of heat release, ion current and injection signal at an engine load of 60Nm and 1800 rpm. The traces obtained before and after swapping of the instrumentation in the tow cylinders are shown in two different colors. The figure shows a very good match between the two sets of traces at this light load of 60 Nm and 1800 rpm.

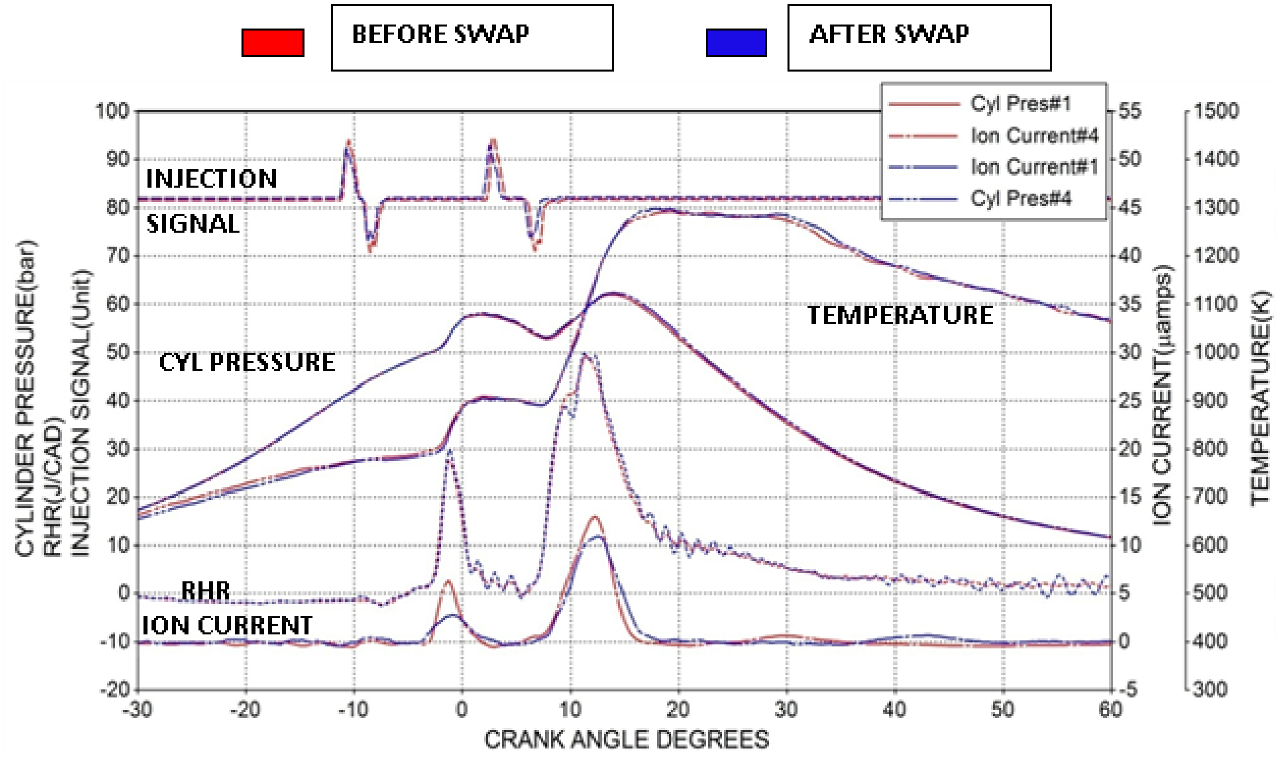

Figure 5-1. Traces taken in cylinder number 1, before and after swapping the instruments with cylinder number 4 at a load of 60Nm at 1800 rpm.

In Figure 5-2, the cylinder to cylinder variation between #1 and #4 is shown with respect to cylinder pressure, rate of heat release, ion current trace and injection signal at a heavier load of 150 Nm at 1800rpm. The injection duration as well as injection timing remained same during both the cases. There were some differences in the in-cylinder temperature plots although the in-cylinder pressure remained similar. The ion current signal also produced some noticeable cylinder to cylinder variation.

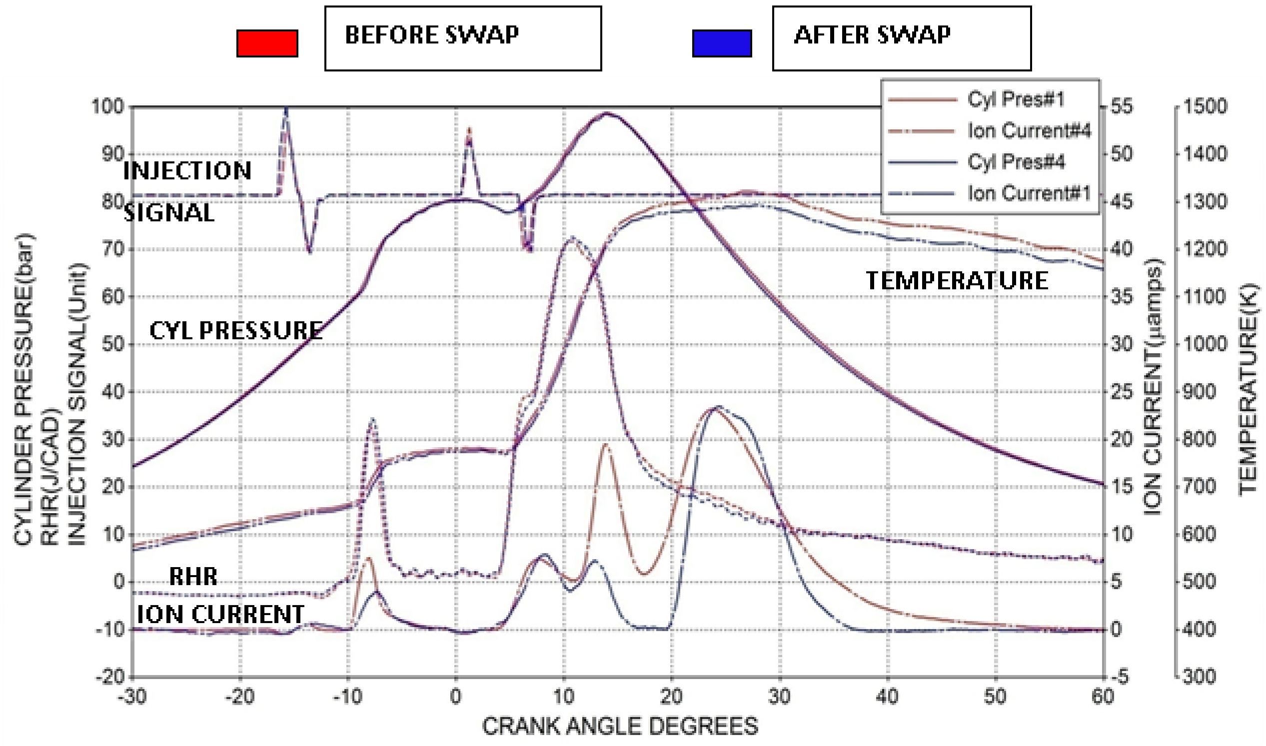

Figure 5-2. Traces taken in cylinder number 1, before and after swapping the instruments with cylinder number 4 at a load of 150 Nm at 1800 rpm.

Figure 5-3 and Figure 5-4 show in dashed blue the lower and upper borders of the cylinder gas pressure in cylinder number 1, recorded for 100 consecutive cycles at engine loads of 60 Nm and 150 Nm respectively. The same figure also shows the overlapping solid lines in red and blue colors for the average values of the in cylinder gas pressure in cylinders #1 and #4 for the same engine condition. The figure indicates clearly that the cylinder to cylinder variations were within the cycle to cycle variations.

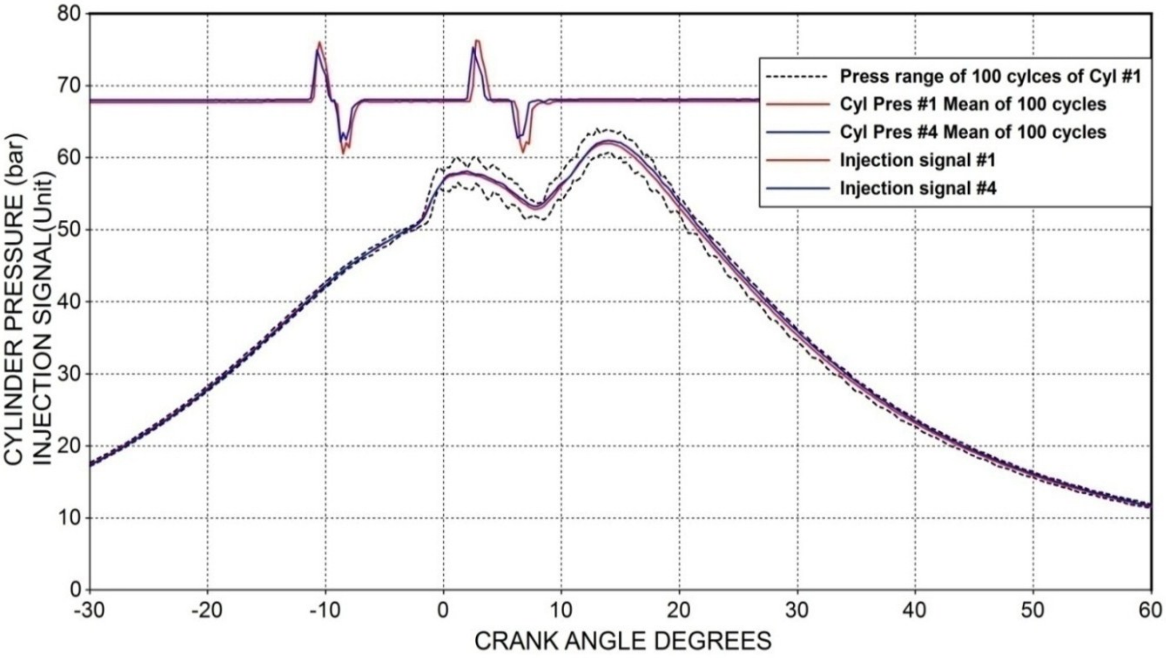

Figure 5-3. Range of cycle to cycle variation and cylindrical variation at 60 Nm – 1800 rpm

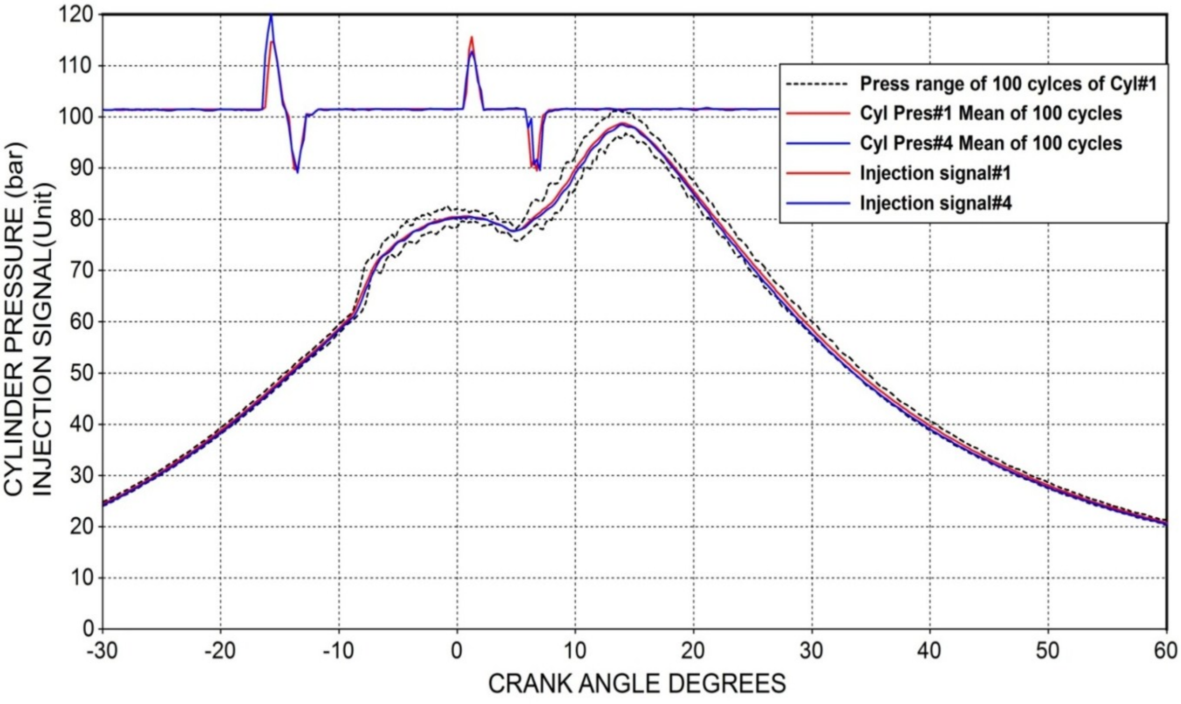

Figure 5-4. Range of cycle to cycle variation and cylindrical variation at 150 Nm – 1800 rpm.

In an attempt to quantify the variations shown in figures 5-3 and 5-4 the coefficient of variation (COV) is calculated for the IMEP [3]. The coefficient of variation is the ratio of standard deviation to the mean value. The COV in the IMEP before and after swapping the instrumentation in cylinders 1 and 4 is calculated at the two loads. Also, the COV of IMEP for the 100 consecutive cycles is calculated at the two loads. The values for the COVs are given in Table 5-1. It can be seen that the COV in IMEP due to cylinder to cylinder variations is comparable to the COV due cycle to cycle variation at the light load of 60 Nm and is lower than cycle to cycle variation at 150 Nm.

Table 5-1. Coefficient of variation (COV) in IMEP for the cycle to cycle and cylinder to cylinder.

LOAD	**IMEP, COV CYCLE TO CYCLE**	**IMEP, COV CYLINDER TO CYLINDER**
60 NM	1.66%	1.81%
150 NM	1.29%	1.02%

.

5.2 *Sample results and analysis with ULSD*

The ion current signal was investigated under different steady state engine conditions for different loads and speeds using ULSD fuel. The ECU followed a split injection strategy at all tested points. Figure 5-5 shows the in-cylinder pressure, temperature, RHR, ion current signal and injection signal traces for ULSD at an engine load of 150Nm and 1800rpm. SOPP of ULSD occurred at 16.25° bTDC and had injection duration of 3.75 CAD.

The following are the main features of the cylinder gas pressure and the ion current traces. The in cylinder pressure trace shows two peak pressures due to dual combustion events. The first injection event or the pilot injection, which was characterized by the short injection duration, occurred early and it was then followed by the second injection event or the main injection event with longer injection duration. The pilot injection produced premixed combustion seen as a sharp rise in the rate of heat release. The premixed combustion produced in the pilot injection was typical for all test points with ULSD. The ion current signal very well captured this combustion event and also corresponded well with rate of heat release trace. The combustion of the main injection event was characterized by premixed and mixing (diffusion) controlled combustion. Although it is difficult to separate specific combustion zones in the rate of heat release, ion current signal gives more information pertaining to these combustion zones. Ion current signal may have two or more peaks depending on the engine operating conditions, particularly the load.

The following is a detailed analysis for the combustion process and the ion current. The auto ignition of the pilot fuel injection caused the in-cylinder pressure to rise before TDC. The RHR shows that fuel evaporation started around 13.75° bTDC. The negative temperature coefficient regime is not depicted at 150 Nm. The high temperature combustion for ULSD started at 9.75° bTDC and reached LPPCp at 8° bTDC with an amplitude of 32.77 J/CAD. The ion current signal produced during the pilot combustion of ULSD started to rise at 9.75° bTDC and reached a peak at 8°bTDC with an amplitude of 7.98 µamps.

For the main combustion event, ULSD produced the SOPM at 0.75°aTDC and injection duration of 6.75 CAD. It was observed that ULSD start of combustion due to the main injection at 3.75° aTDC. LPPCm of ULSD was located at 6.25° aTDC. Since a higher amount of fuel was injected during the main injection at 150Nm, the main combustion was dominantly diffusion/mixing controlled combustion. Location of peak of diffusion combustion (LPDC) for ULSD was at 11.25° TDC with an amplitude of 68.83J/CAD respectively.

During the main combustion event; ULSD produced ion current signal with three distinctive peaks. After the completion of the pilot combustion process, ion current signal gradually decayed to zero. Ion current signal followed the rate of heat release trace and started to rise again at 4.5° aTDC and reached its first peak amplitude (PIC 1) of 7.82 µamps at 7.75° aTDC. After the first peak, amplitude of ion current signal dropped to a minimum and rose again to produce the second peak (PIC 2) with an amplitude of 19.87µamps at 13.75° aTDC. The second peak of ion current was produced from the diffusion/mixing controlled combustion flames. A third ion current peak (PIC 3) was observed with maximum amplitude of 23.60 µamps at 23.75° aTDC. The possible source of third peak is the oxidation of the incomplete combustion products of the main injection.

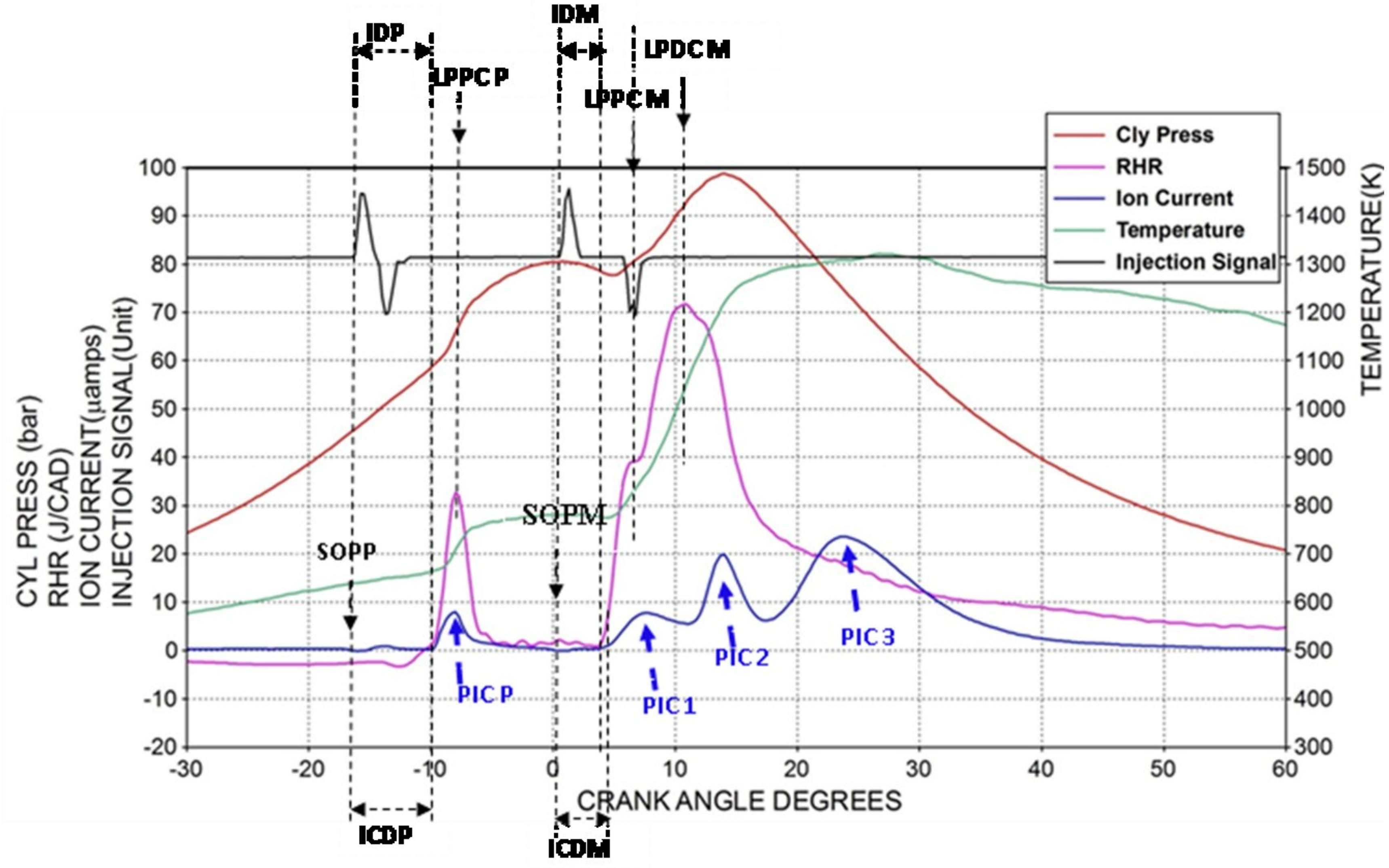

Figure 5-5. Sample traces of pressure, RHR, ion current, temperature at engine load of 150Nm at 1800rpm with ULSD

CHAPTER 6

IONIZATION AND COMBUSTION CHARACTERISTICS WITH ULSD

6.1 *Data processing*

The data was acquired using a high speed data acquisition system and then averaged over 100 consecutive cycles at steady state conditions, in order to eliminate any cycle to cycle variations. The data acquisition system recorded the data for in cylinder pressure, injection pulse signal, injection pressure, in-cylinder ion current, intake manifold pressure, NO and opacity in exhaust on a crank angle degrees basis. A total of 2880 points were obtained for each signal in one cycle as the resolution of the shaft encoder was 0.25. All the data points were recorded more than once to confirm the repeatability of the data.

To process the cylinder pressure data, a five point moving average filter was used whereas a three point moving was used for the ion current signal. This was done in order to eliminate any noise in the acquired signal. The filter was chosen such that anything lower was not effective and using a higher degree of smoothening had a tendency to flat out the peaks.

6.2 *Effect of load*

This study shows the effect of load at three different speeds; 1600, 1800, 2000 rpm, on ion current signal, auto-ignition, combustion, performance, and emission characteristics. During each speed, the engine load was varied from no load to 150 Nm. As the engine was operated with an OEM ECU which controls the engine operating parameters including timing, duration of fuel injection, injection pressure, and intake manifold pressure. Exhaust gas recirculation was not used in this study in order to avoid the cylinder to cylinder variation as discussed in chapter 5. All the engine operating parameters were monitored as well as recorded for each steady state condition and analyzed with respect to the variation in load.

6.3 *Engine operation at 1600 rpm*

The following section covers the analysis during the engine operation at 1600rpm. Figure 6-1, Figure 6-2 and Figure 6-3 show the in cylinder pressure, rate of heat release, ion current signal and in- cylinder temperature signal for varying engine load from no load to 150 Nm at 1600rpm. Figure shows two injection events - pilot injection which occurs early before TDC with a short duration and the main injection with a longer duration which occurs after TDC. As the engine load increased from no load to 150Nm, it is observed that the start of injection of pilot and main were advanced. The start of injection pulse - pilot (SOPP) for no load and 150 Nm occurred at 8.25° bTDC and 15.25° bTDC respectively.

Figure 6-1 shows in-cylinder pressure and ion current for varying engine load at 1600 rpm. The in-cylinder pressure produced two peak pressures corresponding to combustion produced from the two injection events. The peak pressure produced due to the pilot combustion event occurred close to TDC whereas peak pressure produced due to main combustion occurred later in the expansion stroke. It was observed that the intake pressure was increased by turbo charging as the load increased.

Figure 6-2 shows rate of heat release traces and ion current signals for varying engine load at 1600rpm. The pilot fuel injection burned mainly in the premixed combustion mode. For the main injection event, RHR produced one or two peaks depending on the engine load. During no load and lower engine loads, the combustion consisted mainly of premixed combustion and characterized by a peak. As the engine load increased, a larger amount of fuel was injected during the main injection and the main combustion was dominantly diffusion/mixing controlled combustion. A second peak which was mainly produced due to the diffusion combustion was observed in the heat release trace.

The ion current sensor was able to capture both combustion events and produced distinctive signals. The ion current signal was characterized by two to four peaks depending on the applied load. At all load points, the pilot combustion produced a single peak (PICP) in ion current whereas the main combustion event produced one, two or three peaks as seen the figures. At no load of 20Nm, there is no indication of PIC 2 or PIC 3, although there is a clear PIC 1. At 60 Nm and higher loads, the PIC 2 and PIC3 started to develop. It was observed that the location of ion current peaks - LPIC 1 and LPIC 2 followed the location of the peak of premixed combustion (LPPC) and the peak due to diffusion - mixing controlled combustion (LPDC) respectively. The third peak of ion current corresponded to the oxidation of the incomplete combustion products later in the expansion stroke.

Figure 6-3 shows in-cylinder temperature trace and ion current signal for varying engine load at 1600rpm. It can be observed that the temperature increased twice corresponding to the pilot and main injection events. The rise in temperature due to the pilot injection was observed to be comparatively small when compared to the temperature rise due to the main injection.

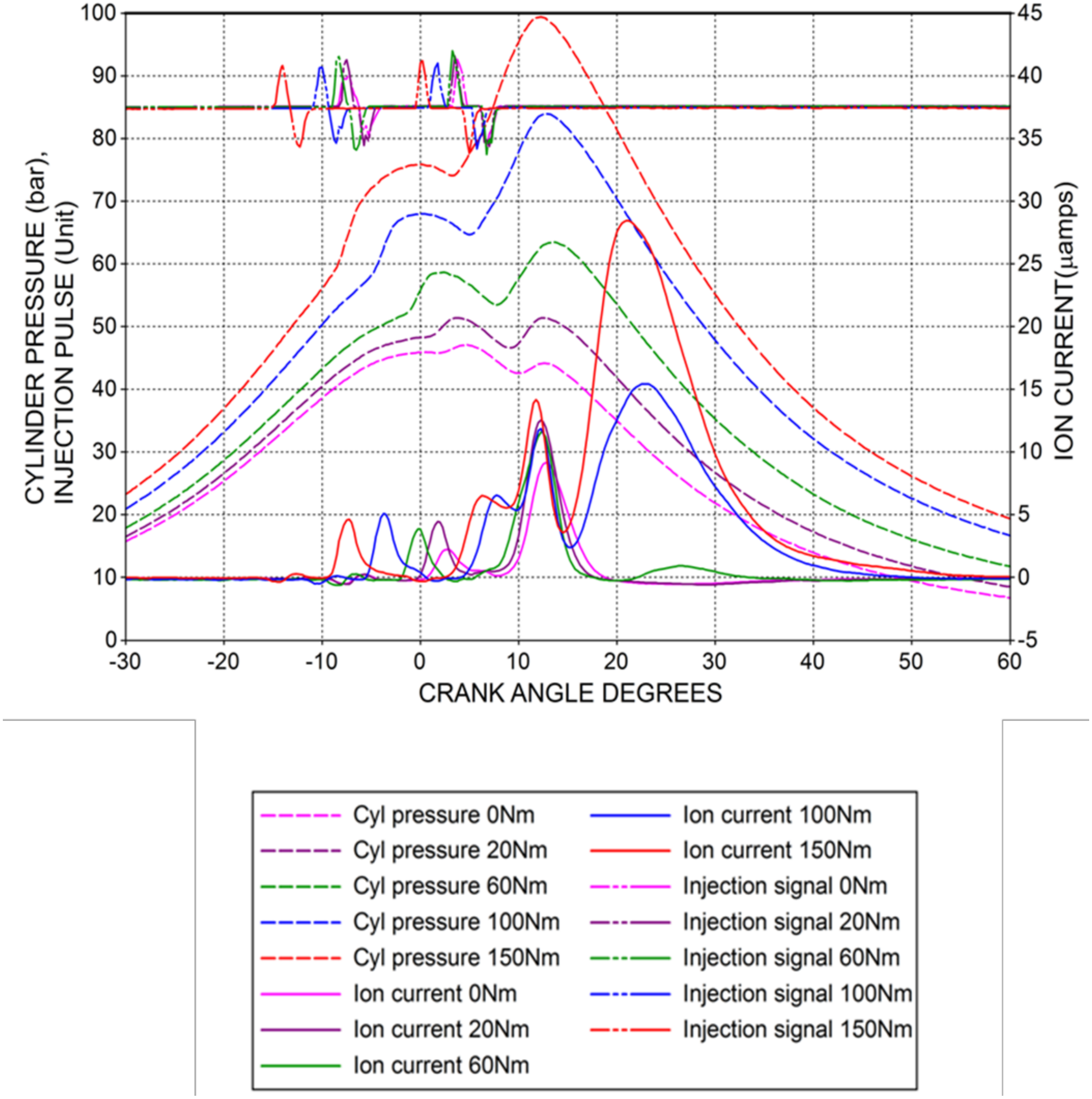

Figure 6-1. In-cylinder pressure and ion current signal for different engine loads at 1600 rpm.

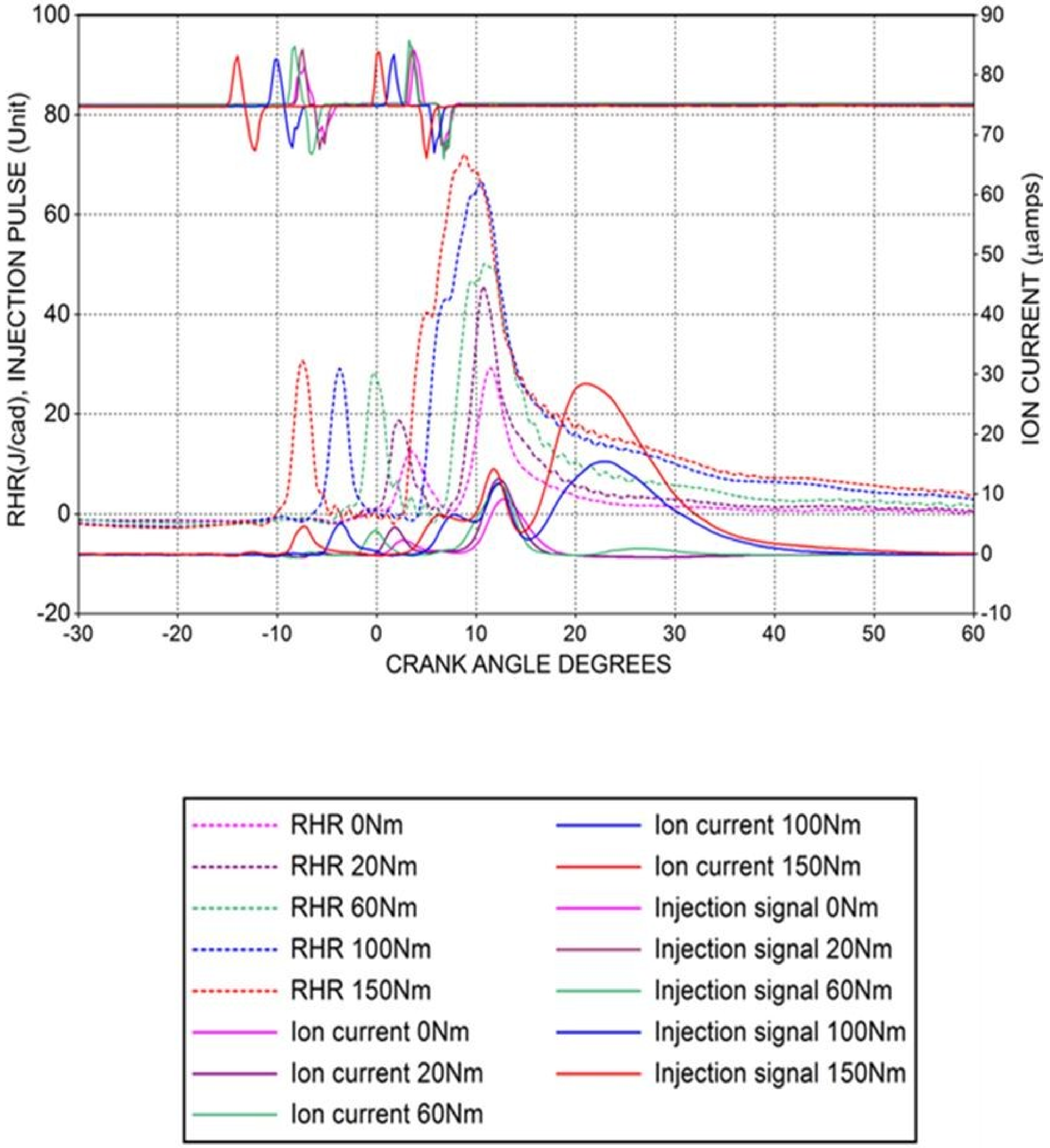

Figure 6-2. RHR and ion current signal for different engine load at 1600 rpm.

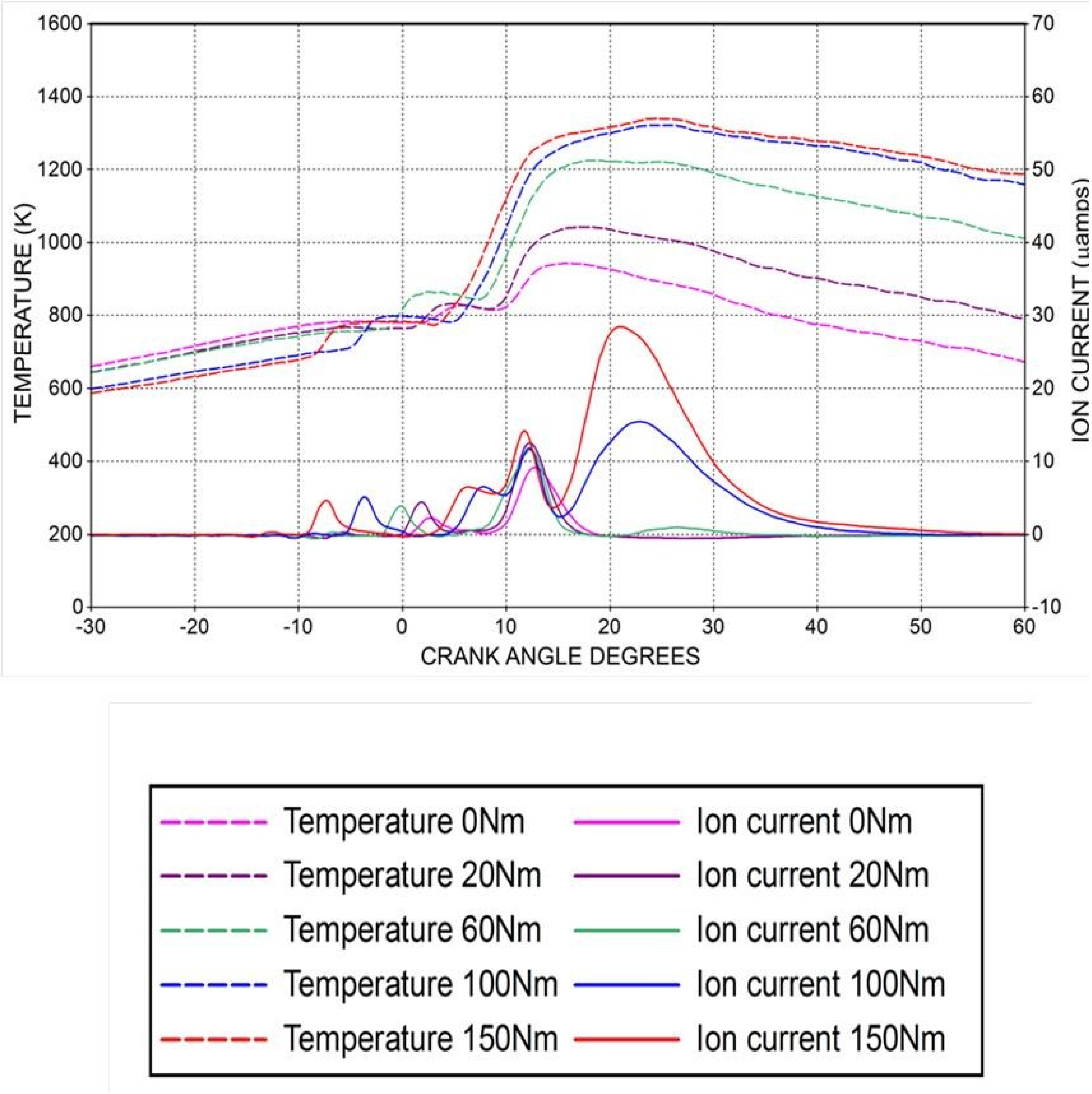

Figure 6-3. In-cylinder temperature and ion current signal for different engine loads at 1600 rpm

Figure 6-4 shows the pilot and main injection pulse duration at 1600 rpm. The pilot injection pulse duration was 4.25CAD at no load which then decreased to 3.75CAD and remained constant at higher engine loads. The main injection pulse duration increased with the increase in load. The main injection pulse duration increased from 4.75CAD at no load to 6.5 CAD at 150 Nm.

In Figure 6-5 shows the SOP (start of injection pulse), SIC (start of ion current), and SRHR (start of rate of heat release) at different IMEPs. Injection parameters related to the pilot injection are denoted by P (pilot) and those related to the main injection by M (main) like in SOP P and SOM M and so on. The engine load was varied from 1.92 bar to 11.7 bar IMEP. ECU adopted an injection strategy where a pilot injection was followed by a main injection event in all the test points. The ion current signal was observed twice in this injection strategy, represented in the figure as the start of ion current for pilot and main injection denoted by SIC P and SIC M respectively. The test was repeated more than once to confirm the injection strategy followed by the ECU. In order to confirm the same, the start of rate of heat release was analyzed and shown in the figure as SRHR. SIC was found to advance along with the SOP as the load was increased and this trend was followed for both pilot and main injection events. It was also observed that the SIC closely followed the SRHR. Detailed analyses for various correlations of ion current signal are discussed later in this section.

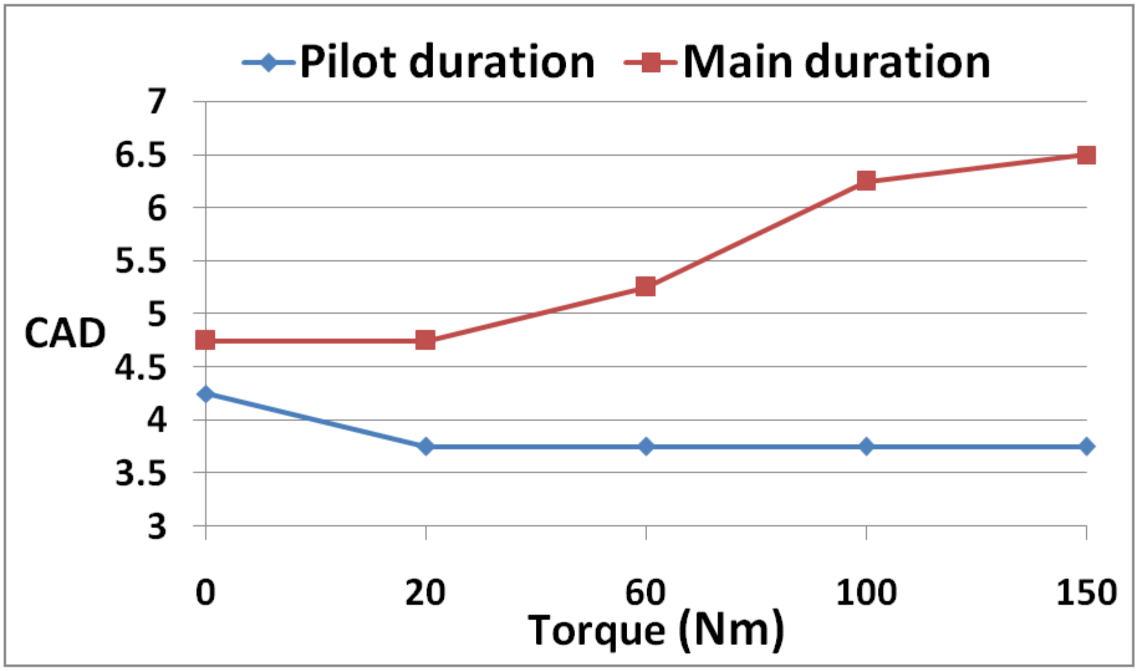

Figure 6-4. Data analysis showing the pilot and main injection duration at 1600rpm.

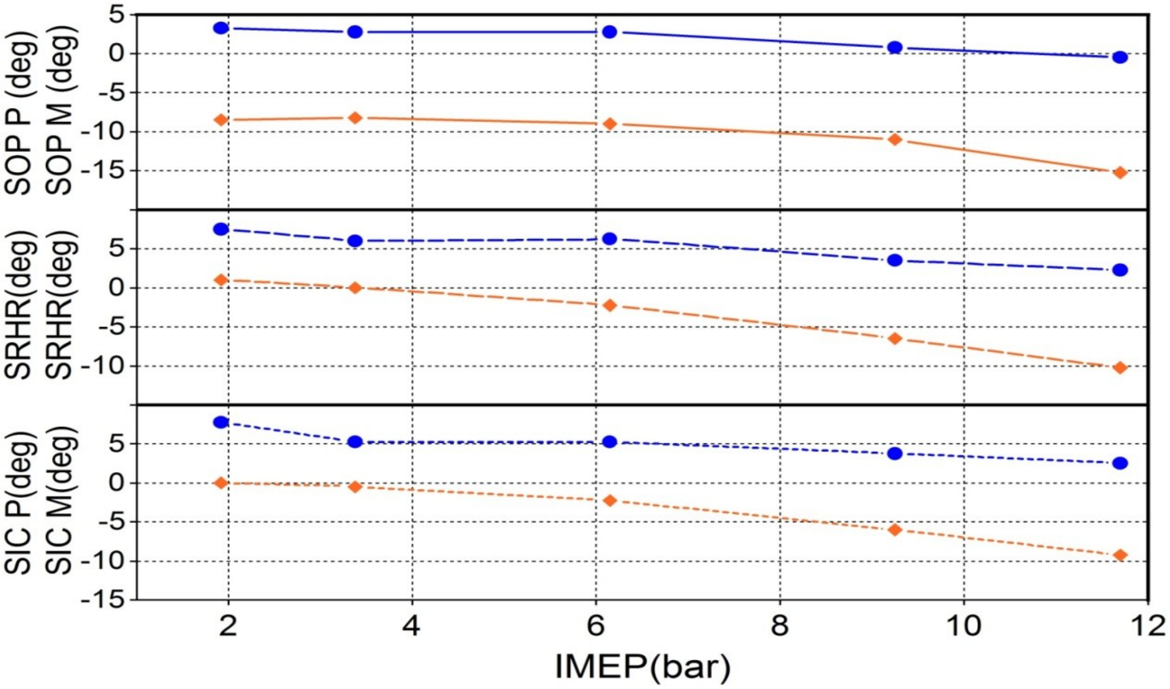

Figure 6-5. Data analysis showing SOP, SRHR, SIC Vs. IMEP @ 1600 RPM for pilot and main injections

Various engine operating parameters, engine out emissions, and performance parameters were processed, analyzed and plotted for different loads as shown in Figure 6-6, Figure 6-7 & Figure 6-8 respectively. As the engine was run on the OEM ECU, analyzing combustion, performance and emission characteristics gave an insight into various strategies used by the engine.

Figure 6-6 shows the manifold absolute pressure, fuel injection pressure, and equivalence ratio at different loads. The intake pressure was observed to increase from 1.11 bar at 1.92 bar IMEP to 2.02 bar at 11.7 bar IMEP. The rate of boosting of intake air was found to increase as the load increased which can be observed as the higher slope of MAP at higher loads. The injection pressure increased with increase in load, starting from 483 bar at IMEP of 1.92 bar to 831 bar at an IMEP of 6.15 bar. The maximum injection pressure of 934 bar was recorded at the highest load of 11.7bar. The fuel injection pressure rose very sharply to 831 bar at a medium load, after which the rate slowed down and max injection pressure recorded was 934 bar. The equivalence ratio (ϕ) was also calculated from the lambda value obtained from the Lambda meter and plotted at different loads. The overall equivalence ratio at all loads were less than one. It is observed that the ϕ increased as the load was increased. It ranged from 0.17 at no load to 0.63 at 11.7 IMEP.

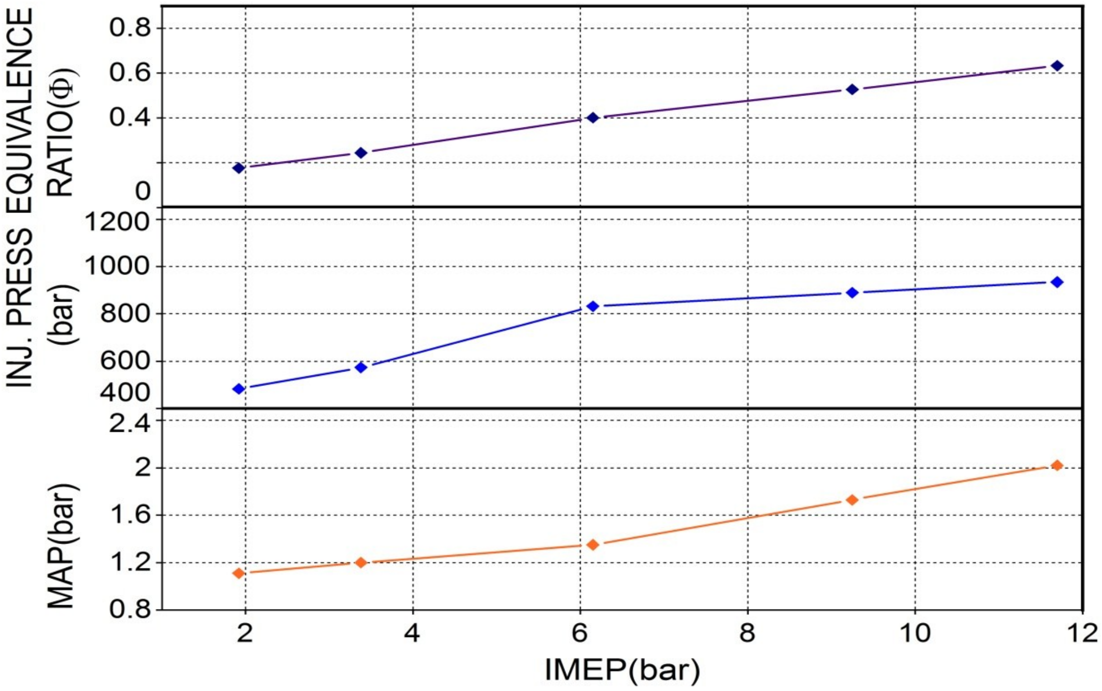

Figure 6-6. Data analysis showing equivalence ratio, injection pressure, MAP Vs. IMEP @ 1600 RPM

NO emissions and opacity percentage were measured during all the test points. Emissions were plotted against load as shown in Figure 6-7. The NO formation was observed to increase with the load linearly as the engine was isolated from EGR. The NO emission was 175 ppm at no load and it rose to 947 ppm at 11.7 bar IMEP. The opacity percentage was observed to be considerably low at all the test points since the OEM ECU are calibrated to produce very low soot values due to strict emission regulations. At the lowest load, the opacity percentage was 0.34 and it increased to 0.51 at highest load. Even though the opacity increased with respect to the increase in load, it was observed that the rate of rise is very low since the injection pressure is higher at higher loads, providing better atomization and better mixing and leading to comparatively lower soot values.

The indicated thermal efficiency and ISFC against load as shown in Figure 6-8. The ISFC decreased with increase in load till 9.25 bar IMEP and again increased at 11.7bar. Thermal efficiency which followed the reverse trend of ISFC, recorded a highest efficiency of 50.2% at 9.25 bar IMEP.

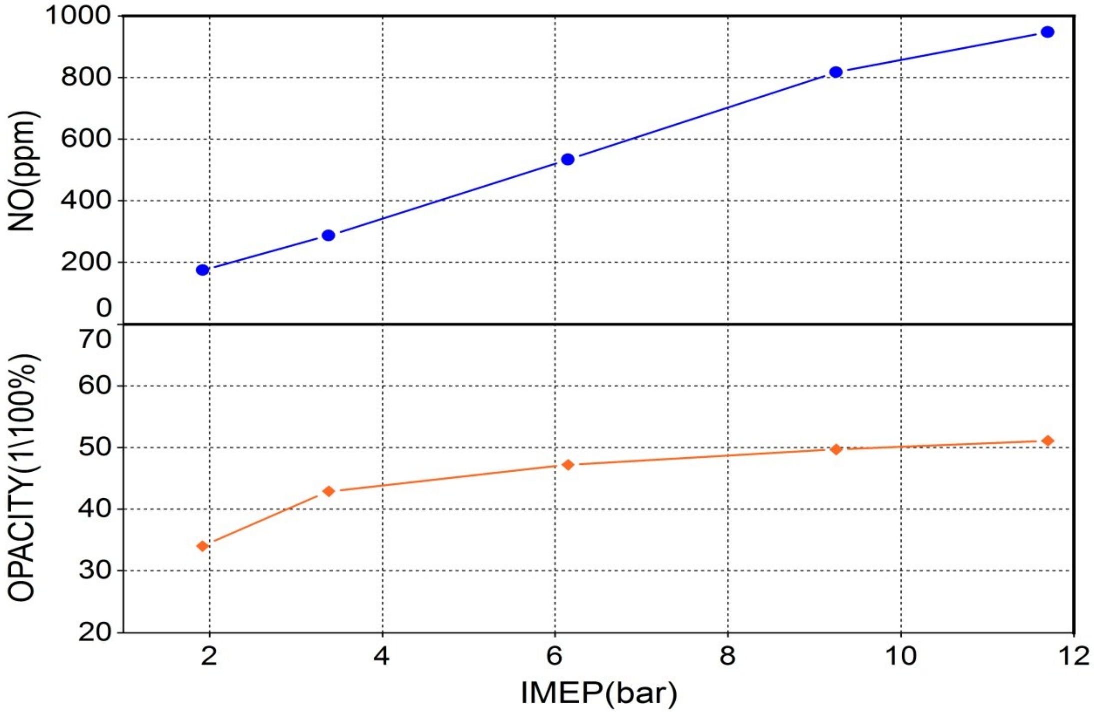

Figure 6-7. Data analysis showing NO and opacity at 1600rpm

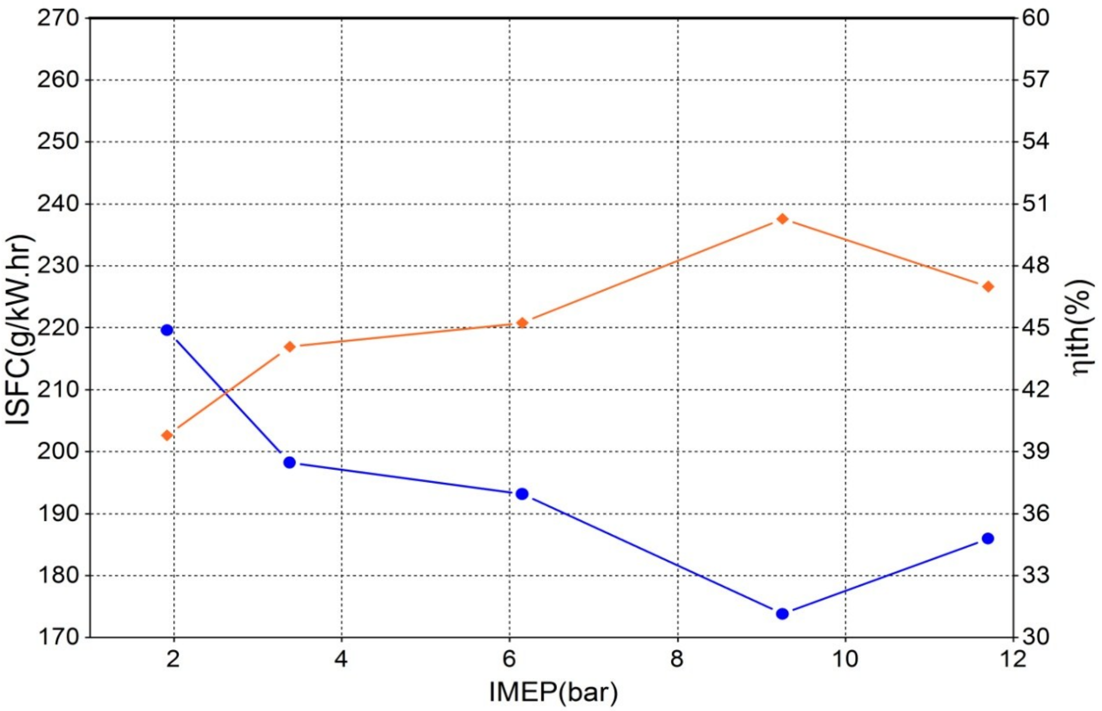

Figure 6-8. Data analysis showing ISFC and indicated thermal efficiency at 1600rpm

Auto-ignition analysis was done at different loads with ULSD at 1600 rpm. Fuel properties and engine conditions affects the auto ignition process which in turns controls the fuel vaporization, atomization and mixing processes. The delay period and auto ignition of the charge play a key role in the performance and emission characteristics. The ignition delay was calculated for each test point of the load and expressed in terms of crank angle degrees (CAD). Ignition delay was calculated from the start of injection pulse to the start of high temperature combustion.

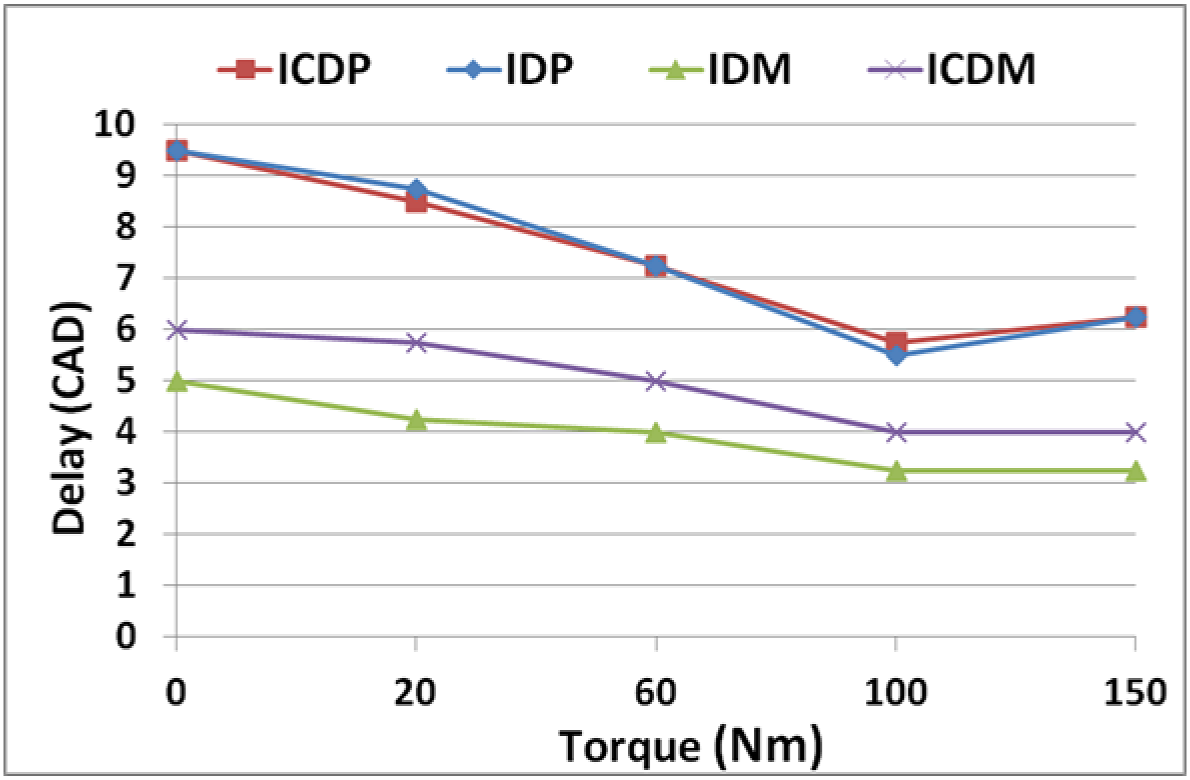

Figure 6-9. Data analysis showing ignition delay and ion current delay for pilot and main injections events for varying loads at 1600 rpm.

Figure 6-9 shows the comparison of the ignition delay and ion current delay for the pilot and main injection events at 1600 rpm. Ion current delay (ICD) was calculated from the start of injection signal pulse to the start of ion current, expressed in crank angle degrees. Ignition delay of pilot combustion was observed to decrease with the increase in engine load. Ion current delay also followed the same trend as that of ID.

While analyzing the ignition delay of main combustion (IDM) it can be observed that it decreased with the increase in load. The IDM was found to be lower than the IDP since the temperature and pressure inside the cylinder had been increased as a result of the pilot combustion process which helped in the faster auto ignition of the fuel injected during main event. The ion current delay of main event (ICDM) followed the same trend of IDM. However, the ICDM was found to be higher than IDM.

Figure 6-10 and Figure 6-11 shows the correlation between ID P and ICD P as well as ID M and ICD M respectively. It can be observed that the correlation between ion current delay and ignition delay produces a regression coefficient (R^2) of 0.9932 for the pilot combustion and 0.926 for the main combustion. During pilot combustion, the premixed combustion fraction is very strong and the ion contribution from the premixed flame is high. However, during the main combustion event, the premixed fraction is weak and diffusion - mixing controlled combustion is strong. This can be observed as the weaker correlation between the ID M and ICD M compared to the corresponding one during pilot event.

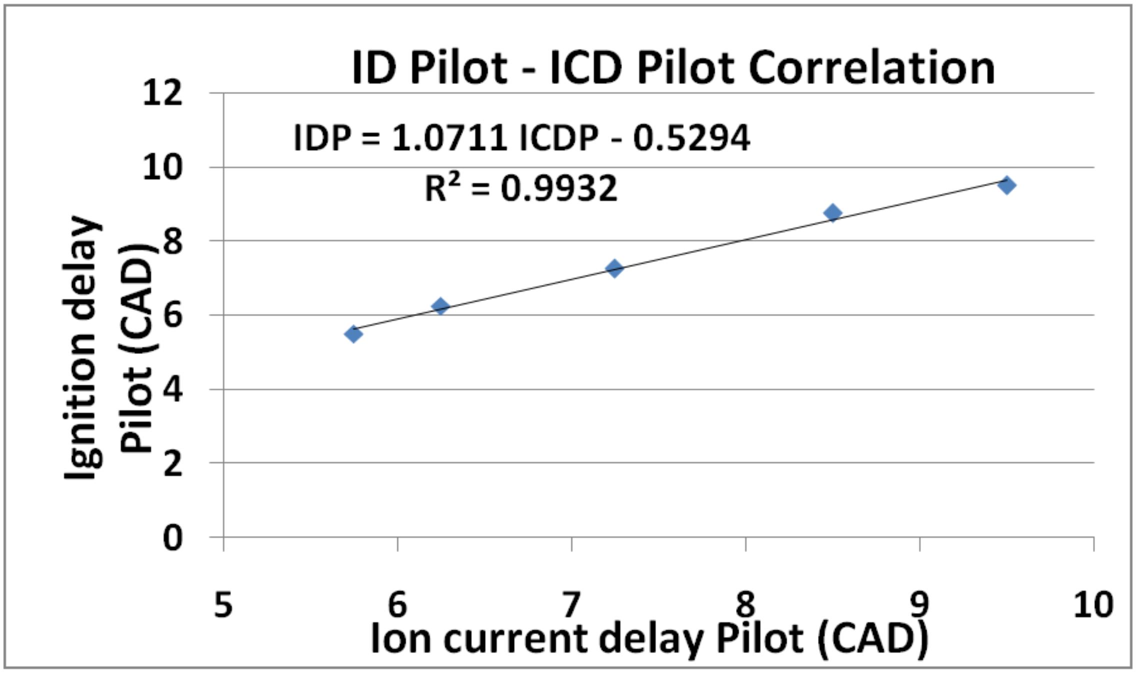

Figure 6-10. Data analysis showing the correlation between ID P and ICD P at 1600rpm.

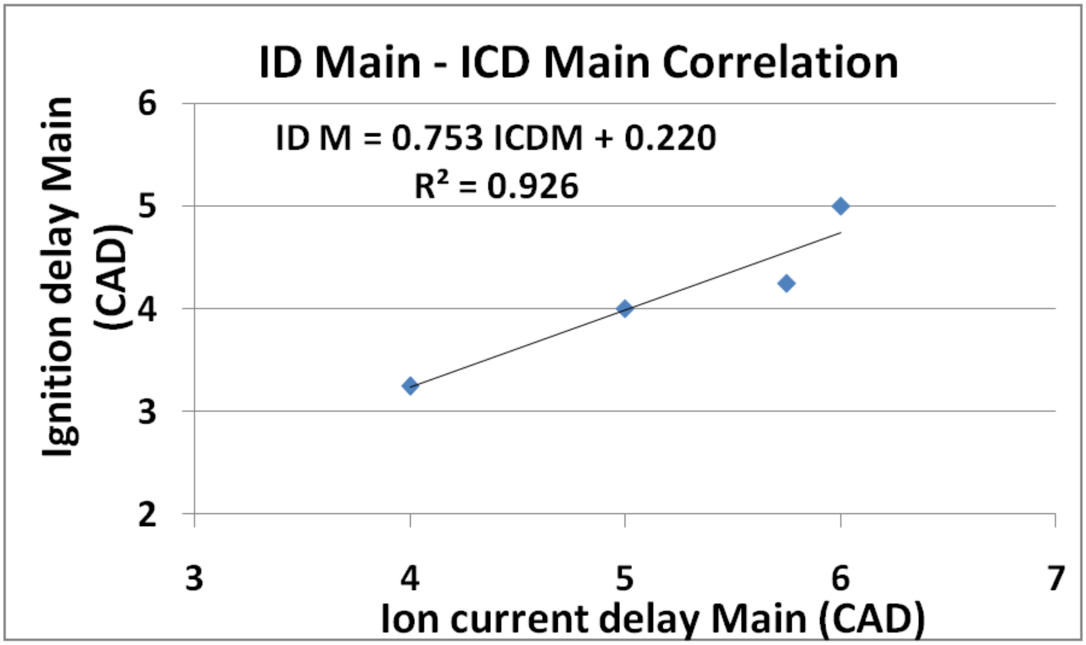

Figure 6-11. Data analysis showing the correlation between ID M and ICD M at 1600rpm.

The ion current signal was studied with respect to different parameters that changed under various operating conditions of the engine. The start of ion current (SIC) was plotted against the start of injection pulse of both main and pilot injections as shown in Figure 6-5. As discussed before, ion current sensor detected two starts associated with both injection events. The signal not only detected two starts, it also correlated well with the start of RHR as seen in the same figure.

Various correlations of ion current signal with rate of heat release trace were investigated. The magnitude and location of the different peaks of the ion current signal contain information regarding various combustion events occurring inside the cylinder. The location of different peaks of ion signal were analyzed for pilot as well as main combustion events and analyzed with respect to the corresponding combustion events from RHR trace. Figure 6-12 shows the location of ion current peaks and various peaks of RHR. The location of peak of ion current of pilot combustion (LPICp) closely followed location of peak of premixed combustion due to pilot (LPPCp). Also, the location of the peaks of ion current due main combustion (LPIC 1, LPIC 2) corresponded to the LPPCm and LPPCm respectively. The third peak of ion current was observed at higher loads where there was an increase in diffusion/mixing controlled flame. Figure 6-13 shows the peak amplitudes of rate of heat release trace and ion current signal for different loads at 1600 rpm. The premixed combustion fraction of the pilot increased with the increase in the load which can also be observed in the increasing magnitude of PPCp. The third peak of ion current was observed to develop around 6 bar IMEP and its amplitude increased with increase in engine load.

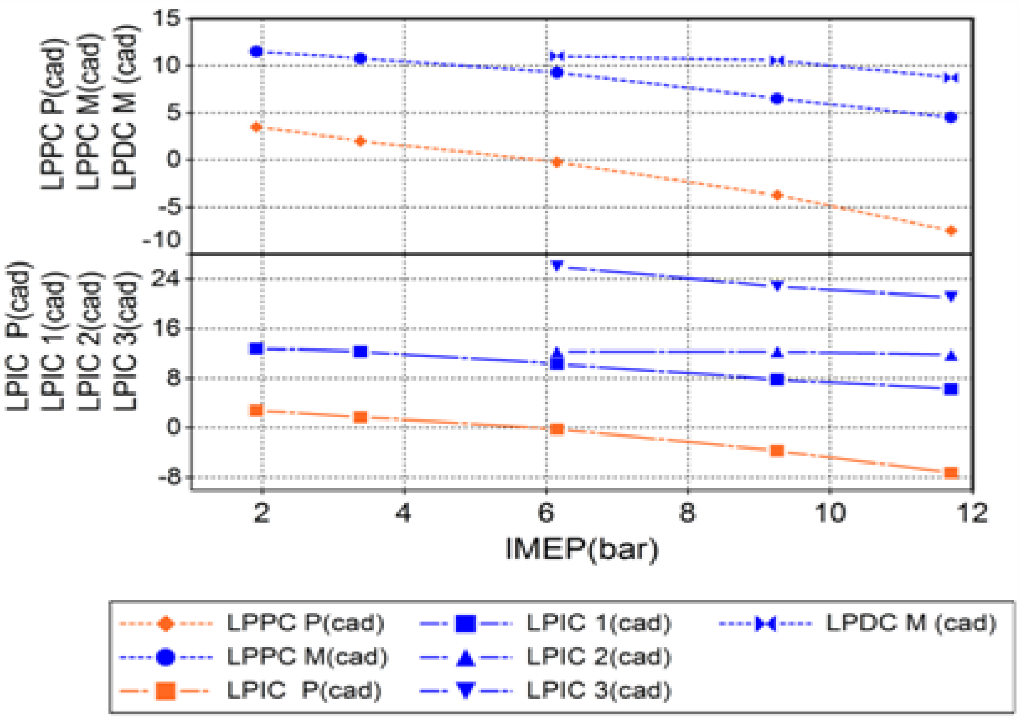

Figure 6-12. Data analysis showing peak locations of RHR trace and ion current signal for different loads at 1600 rpm.

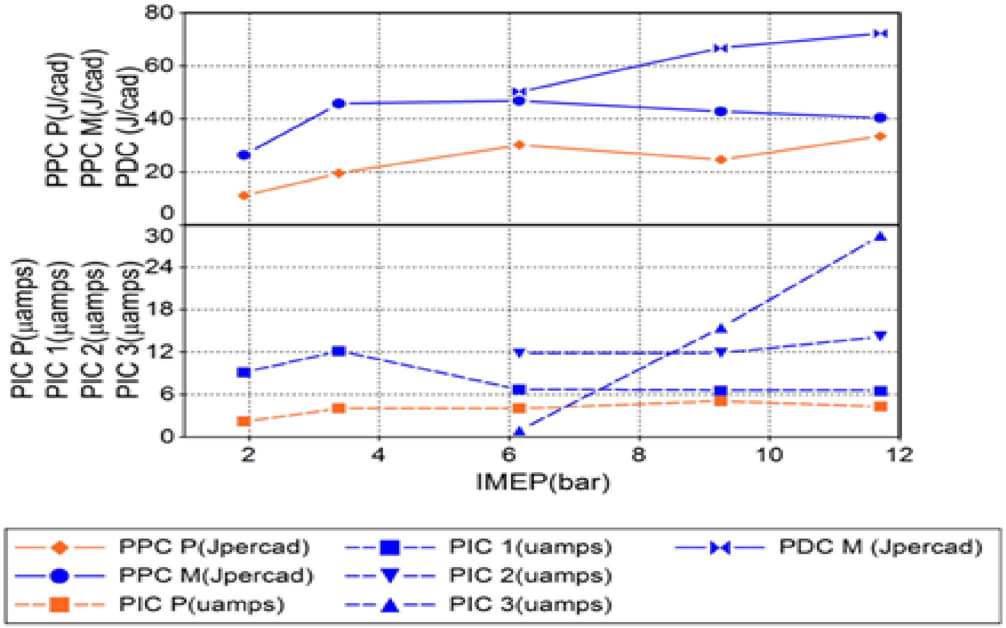

Figure 6-13. Data analysis showing peaks amplitude of RHR and ion current signal at 1600rpm for pilot and main injections.

The plots here shows us that the amplitude and location of ion current peaks are sensitive to varying engine operating parameters such as the injection pressure, injection timing and intake pressure and engine load. The following covers correlations made between the start of ion current signal and the first peak of ion current signal with the location of peak of premixed combustion. The Figure 6-14 shows the correlation between SICp and LPPCp for different engine loads at a constant speed of 1600 rpm. LPPCp was observed to have an offset of 2.85° CAD and the regression coefficient, R^2, was 0.989. Figure 6-15 shows the correlation between LPICp and LPPCp for different engine loads at 1600 rpm. The LPPCp was observed to have an offset of 0.25° CAD and a higher regression coefficient of 0.998 in comparison to the former one. The pilot combustion, as seen from RHR trace, is mostly of the premixed combustion fraction and can be observed as the single peak in the ion current signal. The ion contributors for this peak amplitude are from the premixed combustion flame occurring close to the probe.

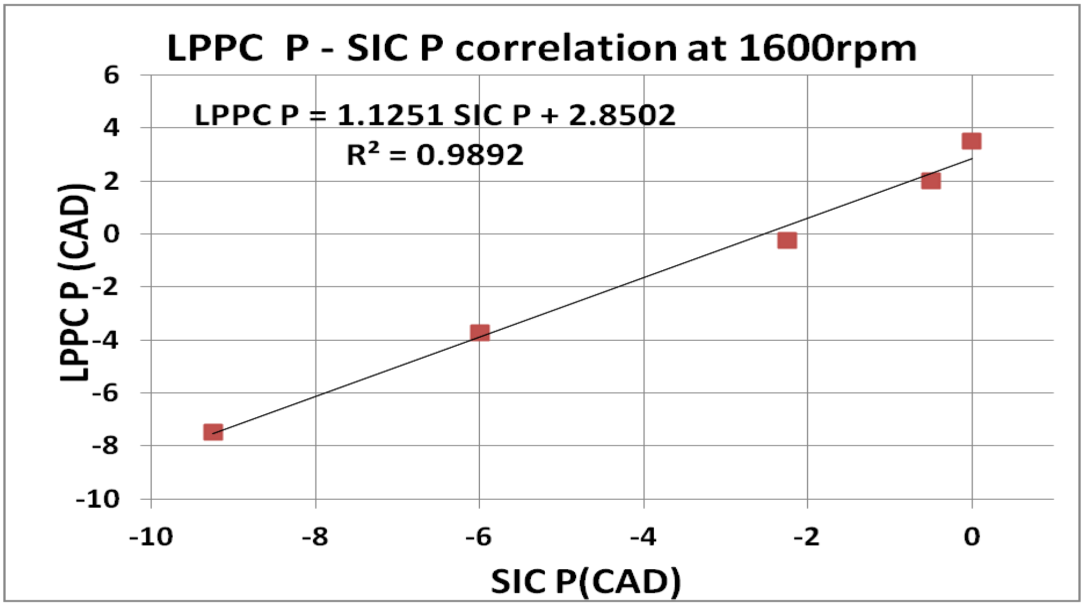

Figure 6-14. Data analysis showing correlations of LPPC P with SIC P at 1600rpm

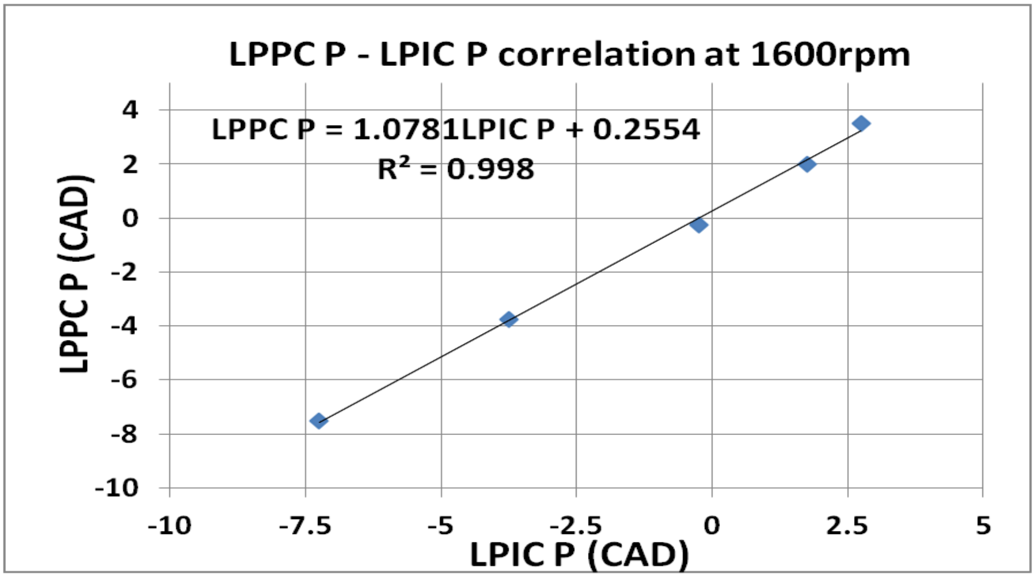

Figure 6-15. Data analysis showing correlations of LPPC P with LPIC P at 1600rpm

Figure 6-16 shows the correlation between LPPCm and SICm for different engine loads at a constant speed of 1600 rpm. LPPCm was observed to have an offset of 8.18 CAD and the regression coefficient, R^2 was 0.79. It was observed that ignition delay as well as the ion current delay of the main injection event has been altered by the pilot combustion event. The pilot combustion increased the in-cylinder pressure and temperature and hence the delay period (both ID and ICD) reduced. Hence the main combustion event comprised mainly of diffusion/mixing controlled combustion. The same can be observed as the weaker correlation during the main combustion event in comparison to the pilot event. Figure 6-17 shows the correlation of LPPCm with LPIC1 for different engine loads at a constant speed of 1600 rpm. The LPPCm was observed to have an offset of 23.18 CAD and a higher regression coefficient of 0.86 in comparison to the correlation with SICm.

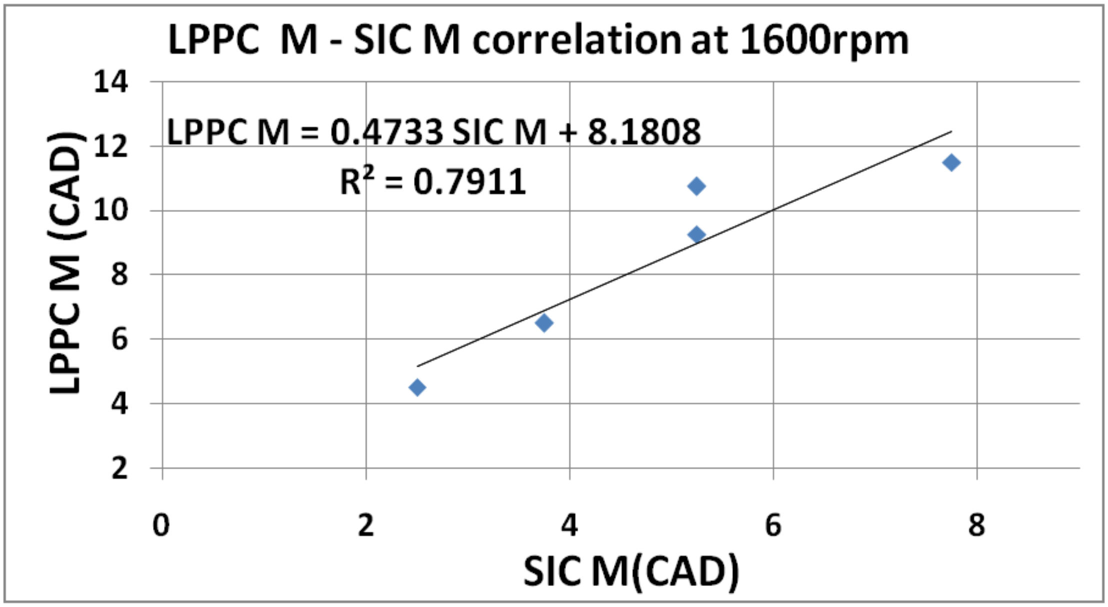

Figure 6-16. Data analysis showing correlations of LPPC M with SIC M at 1600rpm

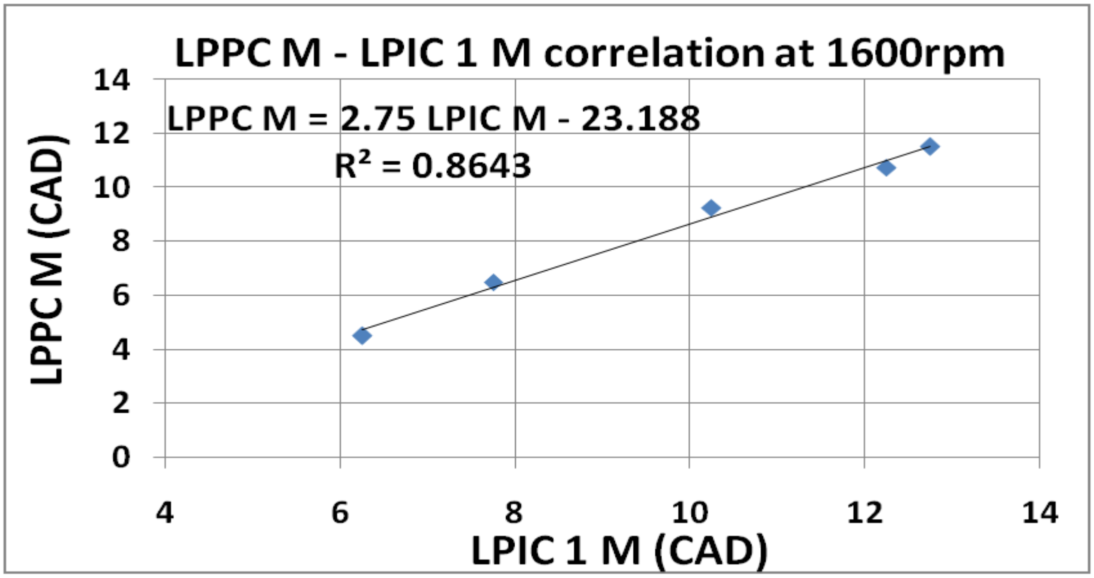

Figure 6-17. Data analysis showing correlations of LPPC M with LPIC 1 M at 1600rpm

6.4 *Engine operation at 1800 rpm*

The following section covers the analysis during the engine operation at 1800rpm. Figures 6-18, 6-19 and 6-20 show in-cylinder pressure, rate of heat release, ion current signal and in-cylinder temperature for varying engine load from no load to 150 Nm at 1800 rpm. The engine operation at 1800rpm shows two injection events - pilot injection which occurs early before TDC with a short duration and the main injection with longer duration which occurs after TDC. As the engine load was increased from no load to 150Nm, it was observed that the start of injection of pilot and main advanced. The start of injection pulse - pilot (SOPP) for no load and 150Nm occurred at 9.25° bTDC and 16.25° bTDC respectively.

Figure 6-18 shows in-cylinder pressure and ion current signal for varying engine load at 1800rpm. Similar to the engine operation at 1600rpm, the in-cylinder pressure produced two peak pressures corresponding to combustion produced from the two injection events. The peak pressure produced due to the pilot combustion event occurred close to TDC whereas peak pressure produced due to main combustion occurred later in the expansion stroke. It was observed that the intake pressure was increased by turbo charging as the load increased.

Figure 6-19 shows rate of heat release trace and ion current signal for varying engine load at 1800rpm. The two injection events produced two separate combustion events which could be observed from the rate of heat release trace. The pilot fuel injection event burned mainly in the premixed combustion mode whereas the main injection event burned mainly in the diffusion/mixing controlled combustion mode. This could be observed from the RHR trace as the single peak amplitude during pilot at LPPCp (location of peak premixed combustion- pilot). For the main injection event, RHR produced one or two peaks depending on the engine load. During no load and lower engine loads, the combustion consisted mainly of premixed combustion and characterized by a peak. As the engine load increased, a larger amount of fuel was injected during the main injection and the main combustion was dominantly diffusion/mixing controlled combustion. A second peak which was mainly produced due to the diffusion combustion was observed in the heat release trace.

Figure 6-20 shows the in-cylinder temperature and ion current signal during different engine loads at 1800rpm. Similar to the operation at 1600 rpm, ion current signal is characterized by two to four peaks depending on the applied load. At all load points, the pilot combustion produced a single peak (LPICp) in ion current whereas the main combustion event may produce one, two or three peaks as seen the figures. At no load and low engine loads, there is no indication of second or third ion current peak, although there was a distinctive first peak. At 60 Nm and higher loads, second and third ion current peaks started to develop. Furthermore, peak in-cylinder combustion temperatures produced considerably higher values during 60Nm in comparison to the lower loads which favored the production of ion current signal. The peak in-cylinder temperatures produced during the main combustion event was considerably higher compared to the combustion produced from pilot fuel injection.

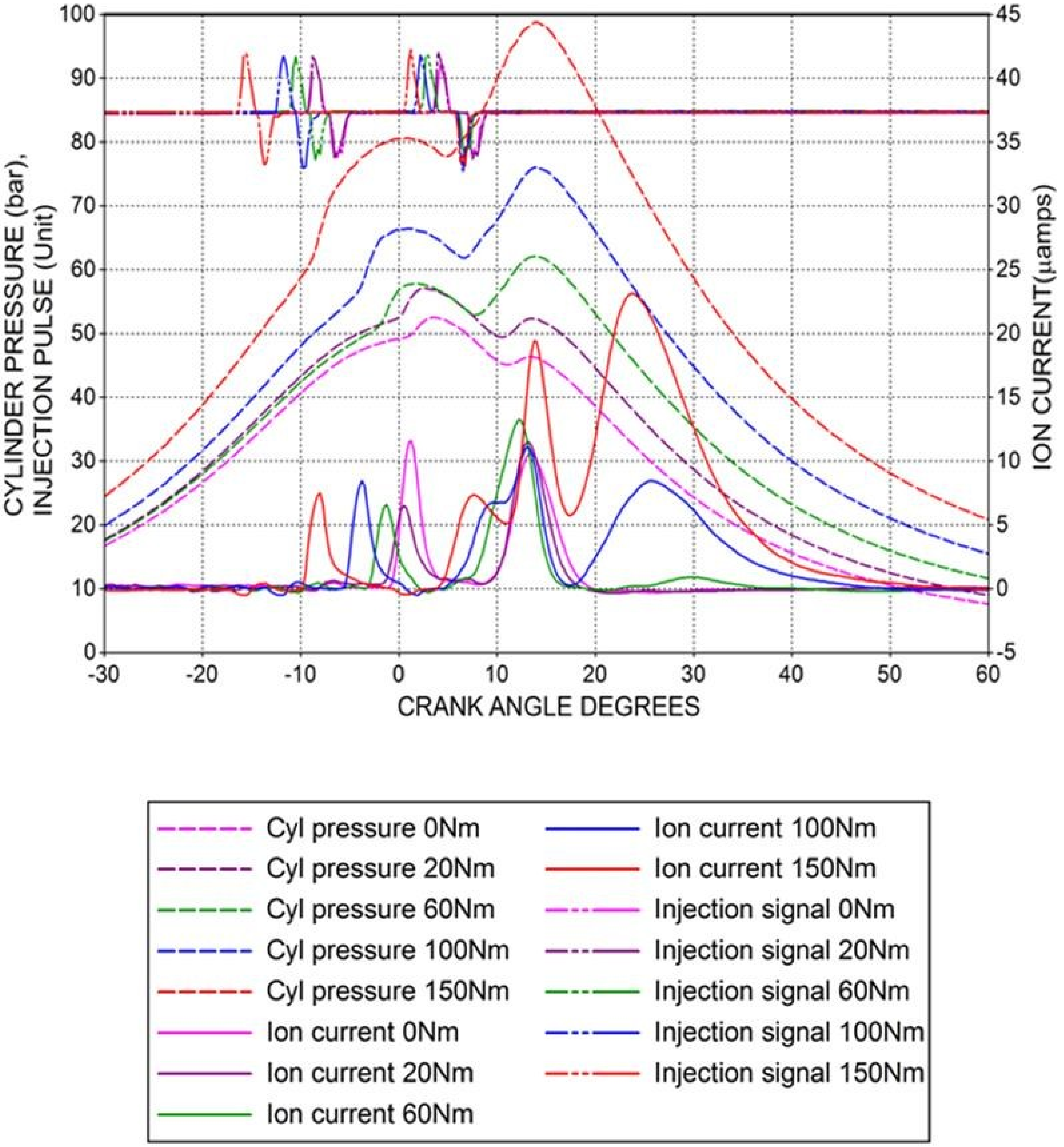

Figure 6-18. In-cylinder pressure and ion current signal for different engine loads at 1800 rpm.

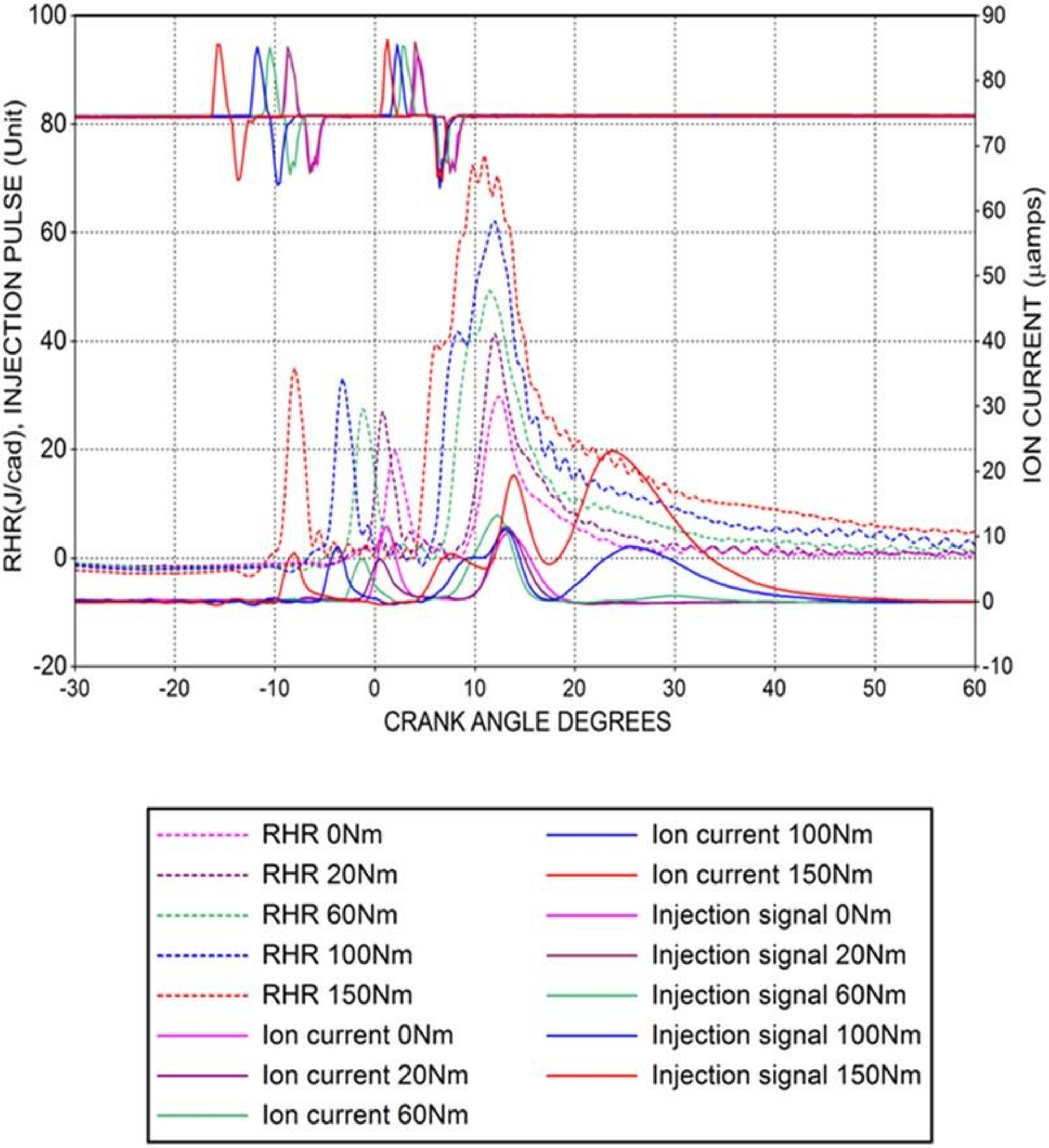

Figure 6-19. RHR and ion current signal for different engine loads at 1800 rpm.

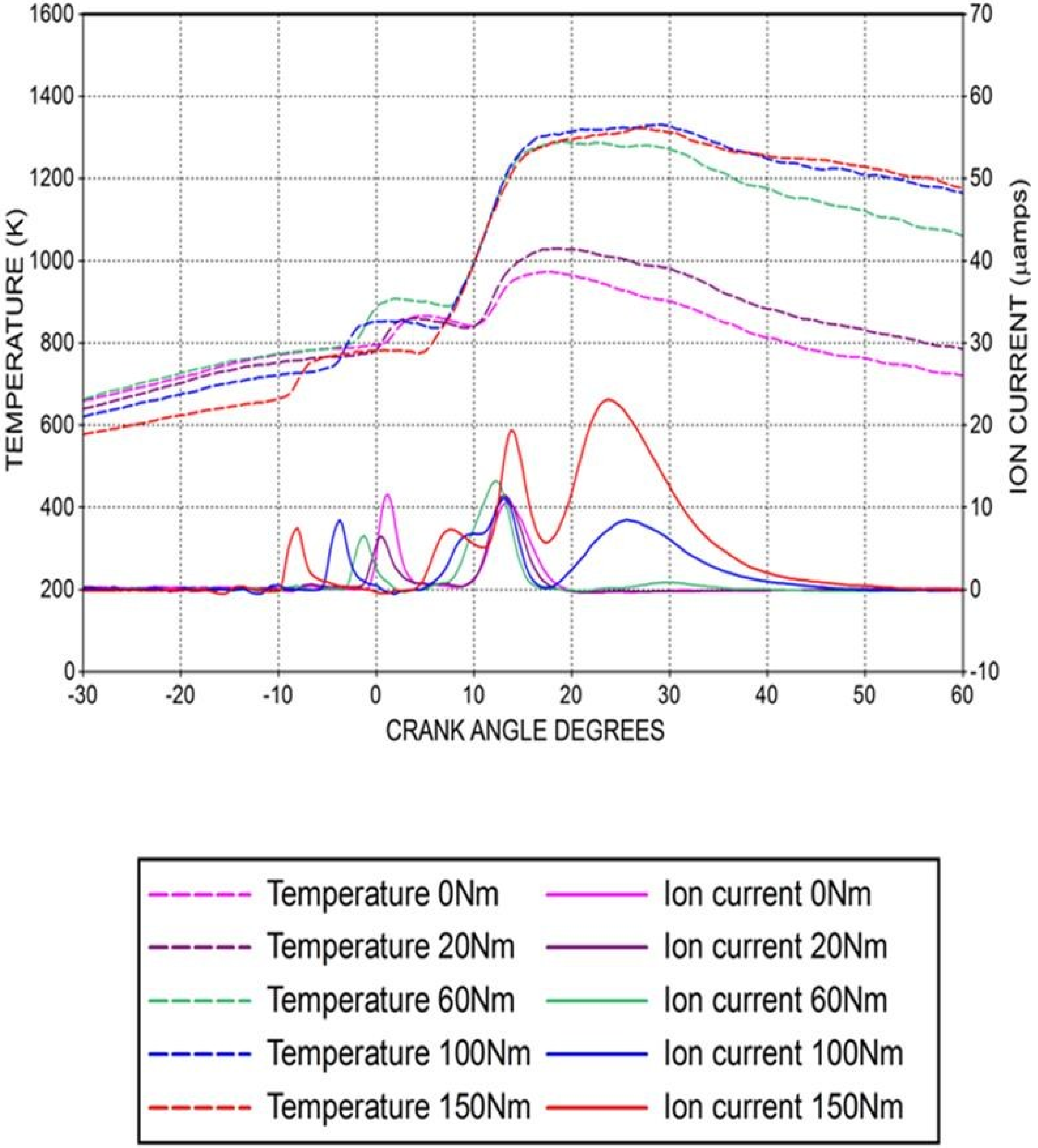

Figure 6-20. In-cylinder temperature and ion current signal for different engine loads at 1800 rpm.

Figure 6-21 shows the pilot and main injection pulse duration at 1800 rpm. The pilot injection pulse duration was 4.25CAD at no load which then decreased to 4CAD at 60Nm and remained the same till 150Nm. The main injection pulse duration increased with the increase in load. The main injection pulse duration increased from 5.25CAD at no load to 7.25 CAD at 150 Nm.

In Figure 6-22 shows the SOP (start of injection pulse), SIC (start of ion current), and SRHR (start of rate of heat release) at different IMEPs. The engine load was varied from 2.31 bar to 12.5 bar IMEP. Similar to the engine operation at 1600 rpm, injection strategy comprised of a pilot and main injection event at all the test points. The ion current signal was observed twice corresponding to the two combustion events. In order to confirm the same, the start of RHR was also analyzed, where two distinctive starts were observed. SOP as well as SIC was found to advance as the load was increased and this trend was observed for both pilot and main injection events. The SIC was found to follow SRHR during pilot and main events. A detailed analysis for various correlations of ion current signals are discussed later in this section. The tests were repeated more than once to confirm the injection strategy followed by the ECU.

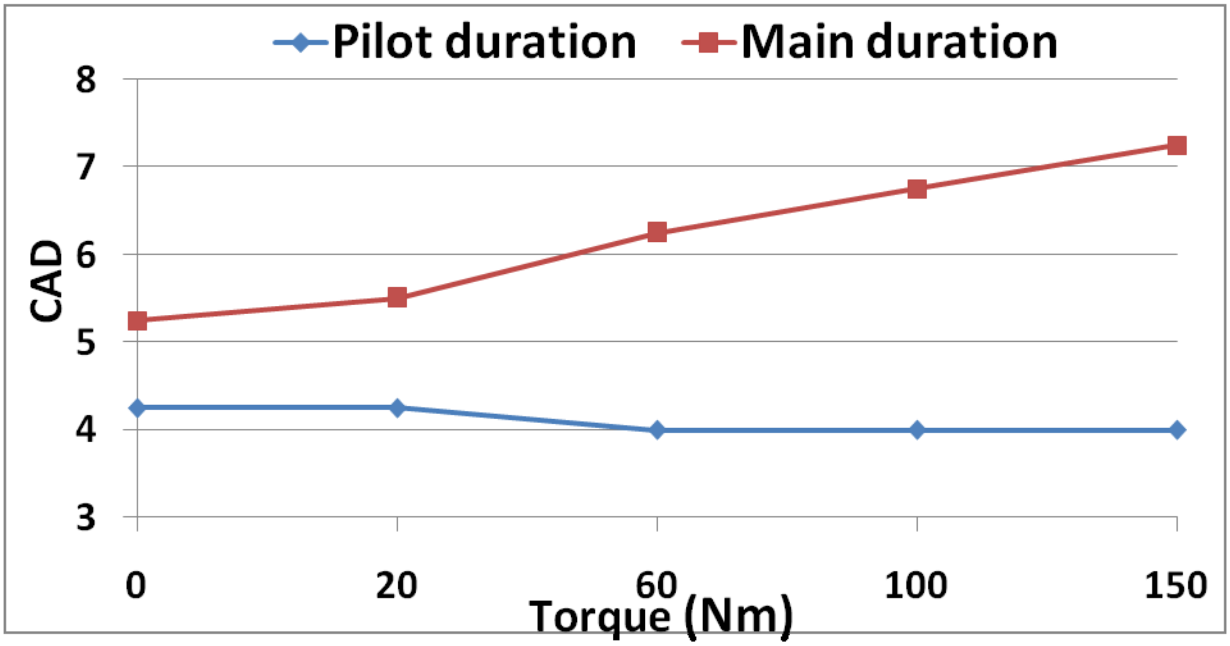

Figure 6-21. Data analysis showing the pilot and main injection duration at 1800 rpm.

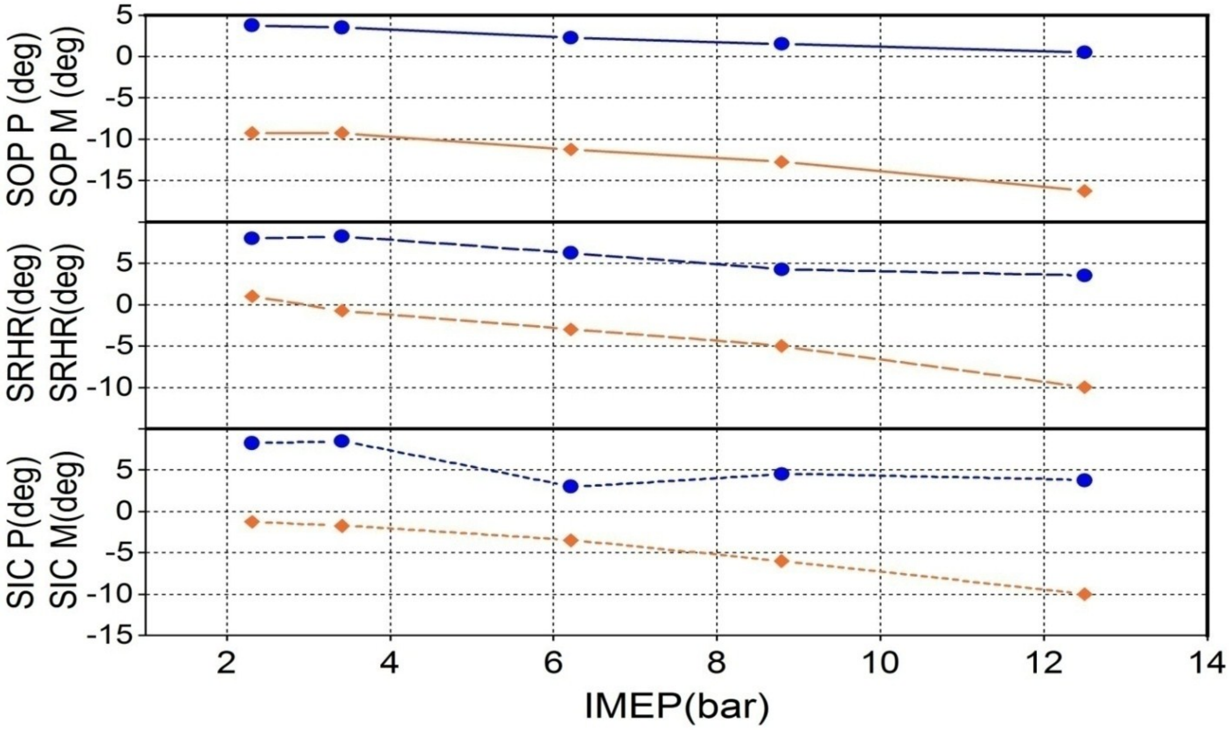

Figure 6-22. Data analysis showing SOP, SRHR, SIC vs. IMEP at 1800 RPM for pilot and main injections.

Various engine operating parameters, engine out emissions, and performance parameters were processed, analyzed and plotted with increase in load as shown in Figure 6-23, 6-24, 6-25.

Figure **6-23** shows the manifold absolute pressure, fuel injection pressure, and equivalence ratio with at different loads. The intake pressure was observed to increase from 1.26 bar at 2.31 bar IMEP to 2.2 bar at 12.5 bar IMEP. The rate of boosting of intake air was found to increase as the load increased, which can be observed in the figure. As the load was increased from 20Nm to 60Nm, the intake air pressure reduced from 1.39 bar to 1.34 bar. The effect of the same was noticeable in the in-cylinder pressure trace. The injection pressure increased with increase in load, starting from 515 bar at an IMEP of 2.31 bar to 895 bar at an IMEP of 6.21 bar. The maximum injection pressure of 1098 bar was recorded at 12.5 bar IMEP. The rate of injection pressure rise was found to slow down once the engine load was 60 Nm, as it can be seen that the rail pressure rose very sharply to 986 bar, after which the rate slowed down and max injection pressure recorded was 1098 bar. Equivalence ratio was calculated from the exhaust lambda value obtained from lambda meter. The equivalence ratio (ϕ) ranged from 0.18 at no load to 0.62 at 12.5 bar IMEP.

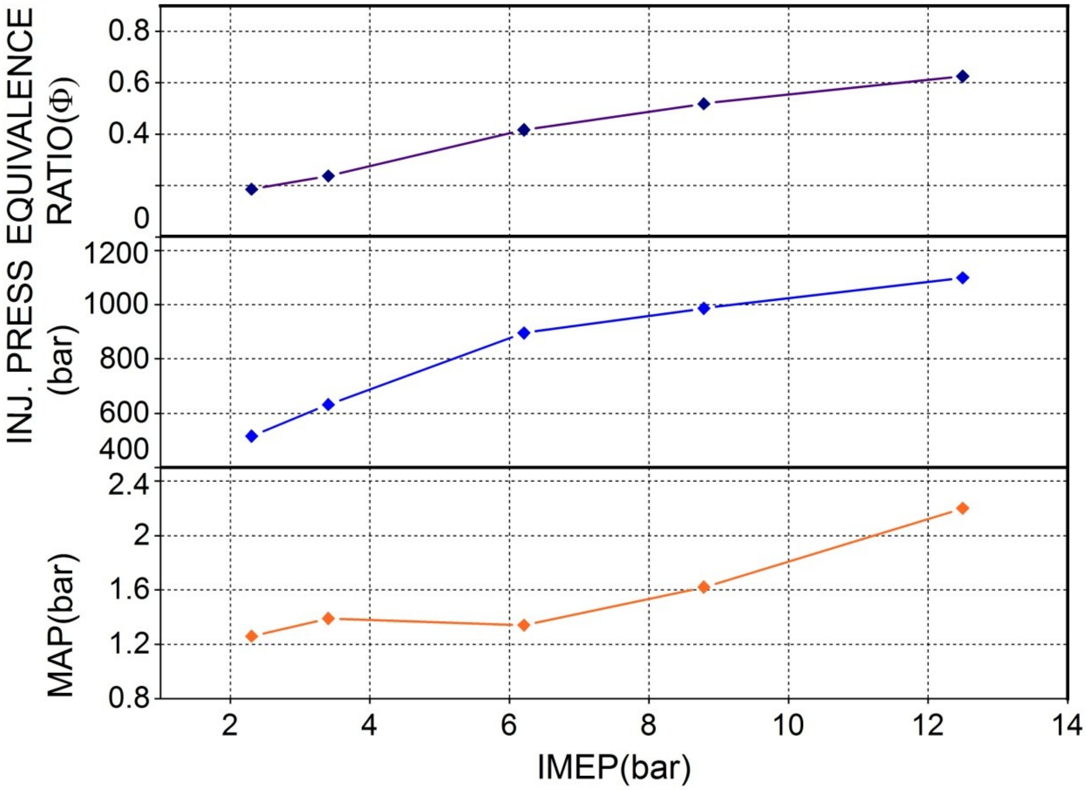

Figure 6-23. Data analysis showing equivalence ratio, injection pressure, MAP vs. IMEP at 1800rpm.

NO emissions and opacity percentage were measured during all the test points. Emissions were plotted against load as shown in Figure 6-24. The NO formation was observed to increase with the load linearly as no EGR applied on the engine. The engine out NO concentration was 206 ppm at no load and it is increased to 906 ppm at the highest load.. At the lowest load, the opacity percentage was 0.21 and it increased to 0.70 at highest load. Even though the opacity increased with respect to the increase in load, it is observed that the rate of rise is very low since the injection pressure is higher at higher loads, providing better atomization and better mixing and leading to comparatively lower rate of increase in soot values.

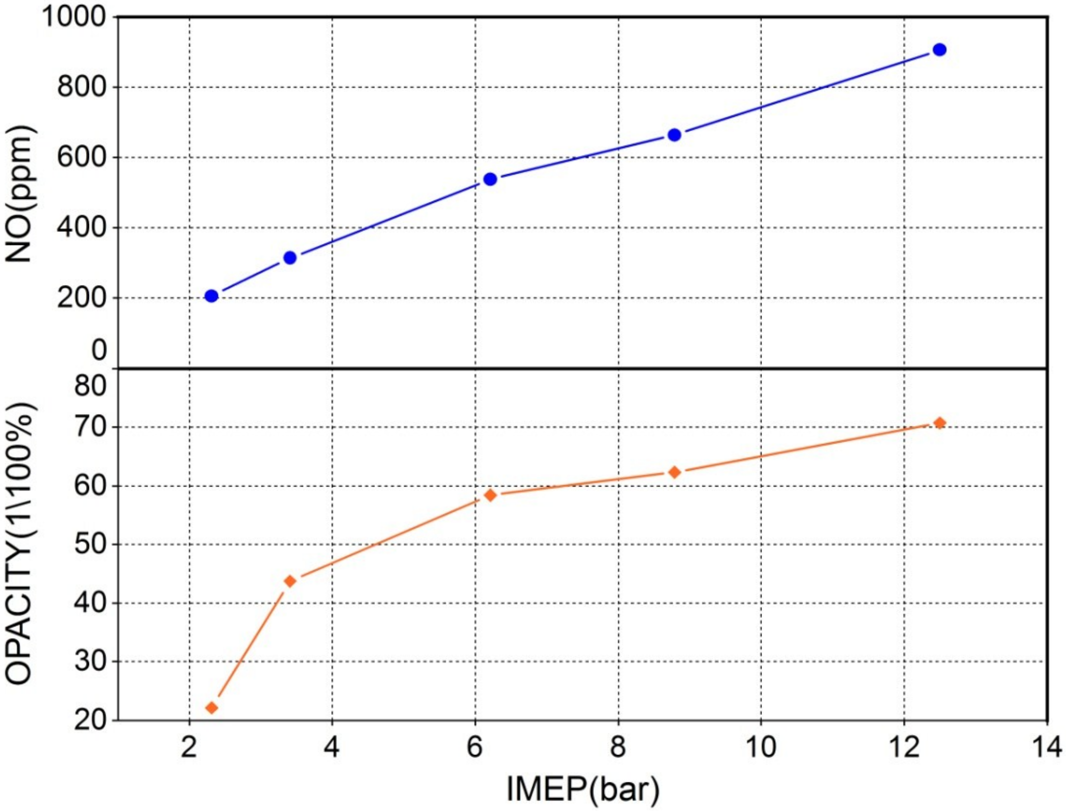

Figure 6-24. Data analysis showing NO and opacity vs. IMEP @ 1800 RPM

The indicated thermal efficiency and ISFC was plotted against engine load at 1800 rpm is as shown in Figure 6-24. Thermal efficiency which followed the reverse trend of ISFC, recorded a highest efficiency of 43.3 % at 6.21 bar IMEP.

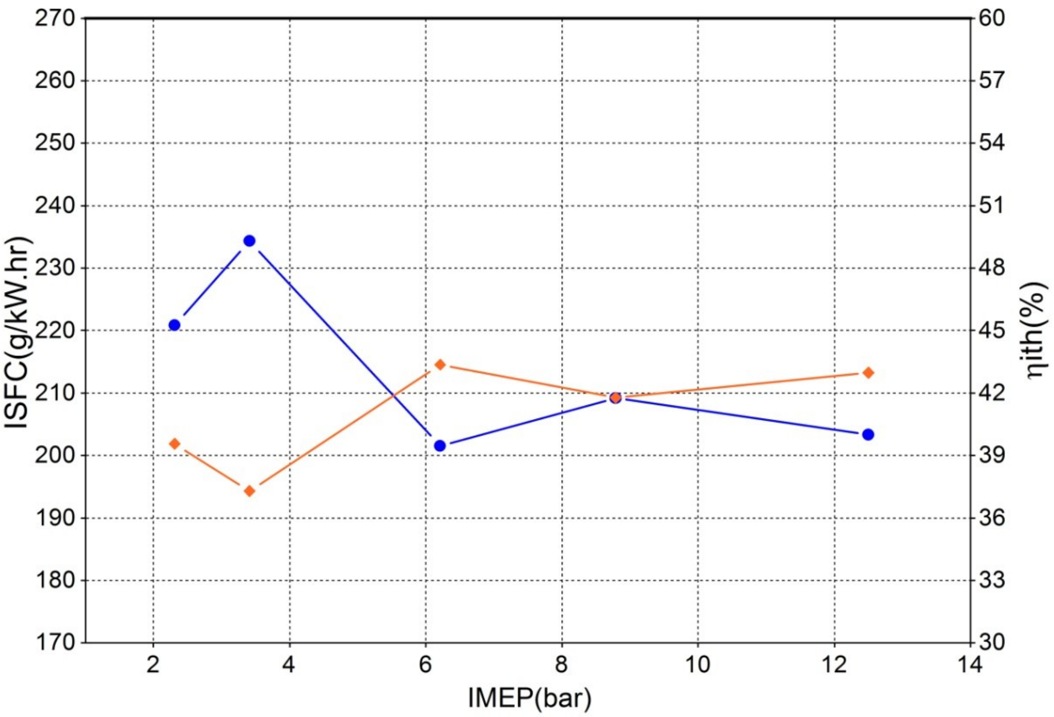

Figure 6-25. ISFC and indicated thermal efficiency vs. IMEP @ 1800 RPM

The following covers the auto ignition analysis for the engine operation at 1800 rpm. Figure 6-26 shows the ignition delay and ion current delay analysis for ULSD 1800 rpm. Ignition delay of pilot combustion is seen to decrease with the increase in engine load. While observing the SOPP, it can be seen that the injection timing advanced in proportion to the increase in load. It can be seen that the ion current delay of pilot (ICDP) followed the IDP.

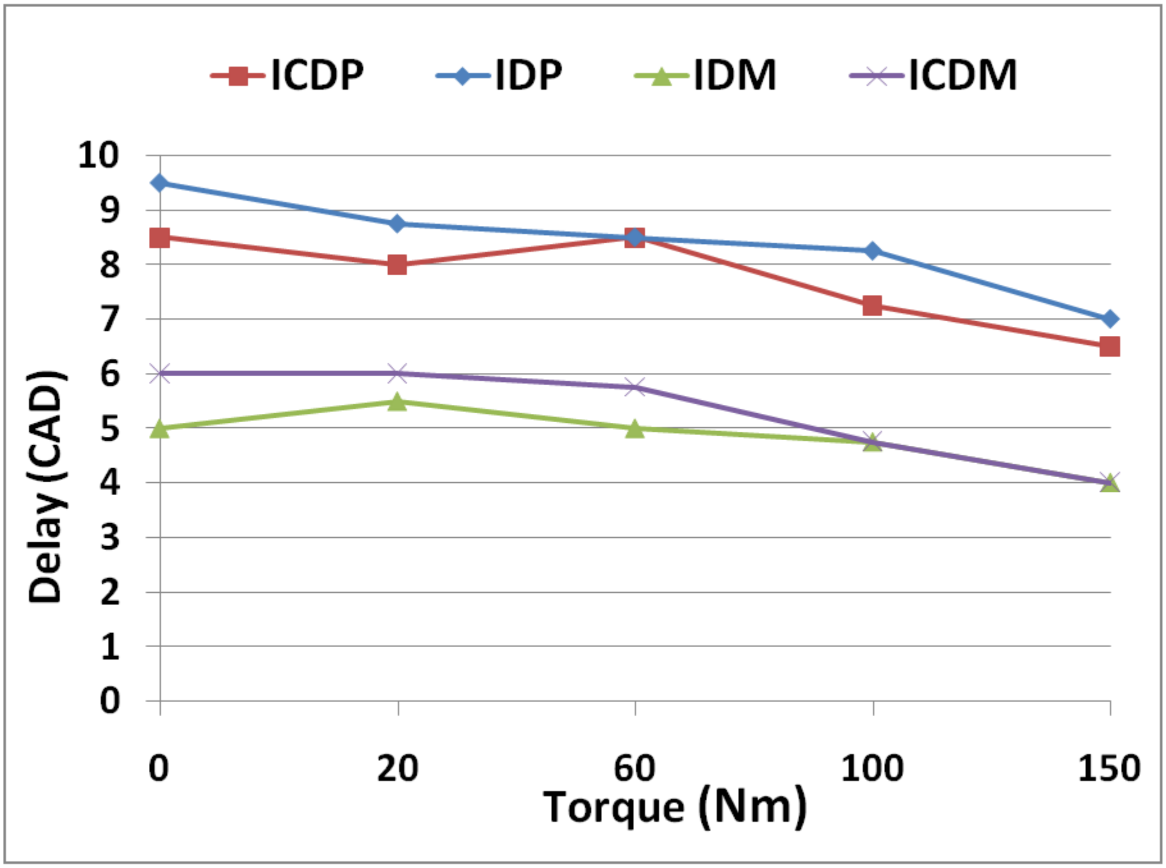

Figure 6-26. Data analysis showing ignition delay and ion current delay for pilot and main injections events at varying loads & 1800 rpm

While analyzing the ignition delay of main combustion (IDM) it can be observed that it decreased with the increase in load. The IDM was found to be lower than the IDP as the in-cylinder temperature and pressure had been increased through the pilot combustion process which helped in the faster auto ignition of the main fuel-air mixture. Although ion current delay of main (ICDM) followed the same trend of IDM, the delay was found to be higher at all load points.

Figure 6-27 and Figure 6-28 shows the correlation between ID P and ICD P as well as ID M and ICD M respectively. It can be observed that the correlation between ion current delay and ignition delay produces a regression coefficient (R^2) of 0.793 for the pilot combustion and 0.838 for the main combustion.

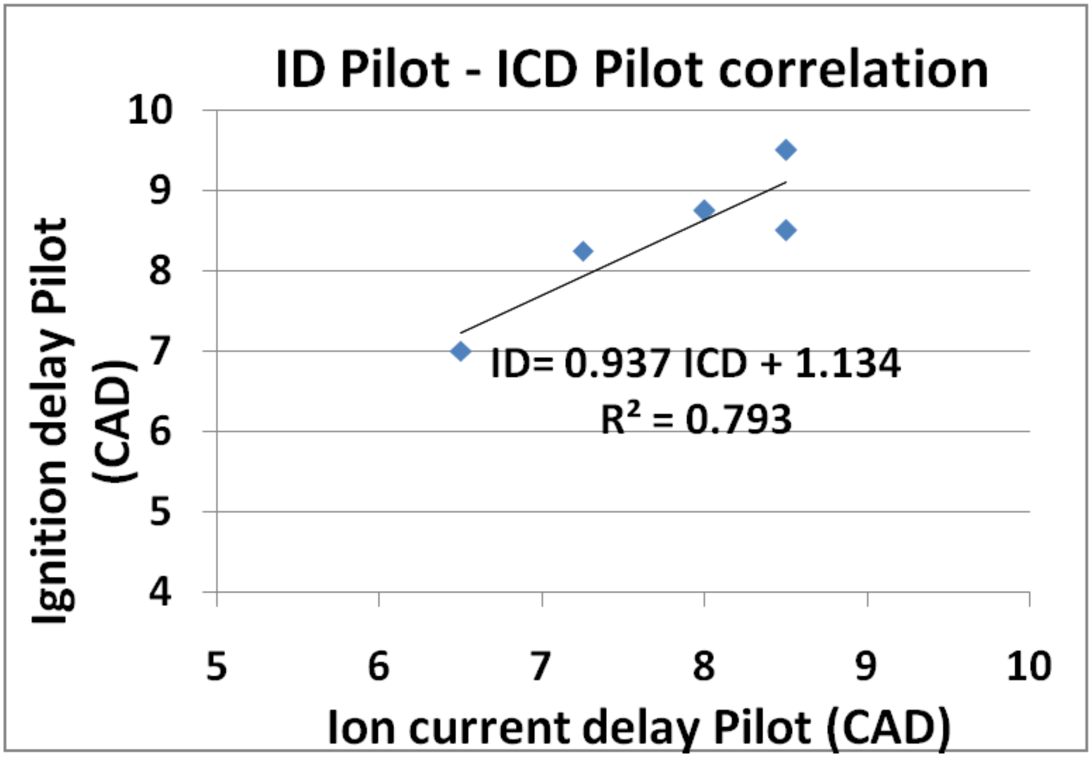

Figure 6-27. Data analysis showing the correlation between ID P and ICD P at 1800rpm.

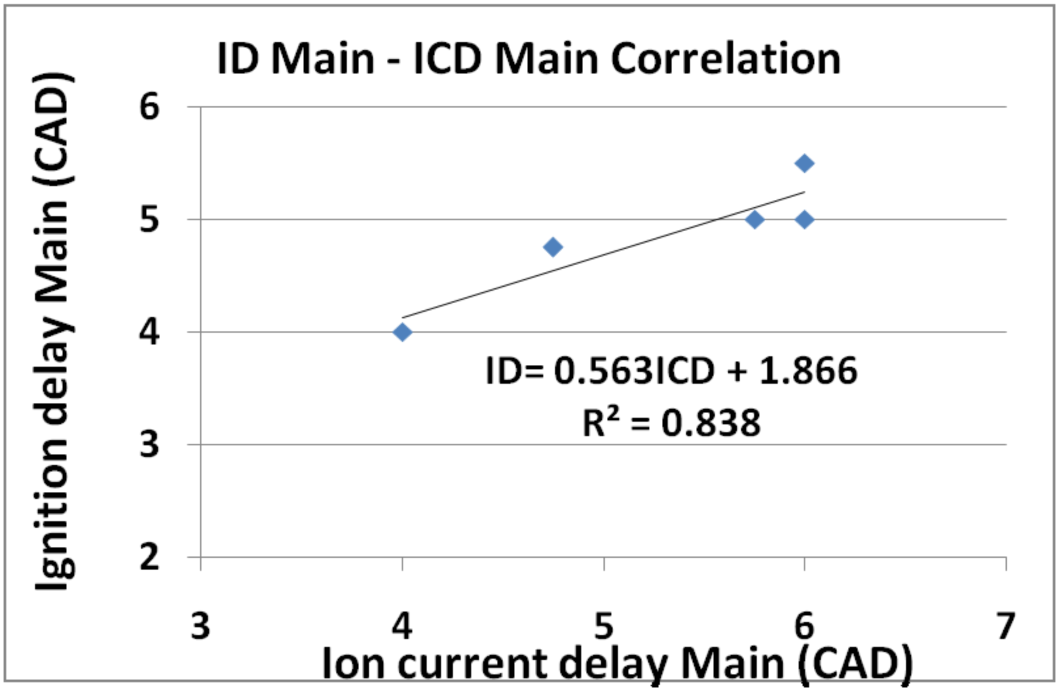

Figure 6-28. Data analysis showing the correlation between ID M and ICD M at 1800rpm

The ion current signal was studied with respect to different combustion parameters that changed under various operating conditions of the engine. The start of ion current (SIC) was plotted against the start of injection pulse of both main and pilot injections as shown in Figure 6-22. The ion current sensor detected two starts associated with both injection events. The signal detected two combustion events as well as correlated with the start of RHR as seen in the same figure.

Various correlations of ion current signal with RHR trace were investigated. The magnitude and location of the different peaks of the ion current signal contains information pertaining to various in cylinder combustion events. The location of different peaks of ion signal were plotted with corresponding peak amplitudes from RHR trace as observed in Figure 6-29. Figure 6-30 shows various peaks of RHR and the location of ion current peaks at 1800 rpm. The location of peak of ion current - pilot (LPICp) closely followed location of peak premixed combustion due - pilot (LPPCp). Also, the location of the peaks of ion current due main combustion (LPIC 1, LPIC 2) followed the location of peak amplitude of RHR. The LPIC 1 and LPIC 2 corresponded to the LPPC M and LPDC M respectively.

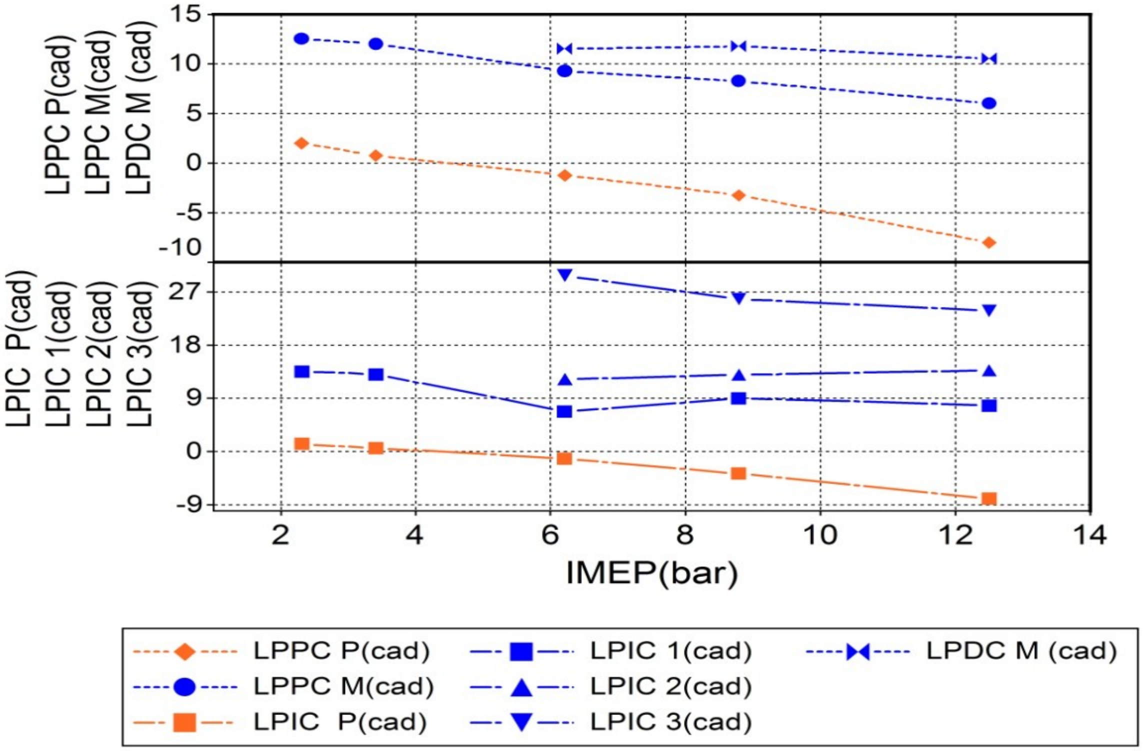

Figure 6-29. Data analysis showing peak locations of RHR trace and ion current signal for different engine loads at 1800 RPM.

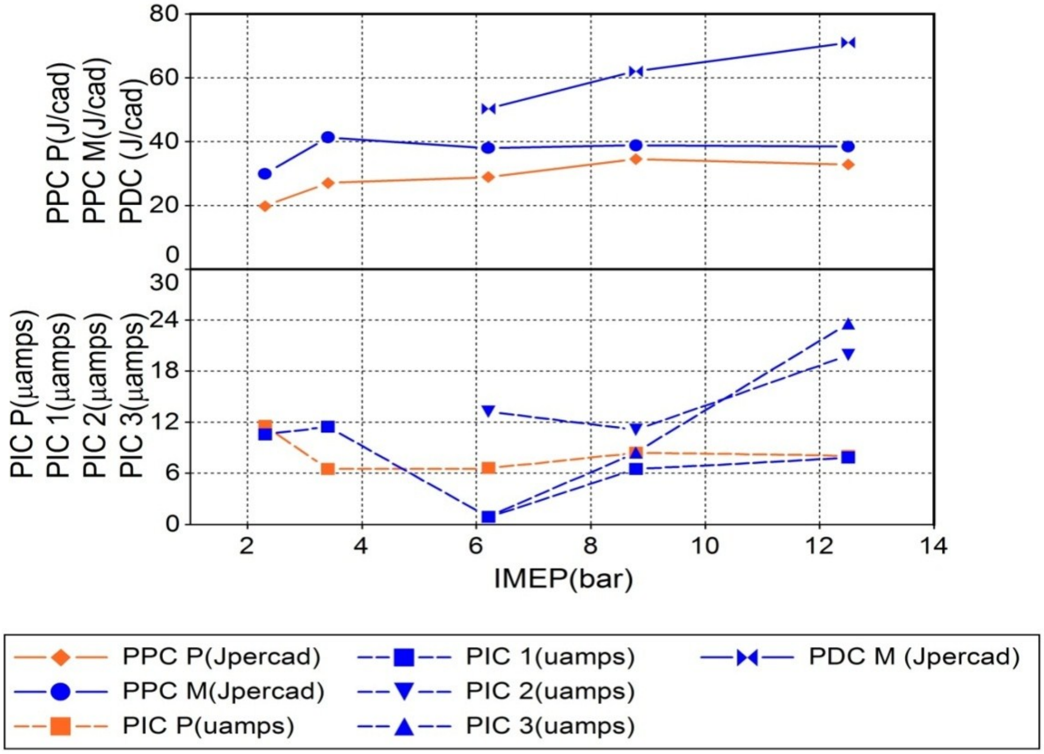

Figure 6-30. Data analysis showing peaks amplitude of RHR and ion current signal at 1800rpm

The following covers correlations made between the start of ion current signal and the first peak of ion current signal with the location of peak premixed combustion. The Figure 6-31 shows the correlation between SICp and LPPCp for different engine loads at a constant speed of 1800 rpm. LPPC P was observed to have an offset of 2.285° CAD and the regression coefficient R^2 was 0.991. Figure 6-32 shows the correlation between LPICp and LPPCp for different engine loads at 1800 rpm. The LPPCp was observed to have an offset of 0.402° CAD and a higher regression coefficient of 0.995 in comparison to the former one. A similar observation was made during the engine operation at 1600 rpm.

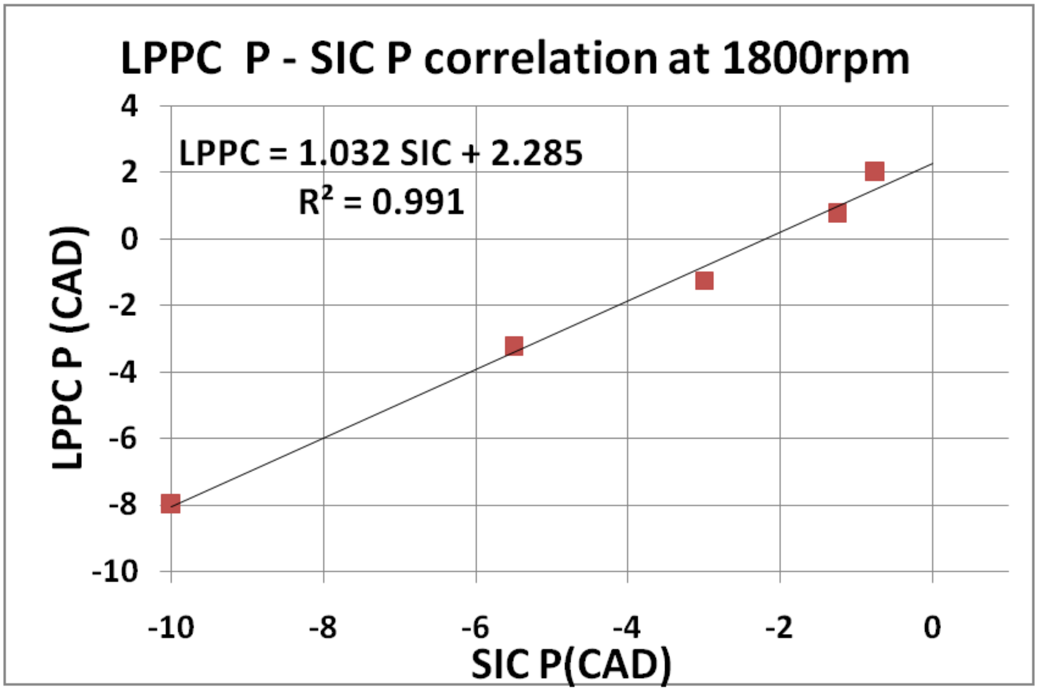

Figure 6-31. Data analysis showing correlations of LPPC P with SIC P at 1800 RPM

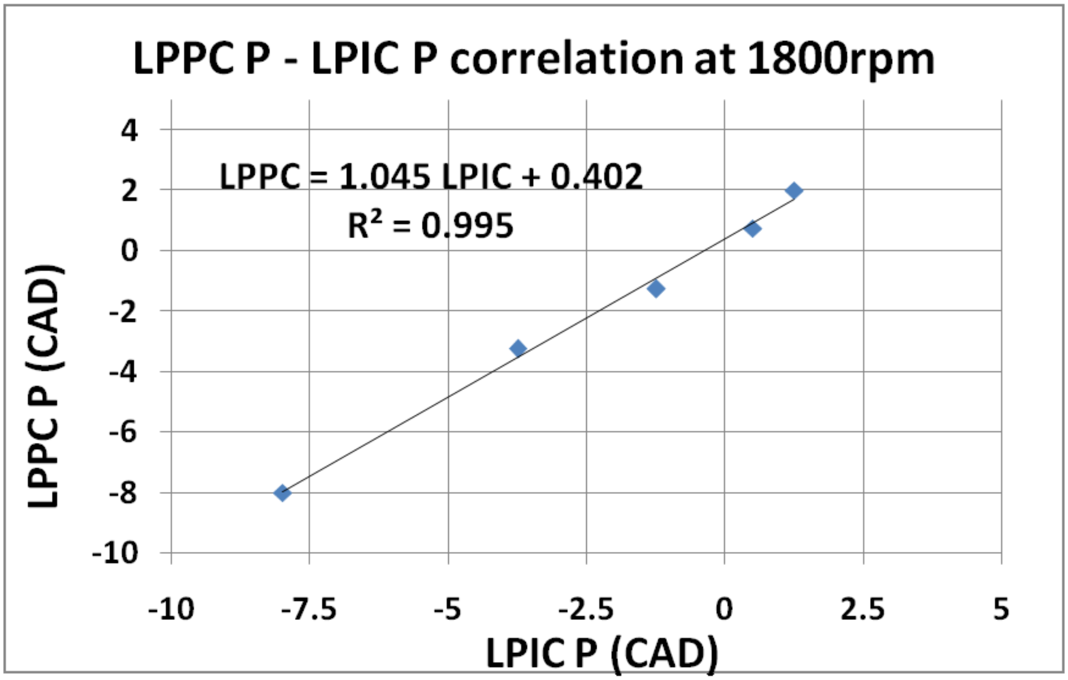

Figure 6-32. Data analysis showing correlations of LPPC P with LPIC P at 1800 RPM

Figure 6-33 shows the correlation between LPPCm and SICm for different engine loads at a constant speed of 1800 rpm. LPPCm was observed to have an offset of 2.13 CAD and the regression coefficient, R^2 was 0.992. Figure 6-17 shows the correlation of LPPCm with LPIC1 for different engine loads at a constant speed of 1800 rpm. The LPPCm was observed to have an offset of 2.2 CAD and a lower regression coefficient of 0.708 in comparison to the correlation with SICm. It is worth noting that during the engine operation at 1600 rpm, LPPC was more correlated to LPIC than SIC.

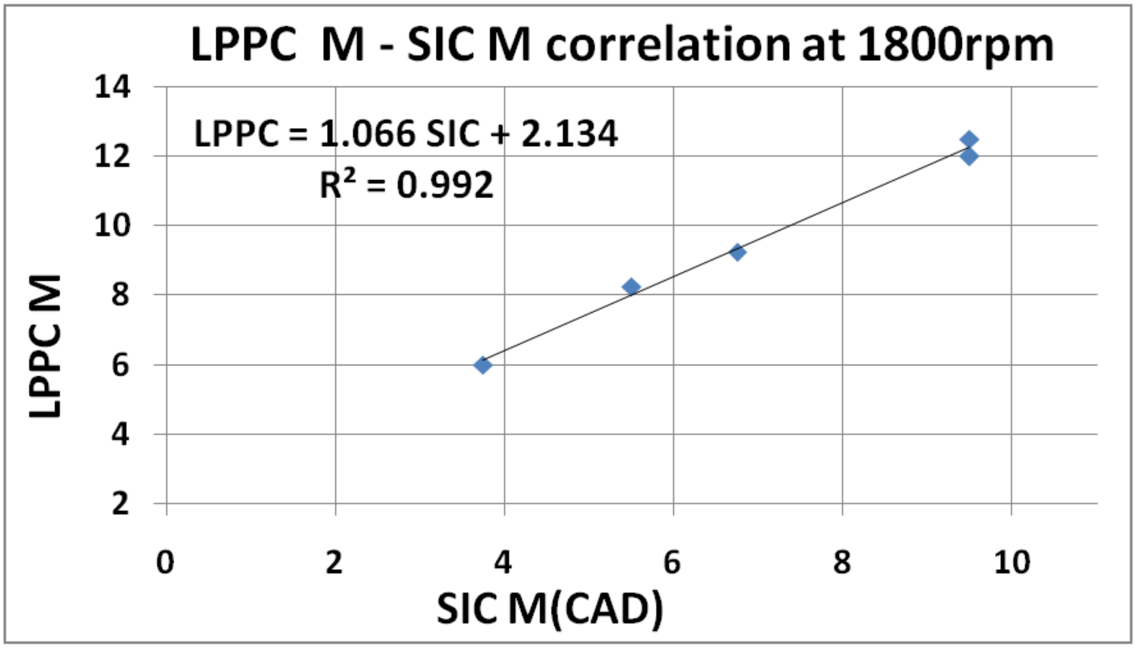

Figure 6-33. Data analysis showing correlations of LPPC M with SIC M at 1800 RPM

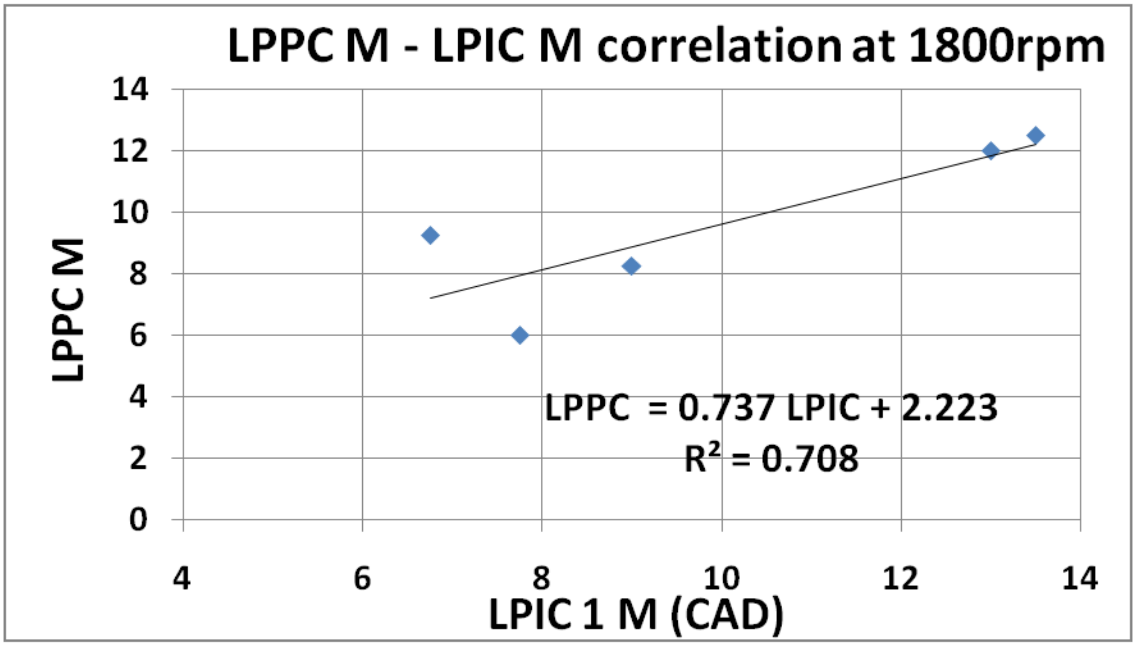

Figure 6-34. Data analysis showing correlations of LPPC M with LPIC 1 M at 1800 RPM

6.5 *Engine operation at 2000 rpm*

The following section covers the analysis during the engine operation at 2000 rpm. Figure 6-35, 6-36, 6-37, shows in-cylinder pressure, rate of heat release, ion current signal and in-cylinder temperature for varying engine load from no load to 150Nm at 2000rpm. The engine operation at 2000rpm also shows two injection events - pilot injection which occurred early before TDC with a short duration and the main injection with longer duration which occurred after TDC. Similar to the engine operation at 1600rpm and 1800rpm, as the engine load was increased from no load to 150Nm, it was observed that the start of injection of pilot and main were advanced.

Figure 6-35 shows in-cylinder pressure and ion current signal for varying engine load at 2000 rpm. Similar to the engine operation at 1600 rpm and 1800 rpm, the in-cylinder pressure produced two peak pressures corresponding to combustion produced from the two injection events. The peak pressure produced due to the pilot combustion event occurred close to TDC whereas peak pressure produced due to main combustion occurred later in the expansion stroke.

Figure 6-36 shows rate of heat release trace and ion current signal for varying engine load at 2000 rpm. The pilot injection event produced a single peak amplitude at LPPCp whereas the main injection event produced both premixed and diffusion/mixing controlled combustion. Hence two peak amplitude were observed during the main injection event, similar to the engine operation at lower speeds as discussed in the previous sections.

Figure 6-37 shows the in-cylinder temperature and ion current signal during different engine loads at 2000 rpm. Similar to the engine operation at lower speeds, ion current signal is characterized by two to four peaks depending on the applied load. At all load points, the pilot combustion produces a single peak (LPICp) in ion current whereas the main injection event may produce one, two or three peaks depending on the engine load. The peak in-cylinder temperatures produced during the main injection event was considerably higher compared to the combustion produced from pilot fuel injection.

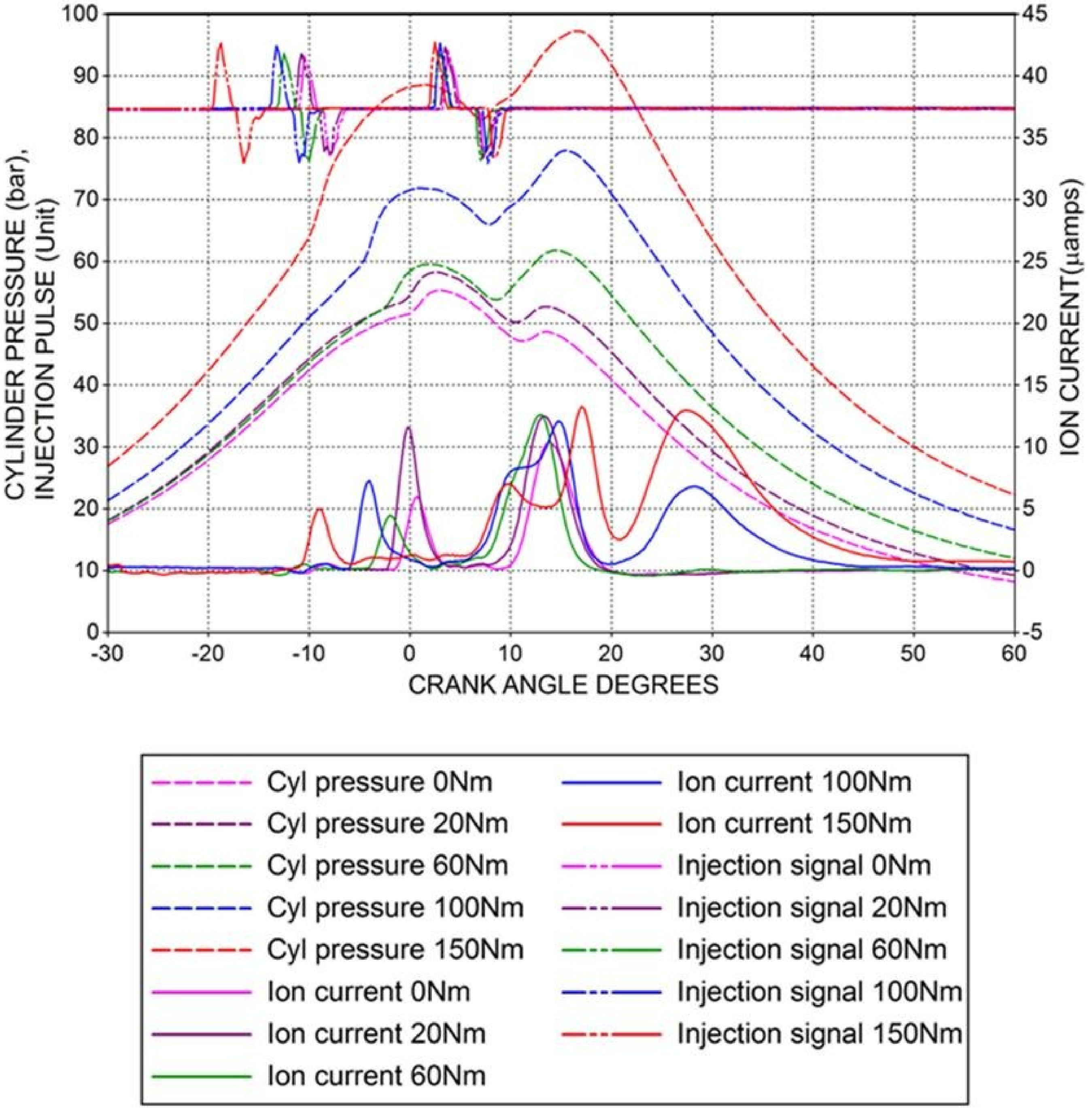

Figure 6-35. In-cylinder pressure and ion current signal for different engine loads at 2000 rpm.

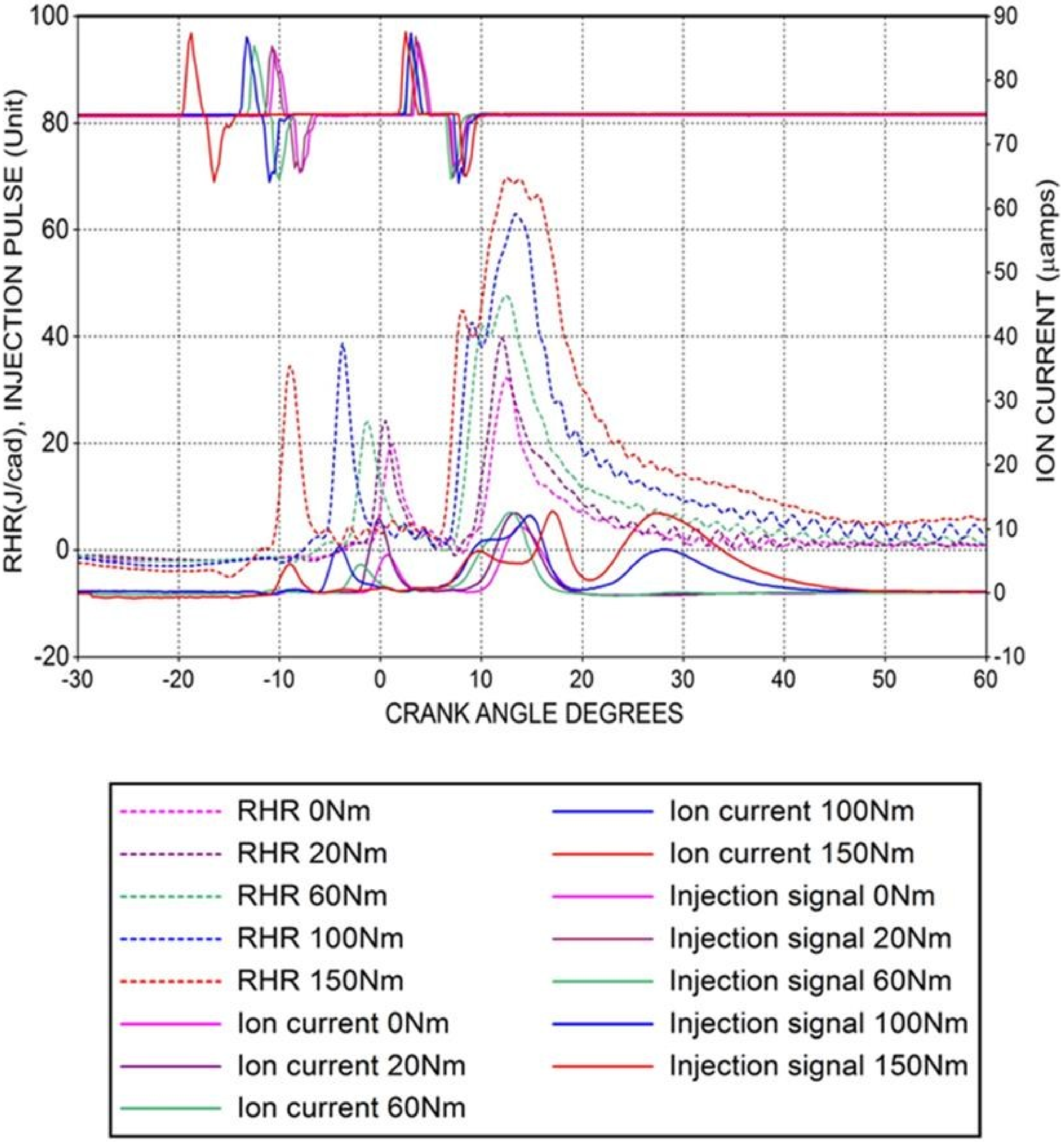

Figure 6-36. RHR and ion current signal for different engine loads at 2000 rpm.

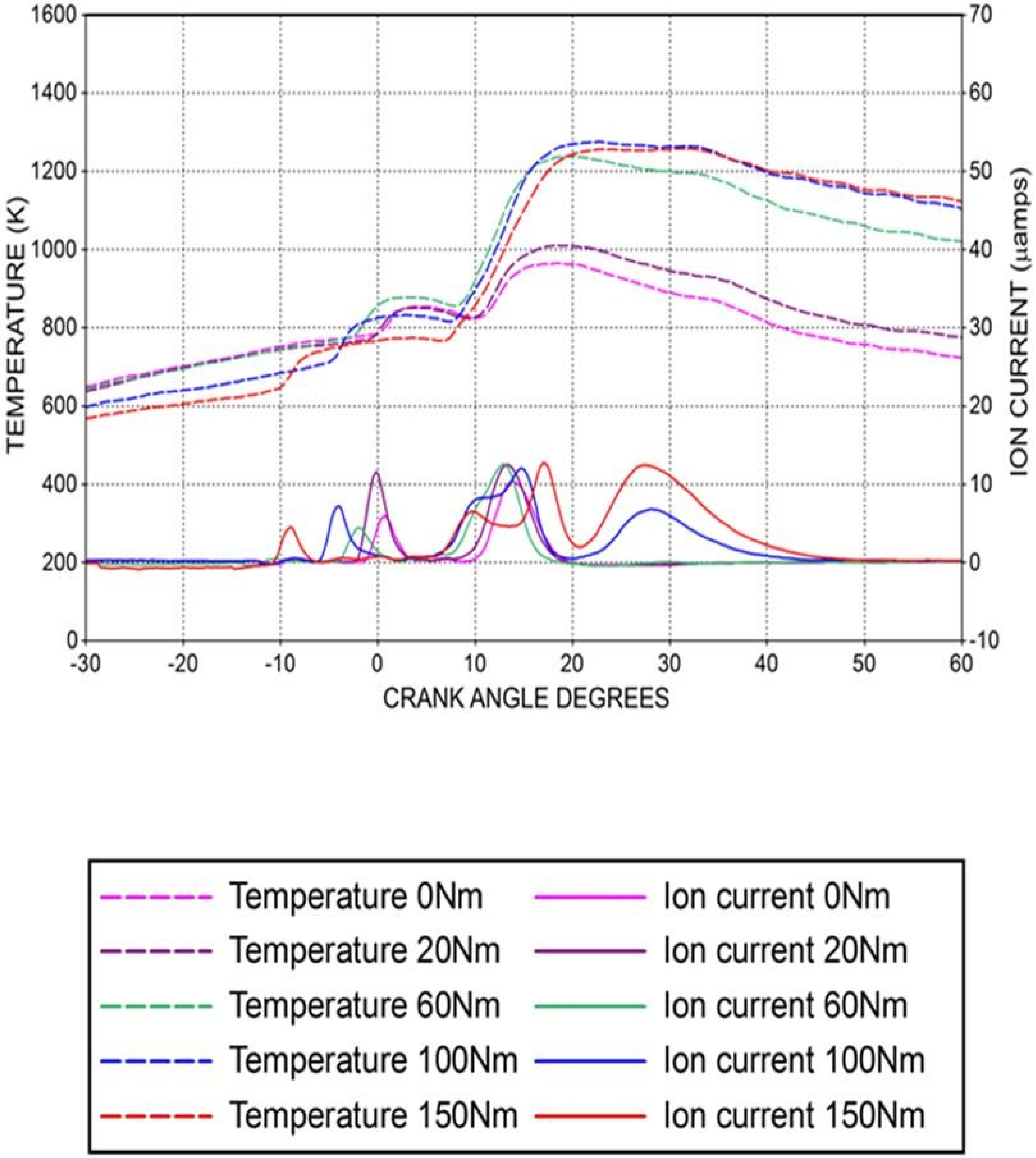

Figure 6-37. In-cylinder temperature and ion current signal for different engine loads at 2000 rpm.

Figure 6-38 shows the pilot and main injection pulse duration at 2000 rpm. The pilot injection pulse duration was 4.75CAD at no load which then increased to 5CAD at 60Nm and further increased to a longer duration of 5.5 CAD at 150Nm. The main injection pulse duration was observed to increase with the increase in load. The main injection pulse duration increased from 5.75 CAD at no load to 8.25 CAD at 150 Nm.

In Figure 6-22 shows the SOP (start of injection pulse), SIC (start of ion current), and SRHR (start of rate of heat release) at different IMEPs.. The engine load was varied from 2.64 bar to 13.3 bar IMEP. Similar to the engine operation at lower speeds, where a pilot injection was followed by a main injection event in all the test points. The ion current signal captured two distinctive combustion events which was also confirmed by the RHR trace. The test was repeated more than once to confirm the injection strategy followed by the ECU. The SIC was found to advance along with the SOP as the load was increased and this trend was followed for both pilot and main injection events.

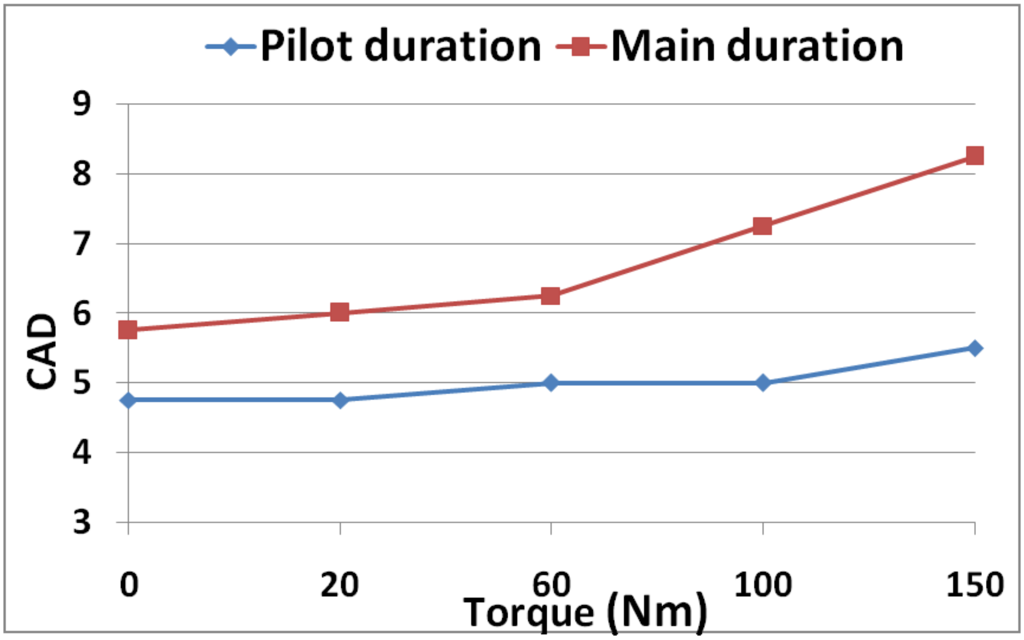

Figure 6-38. Data analysis showing the pilot and main injection duration at 2000rpm

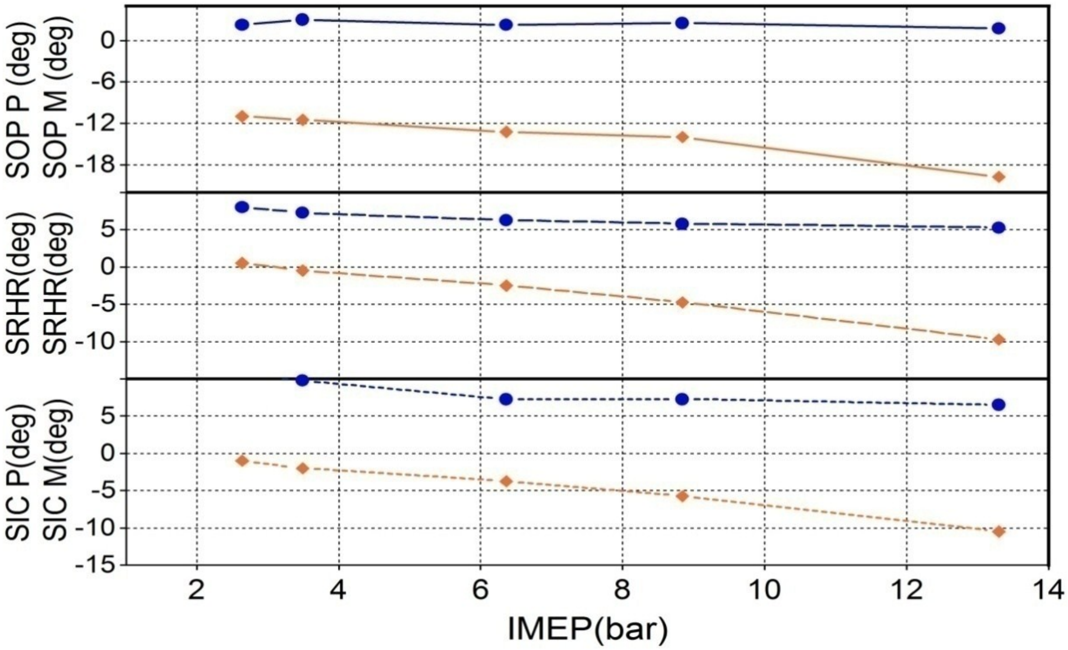

Figure 6-39. Data analysis showing SOP, SRHR, SIC vs. IMEP @ 2000 RPM for pilot and main injections

Various engine operating parameters, engine out emissions, and performance parameters were processed, analyzed and plotted with increase in load as shown in Figure 6-40, 6-41, 6-42.

Figure 6-40 shows the manifold absolute pressure, fuel injection pressure, and equivalence ratio with respect to the change in IMEP. The boost pressure increased with increase in engine load and attained very high values to provide better volumetric efficiency. The intake pressure was observed to increase from 1.34 bar at 2.64 bar IMEP to 2.45 bar at 13.3 bar IMEP. Similar to engine operation at 1800 rpm, the intake air pressure reduced from 1.42 bar to 1.38 bar as the load was increased from 20 Nm to 60 Nm. The injection pressure increased with increase in load, starting from 590 bar at an IMEP of 2.64 bar to 910 bar at 6.3 bar IMEP. The maximum injection pressure of 1219 bar was recorded at 13.3 bar IMEP. The equivalence ratio (ϕ) was calculated and plotted at different IMEPs. It ranged from 0.2 at no load to 0.53 at 13.3 bar IMEP.

In order to analyze the engine performance, indicated thermal efficiency and ISFC were calculated and plotted at different IMEP as shown in Figure 6-41. While the engine was operated at 2000rpm, it produced highest thermal efficiency of 39% during 6.3 and 13.3 bar IMEP. It produced the specific highest fuel consumption while the engine was operating at no load point.

Engine out emissions namely, NOx and opacity percentage were measured during all the test points. Emissions were plotted at different IMEPs as shown in Figure 6-42. Similar to the engine operation at 1600 and 1800rpm NOx emissions increased as the load was increased. The engine out NO concentration was 206 ppm at no load and it is increased to 710 ppm at the highest load. The opacity percentage was observed to be considerably low at all the test points since the OEM ECU was calibrated to produce very low soot due to strict emission regulations. At the lowest load, the opacity percentage was 0.34 and it increased to 0.65 at highest load.

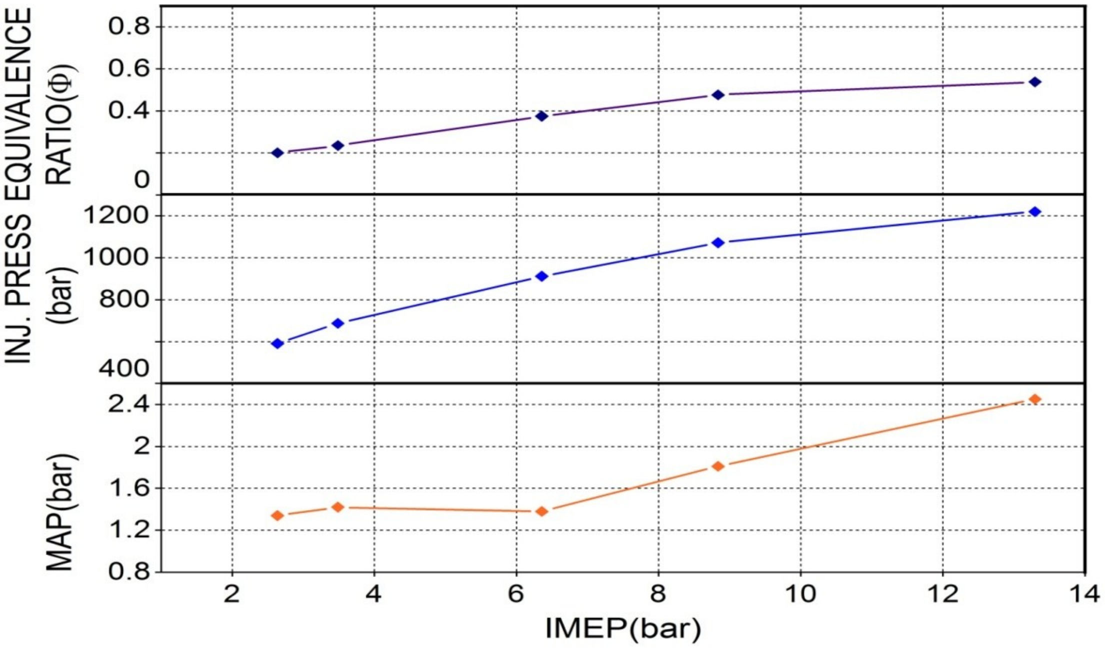

Figure 6-40. Data analysis showing equivalence ratio, injection pressure, MAP vs. IMEP @ 2000 RPM

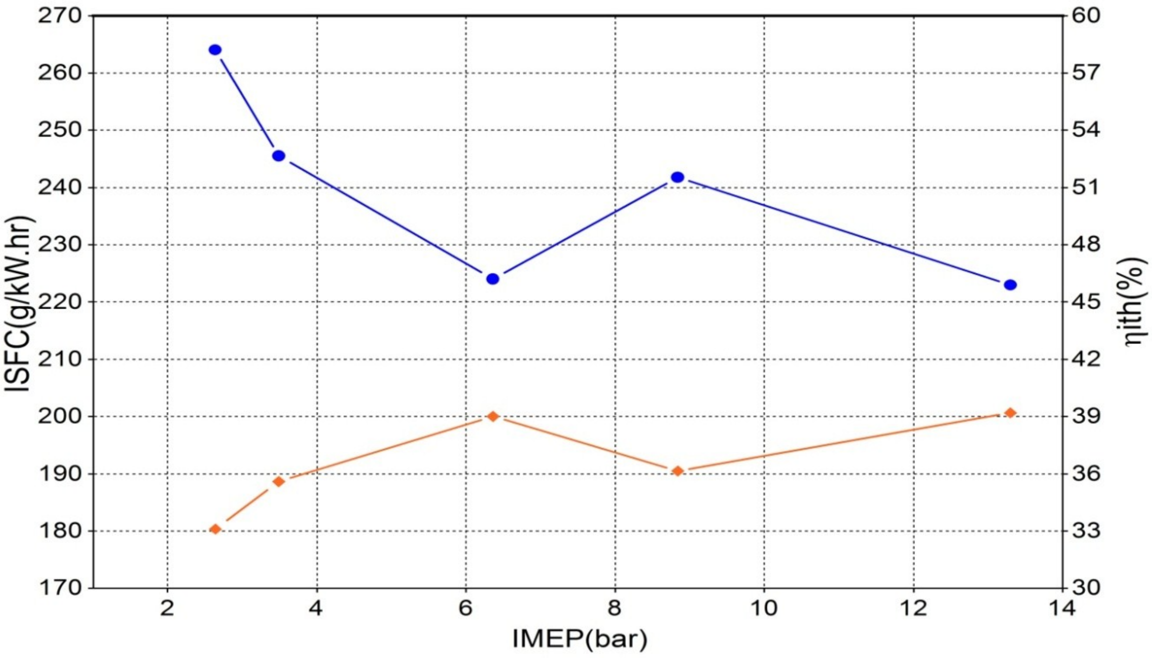

Figure 6-41. ISFC and indicated thermal efficiency vs. IMEP @ 2000 RPM

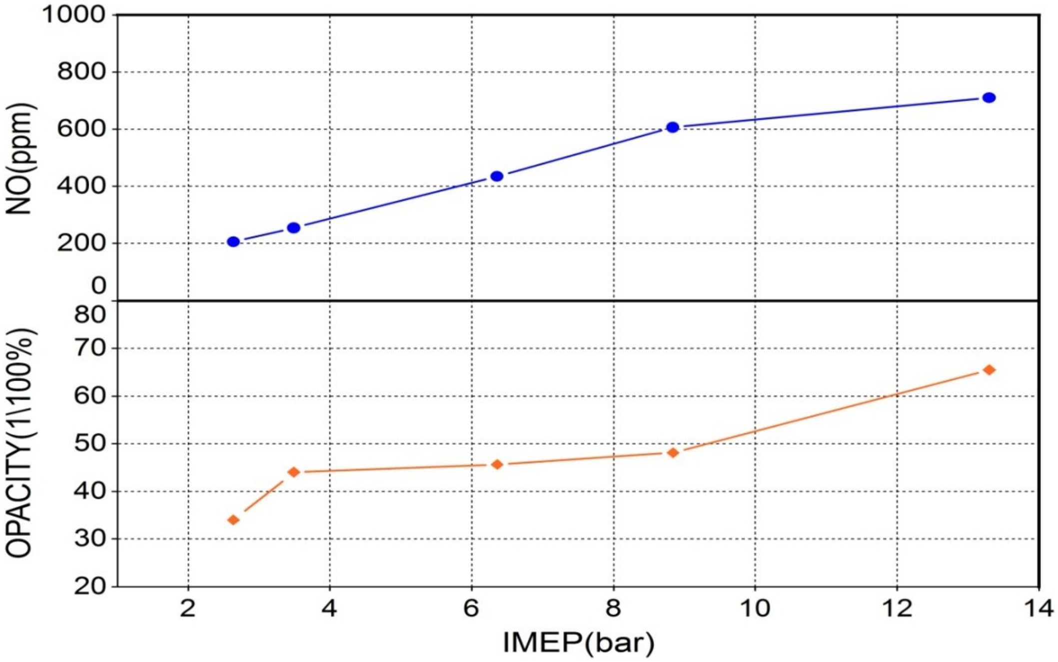

Figure 6-42. Data analysis showing NO and opacity vs. IMEP @ 2000 rpm

The following covers the auto ignition analysis for the engine operation at 2000 rpm. Figure 6-43 shows the comparison of the ignition delay and ion current delay for the pilot and main injection events for increasing engine load at 2000 rpm. Ignition delay of pilot combustion was seen to decrease with the increase in engine load. It can be seen that the ion current delay of pilot (ICDP) closely followed the IDP. While analyzing the ignition delay of main combustion (IDM) it also showed a decreasing trend as the load was increased. The IDM was found to be lower than the IDP as the in-cylinder temperature and pressure had been increased through the pilot combustion process which helped in the faster auto ignition of the main fuel-air mixture. The delay calculated from the ion current signal closely matched the ignition delay.

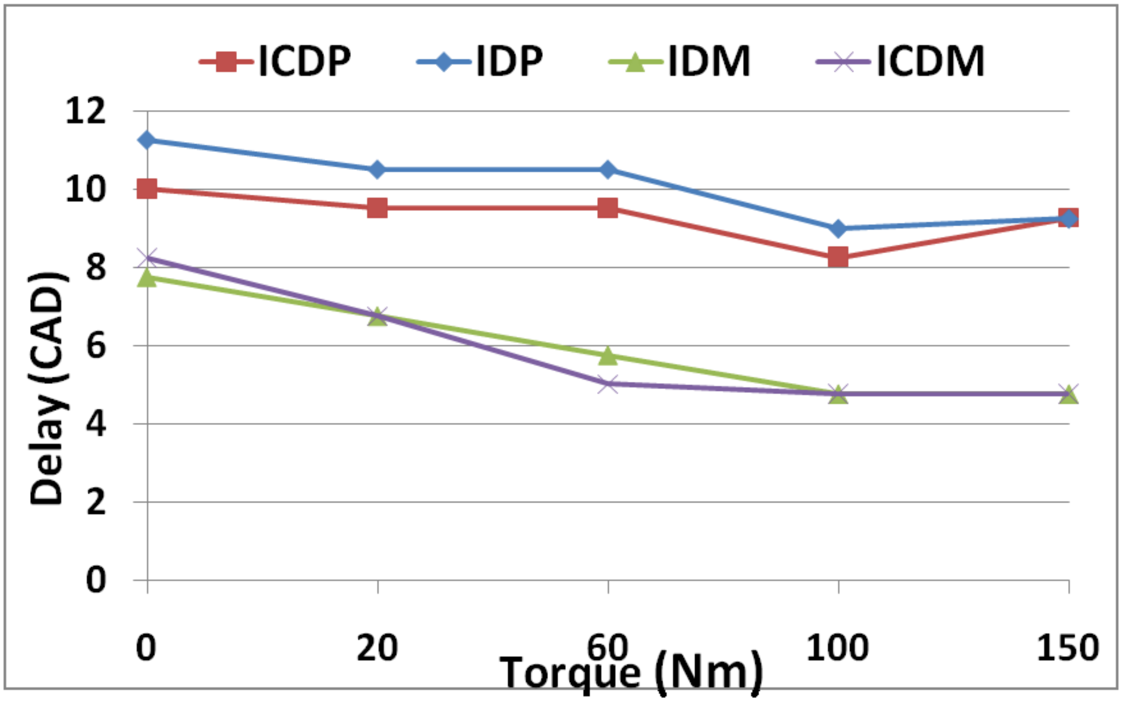

Figure 6-43. Data analysis showing ignition delay and ion current delay for pilot and main injections events at varying loads and 2000 rpm

Figure 6-44 and Figure 6-45 shows the correlation of ID P with ICD P and ID M with ICD M respectively. It can be observed that the correlation between ion current delay and ignition delay produced a regression coefficient (R^2) of 0.793 for the pilot combustion and 0.934 for the main combustion.

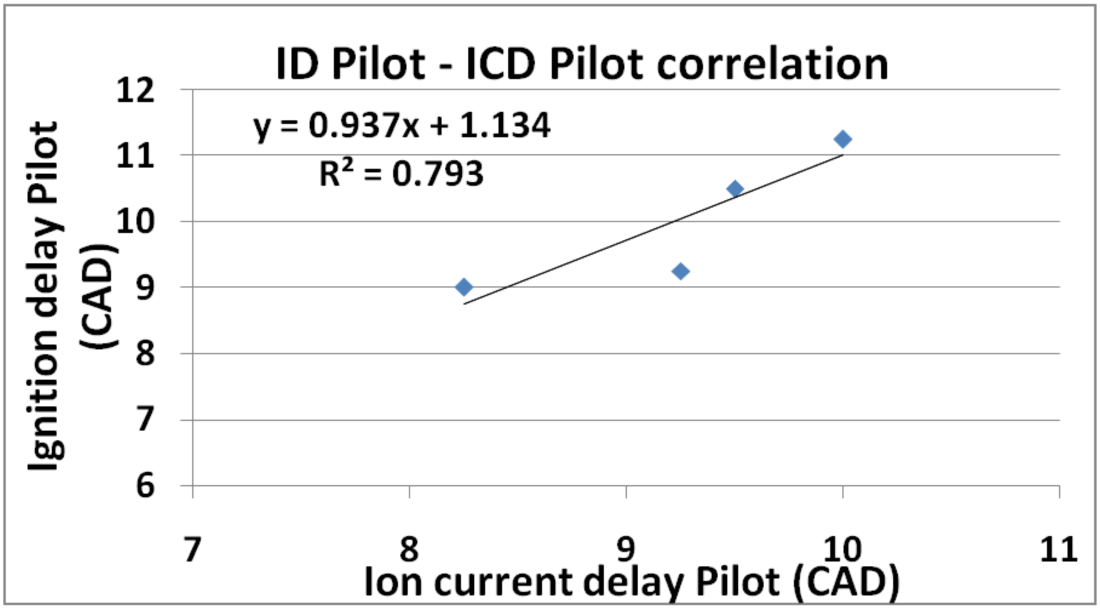

Figure 6-44. Data analysis showing the correlation between ID P and ICD P at 2000rpm.

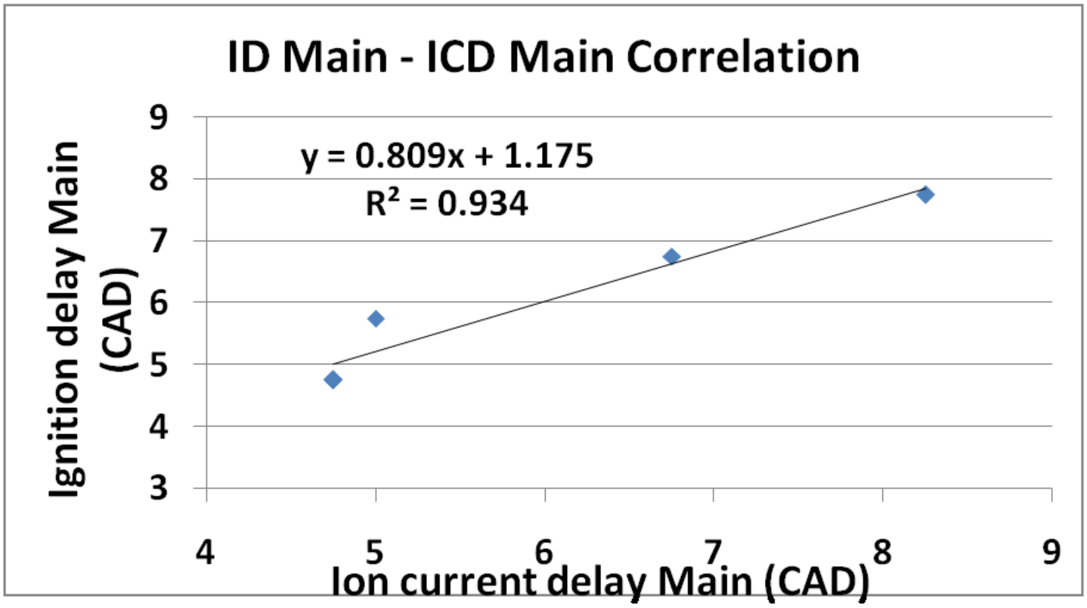

Figure 6-45. Data analysis showing the correlation between ID M and ICD M at 2000rpm

The ion current signal was studied with respect to different combustion parameters that changed under various operating conditions of the engine. The start of ion current (SIC) was plotted against the start of injection pulse of both main and pilot injections as shown in Figure 6-39. As discussed before and similar to the engine operation at 1600 and 1800 rpm, ion current sensor could detect two separate combustion processes.

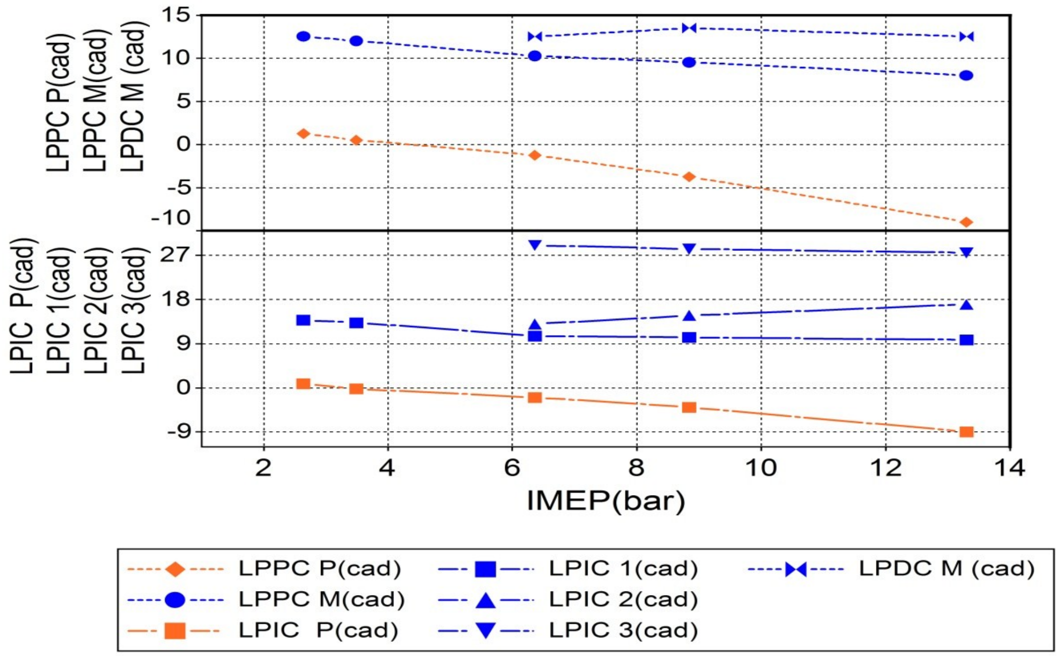

Figure 6-46. Data analysis showing peak locations of RHR trace and ion current signal for different engine loads at 2000 RPM.

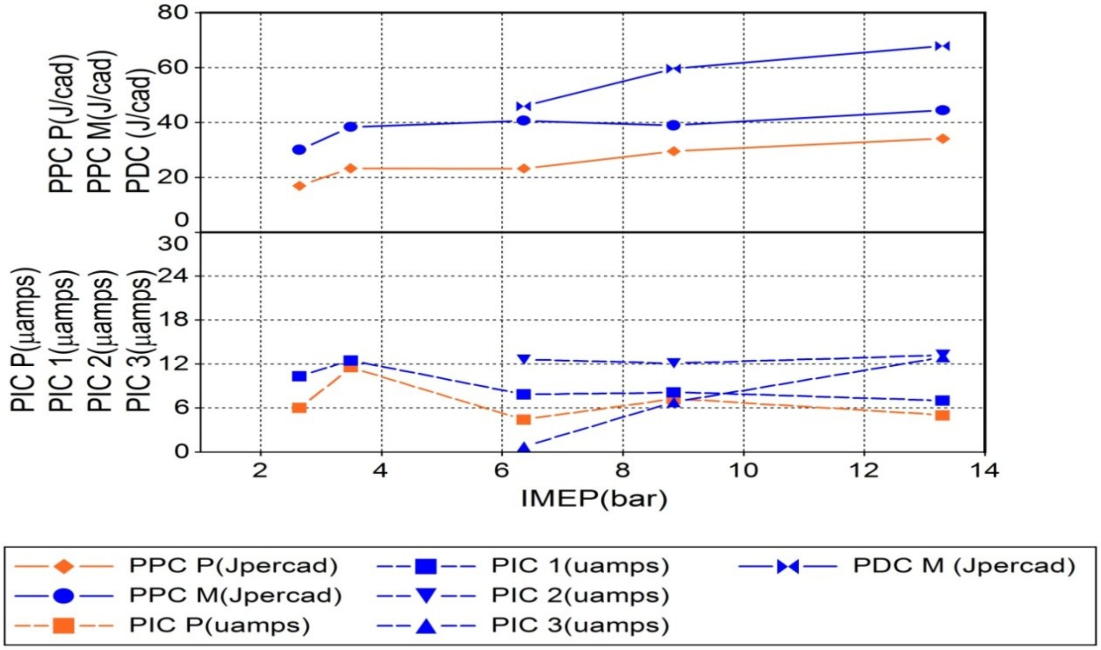

Figure 6-47. Data analysis showing peaks amplitude of RHR and ion current signal at 2000rpm

The following analysis deals with various correlations of ion current signal with RHR trace. The magnitude and location of the different peaks of the ion current signal contains information pertaining to various in cylinder combustion events. The location of different peaks of ion signal were plotted with corresponding peak amplitudes from RHR trace as observed in Figure 6-46. Figure 6-47 shows the peak amplitudes of RHR and ion current signal at 2000 rpm. The location of peak of ion current - pilot (LPICp) closely followed the location of peak premixed combustion due - pilot (LPPCp). It was observed that the both LPPCp and LPICp advanced as the engine load was increased. The location of the peaks of ion current due main combustion (LPIC 1, LPIC 2) followed the location of peak amplitude of RHR. The LPIC 1 and LPIC 2 corresponded to the LPPC M and LPDC M respectively.

The following covers the analysis of correlations made between the start of ion current signal and the first peak of ion current signal with the location of peak premixed combustion. The Figure 6-48 shows the correlation between SICp and LPPCp for different engine loads at a constant speed of 2000rpm. LPPC P was observed to have an offset of 3.053 CAD and the regression coefficient R^2 was 0.997. Figure 6-49 shows the correlation between LPICp and LPPCp for different engine loads at 2000rpm. The LPPCp was observed to have an offset of 0.655 CAD and a higher regression coefficient of 0.998 in comparison to the former one. It is worth noting that both SICp as well as LPICp strongly correlated with LPPCp but LPICp had a higher regression coefficient (R^2) in comparison with SICp during all three chosen speeds.

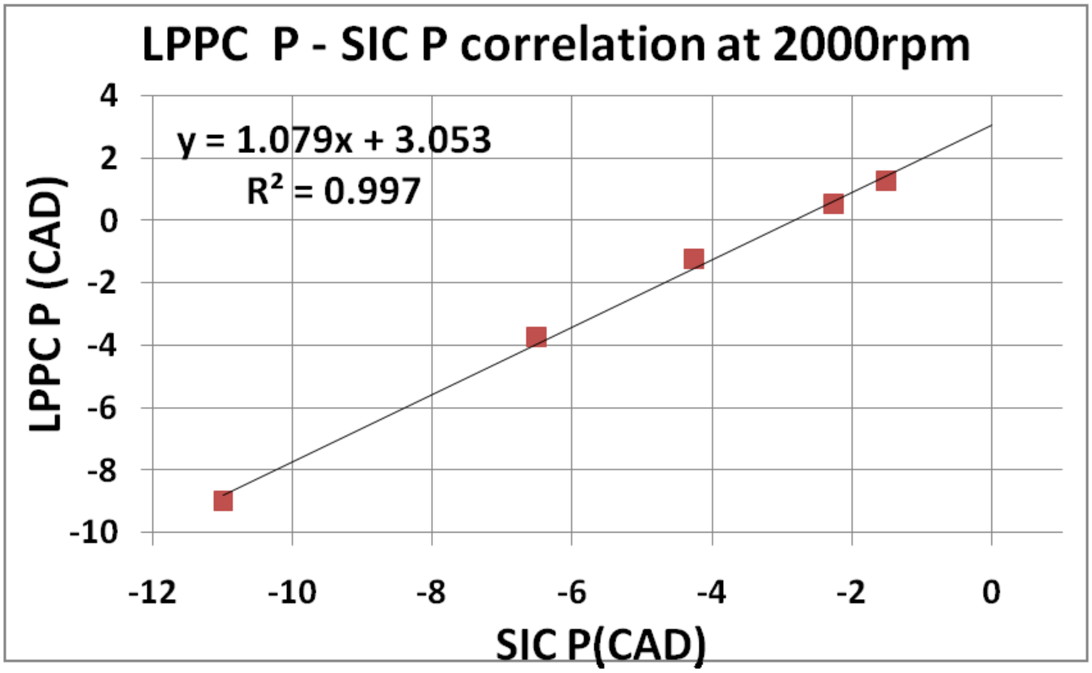

Figure 6-48. Data analysis showing correlations of LPPC P with SIC P @ 2000 RPM

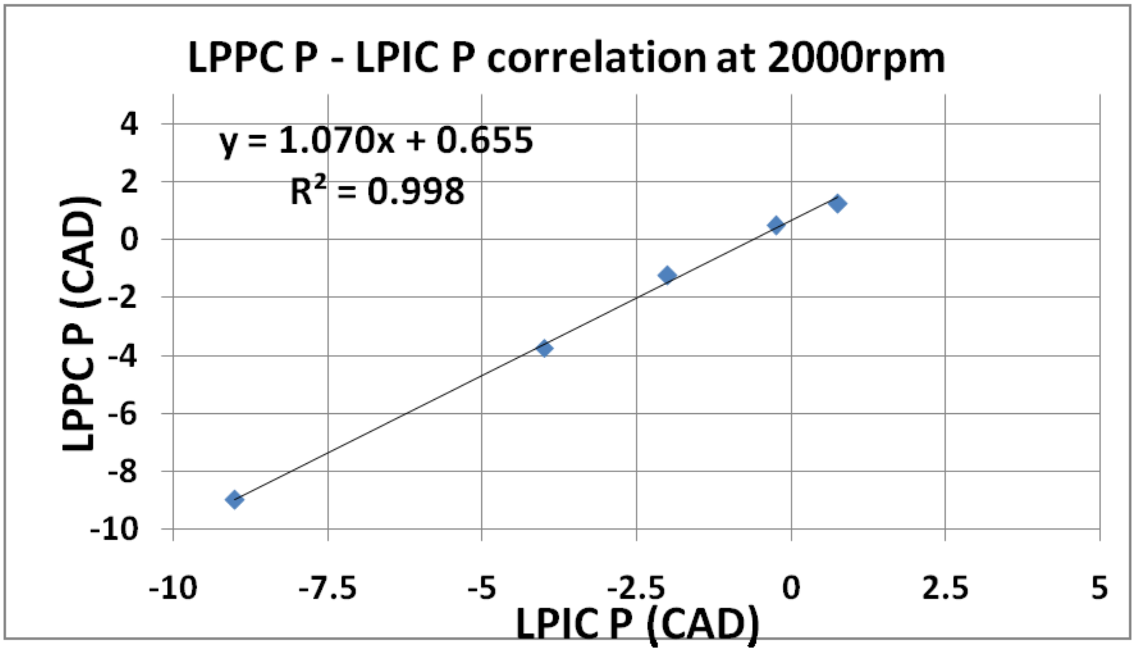

Figure 6-49. Data analysis showing correlations of LPPC P with LPIC P at 2000 RPM

Figure 6-50 shows the correlation between LPPCm and SICm for different engine loads at a constant speed of 2000 rpm. LPPCm was observed to have an offset of 5.71 CAD and the regression coefficient, R² was 0.278. It was observed that the correlation of SIC m with LPPCm was very weak. Figure 6-51 shows the correlation of LPPCm with LPIC1 for different engine loads at a constant speed of 2000 rpm. The LPPCm was observed to have an offset of 0.42 CAD and a regression coefficient of 0.907.

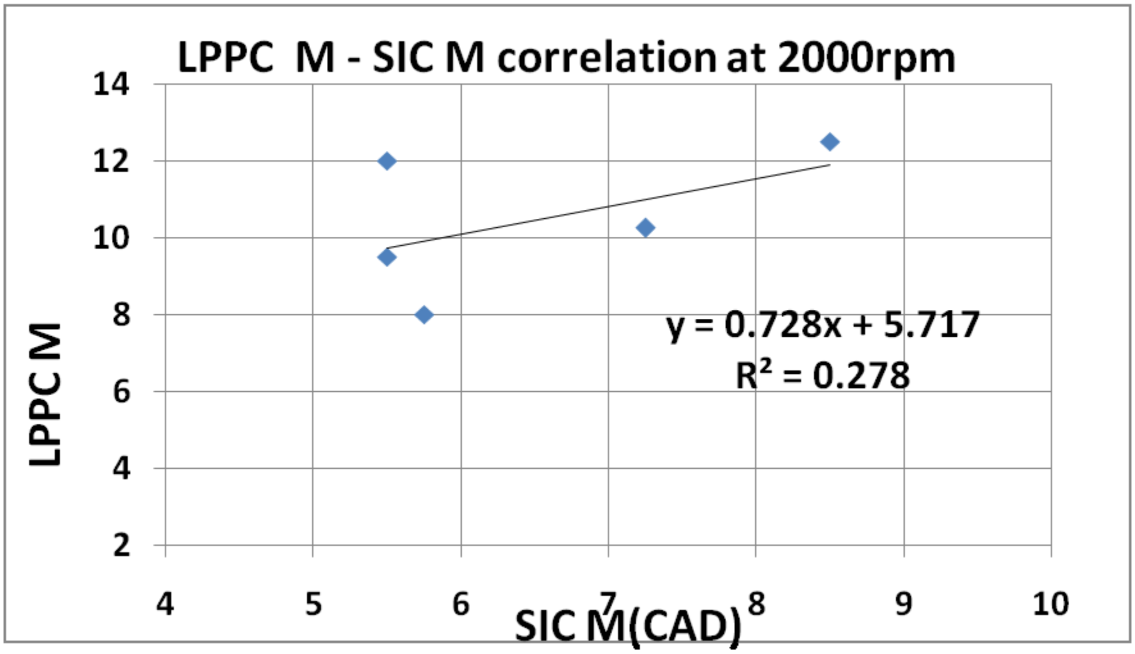

Figure 6-50. Data analysis showing correlations of LPPC M with SIC M at 2000 RPM

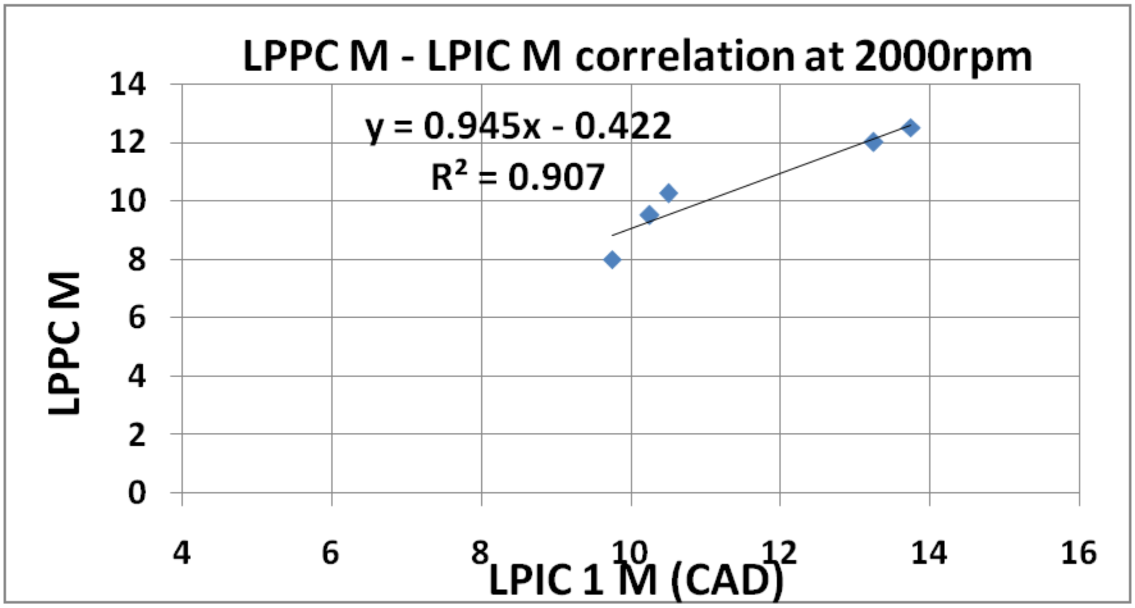

Figure 6-51. Data analysis showing correlations of LPPC M with LPIC 1 M at 2000 RPM

6.6 *Summary*

Detailed experimental investigations were conducted at a series of engine loads and three different engine speeds of 1600 rpm, 1800 rpm and 2000 rpm. Combustion, auto-ignition, performance, engine out emission and ion current characteristics are discussed at each speed. Each sub section details the data analysis, results and discussions associated with the engine operation in a step by step fashion. The engine was operated with original ECU settings and various parameters that changed with engine load such as injection pressure, intake manifold boost pressure, injection events, and injection timing were analyzed during each steady state condition and presented. Effect of changing the above parameters on combustion, performance, auto ignition and emissions are explained in detail. The effect of engine equivalence ratio, indicated fuel efficiency, thermal efficiency ignition delay of pilot and main combustion events, opacity percentage, and NOx emissions are analyzed and discussed. Furthermore, correlations between the ion current signal and different combustion and auto ignition parameters are developed. The results presented show us that the ion current delay correlates with ignition delay during both the pilot and main injection events. The various correlation plots demonstrated a good relationship between ion current signal and rate of heat release trace. Ion current signal was seen to closely follow RHR by location and peak amplitude. This investigation studied the relation of LPPC with start of ion current (SIC) as well as the first peak of ion current. It was observed that during all operating speeds - 1600, 1800, and 2000rpm, there was a strong correlation between LPPCp and LPICp. A similar trend was demonstrated between SICp and LPPCp. However, during the main combustion events, SICm and LPPCm demonstrated a good correlation only during 1800rpm. The correlation deteriorated during higher and lower speeds. The relationship between LPPCm and LPIC1 were also investigated. The best correlation between the same was demonstrated during the 2000rpm which was followed by 1600rpm and 1800rpm.

CHAPTER 7

DATA ANALYSIS AND RESULTS WITH JET AVIATION FUELS

7.1 *Introduction*

With the research being targeted towards the operation of alternative fuels or diesel like fuels on current diesel engines, particularly by US Military and their choice of jet fuels for powering vehicles based on 'Single Fuel Policy', the need for extensive investigation of combustion, performance and emission characteristics using these fuels is necessary [24]. The effect of differences in the physical and chemical properties of diesel and jet fuels would result in the variation of the ignition behavior, engine performance and emissions [25] [26] [24]. Although there were many efforts to quantify the variances between diesel fuel and jet fuels using optimized combustion calibration strategies, the impact of using jet fuels on a chosen calibration strategy has not been greatly investigated [24].

Hence, the main motivation of this work is to investigate the impact of using jet aviation fuels, such as JP-8 and Sasol-IPK, on the operation of modern diesel engine which follows a calibration strategy tuned for ultra-low sulfur diesel (ULSD). The variation in combustion, performance, auto-ignition and emission, of jet fuels and the regular US diesel fuel are compared. Ion current signal characteristics are studied during the operation with these fuels and were utilized to better understand the combustion process. The current study used the OEM ECU for modern high speed automotive diesel engine to conduct the test with different fuels.

ULSD, JP-8, and Sasol-IPK have distinct physical and chemical properties which affect the fuel spray characteristics, fuel atomization, evaporation, auto-ignition, combustion characteristics, and emission formation. This leads to changes in engine brake power, thermal efficiency, and fuel consumption and engine-out emissions [27] [26] [25]. This work is targeted to quantify the effects of using alternative fuels on the above mentioned engine parameters. The analysis of the combustion characteristics would lead to the development of efficient control techniques to operate with alternative fuels in CI engines. Ion current signal has been used to better understand the combustion process using different fuels and also to improve feedback to engine control unit [13].

7.2 *Comparison of fuel properties*

Various physical and chemical properties of ULSD, JP-8, and Sasol IPK are shown in Table 7-1.

The Cetane number (CN) is used to determine the ignition quality of fuels. CN can be explained as the experimental determination of ignition delay under standard conditions and is a reasonable indicator of the auto-ignition quality of the fuel. The ignition delay decreases as the CN of the fuel increases. CN along with the combustion strategy play a major role in the premixed combustion fraction which in turn also affects the emission characteristics. A large variation in CN of ULSD is observed particularly in North American market, which ranges from 40 to 55, and has an average value of 46 [28]. European based modern diesel engine have a specification to use diesel fuels with CN more than 51, as those engines are calibrated to operate on higher CN [29]. Also, JP-8 has a wide variation of CN which ranges from 30 to 50 [24]. In this study, the JP-8 used has CN of 49 whereas Sasol-IPK has CN of 25.4 and ULSD has a CN of 42.3.

Table 7-1 Physical and chemical properties of ULSD, JP-8, Sasol-IPK

FUEL	*ASTM*	*ULSD*	*JP-8*	*Sasol-IPK*
Cetane Number	D613	42.3	49	25.4
Derived Cetane Number	D6890	42.1	50.1	31.1
Flash Point (°C) min	D93	69	49.5	42
Density (@15°C) kg/m3	ASTM 85H	842	798	755
Viscosity(cSt,40°C)	D445	2.438	1.367	1.125
Heating Value (MJ/kg)		41.2	43.2	44.0
Aromatic content	D2425	27.8	16.3	0.2

Density is another important property of fuel. ULSD has the highest density of 842 kg/m^3, whereas Sasol-IPK has the lowest density of 755 kg/m^3 and JP-8 has the density of 798 kg/m^3.

It can be observed that jet fuels have higher energy content compared to ULSD fuel, whereas Sasol-IPK has the highest heating value of 44MJ/kg, closely followed by JP-8 with 43.2MJ/kg and ULSD with 41.2 MJ/kg. Jet fuels have a lower aromatic content compared to ULSD fuels, whereas Sasol-IPK has the lowest with 0.2% aromatic content.

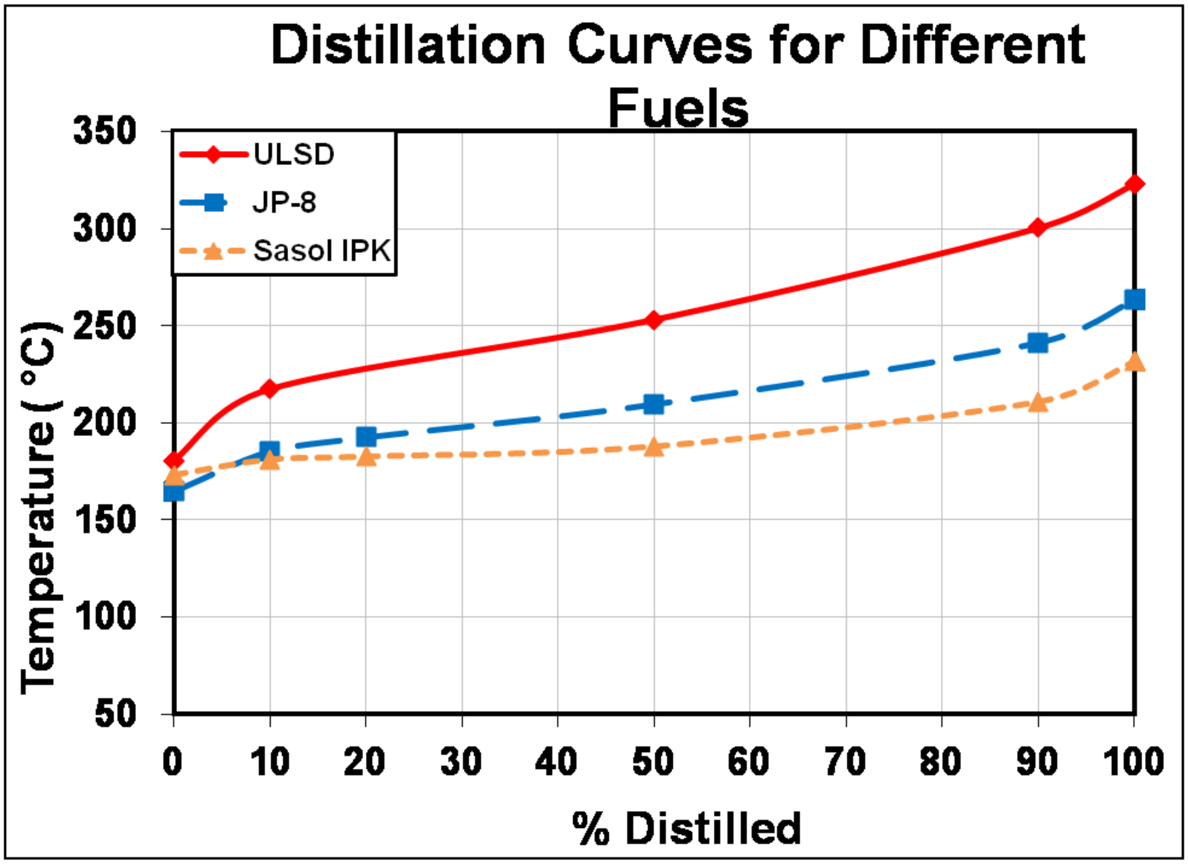

Figure 7-1. ***Distillation curves for ULSD, JP-8, and Sasol-IPK***

The volatility of the fuel impacts mainly the liquid spray characteristics including liquid penetration lengths and fuel evaporation, which in turn affects the combustion and emission characteristics. The distillation curve is obtained by plotting the boiling temperature of the fuel against its volume percent distilled. Figure 7-1 shows the distillation curves for ULSD, JP-8, and Sasol-IPK. The comparison of distillation curves for ULSD and jet fuels shows that the latter has lower distillation temperatures. ULSD fuel has a mixture of heavier compounds when compared to jet fuels. At 10% recovery, the temperature of ULSD is 30° C higher than the jet fuels. At 50% recovery point, the difference between the three fuels can be clearly observed and there is an approximate difference of 75°C between ULSD and Sasol-IPK. At 100% recovery, Sasol-IPK has the lowest recovery temperature 230°C, followed by JP-8 at 265°C and USLD at 325°C.

7.3 *Results and analysis*

Analysis of the combustion process

The combustion analysis in this section will be explained with respect to the in-cylinder pressure, rate of heat release, ion current signal, and the injection signal. All the results are presented for a constant speed of 1800rpm, where engine load was varied from no load to 140 Nm and a comparative analysis during the operation with ULSD, JP-8 and Sasol-IPK is made.

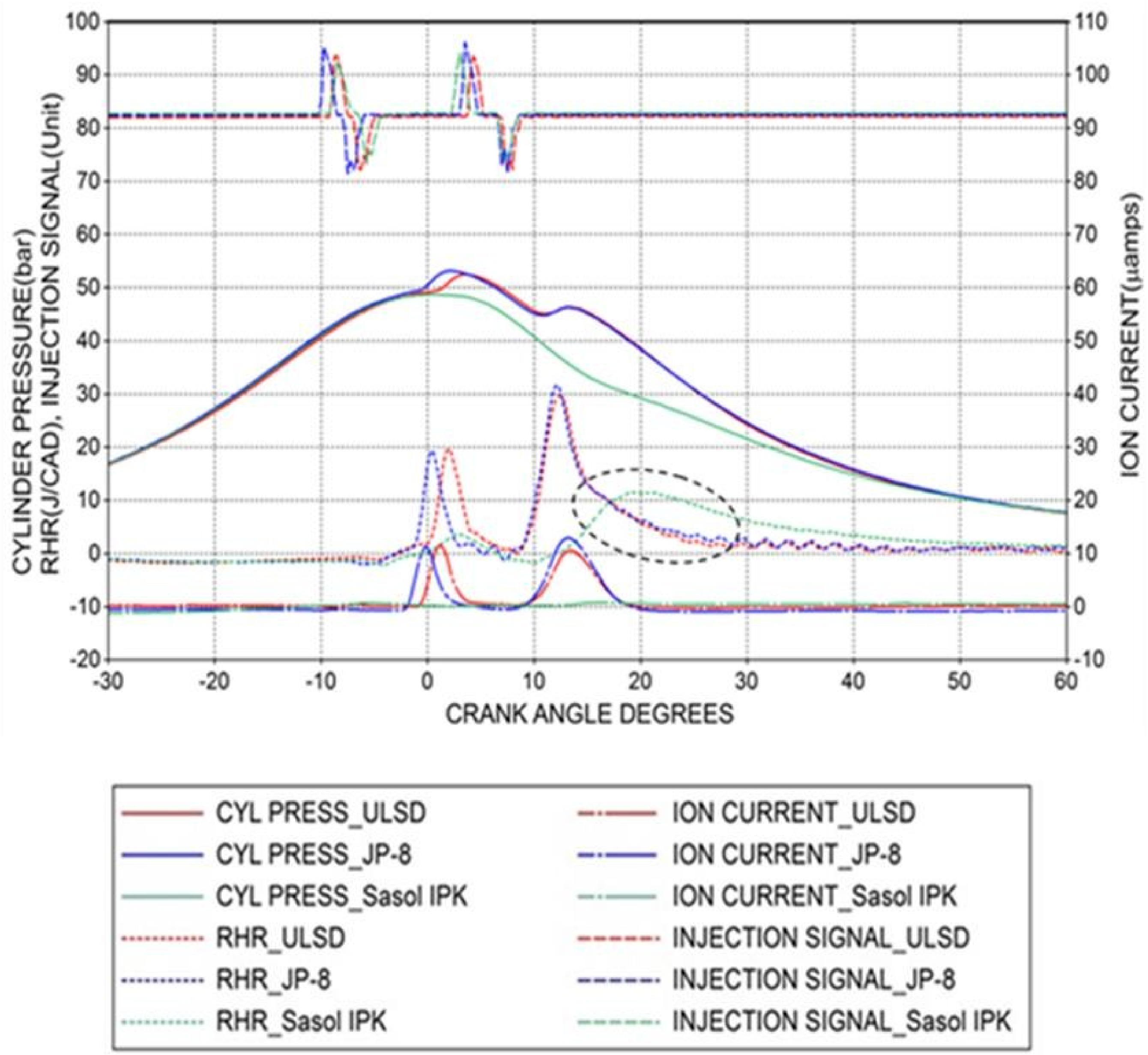

Figure 7-2. Cylinder pressure, RHR, ion current, injection signal for engine operation at no load, 1800rpm for ULSD, JP-8, and Sasol-IPK fuels.

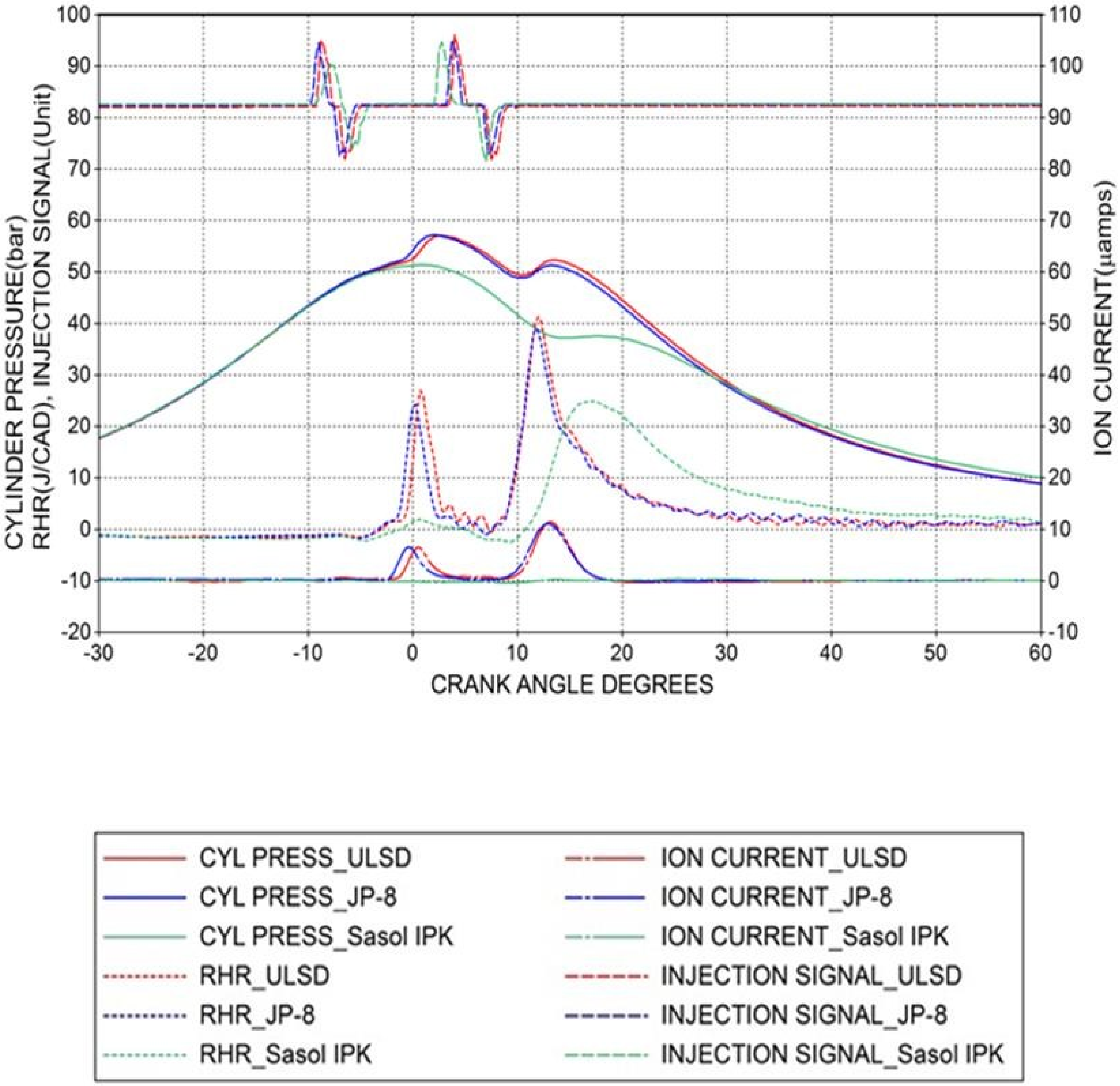

Figure 7-3. Cylinder pressure, RHR, ion current, needle lift traces for engine operation at 20Nm load, 1800rpm speed for ULSD, JP-8, and Sasol IPK fuels.

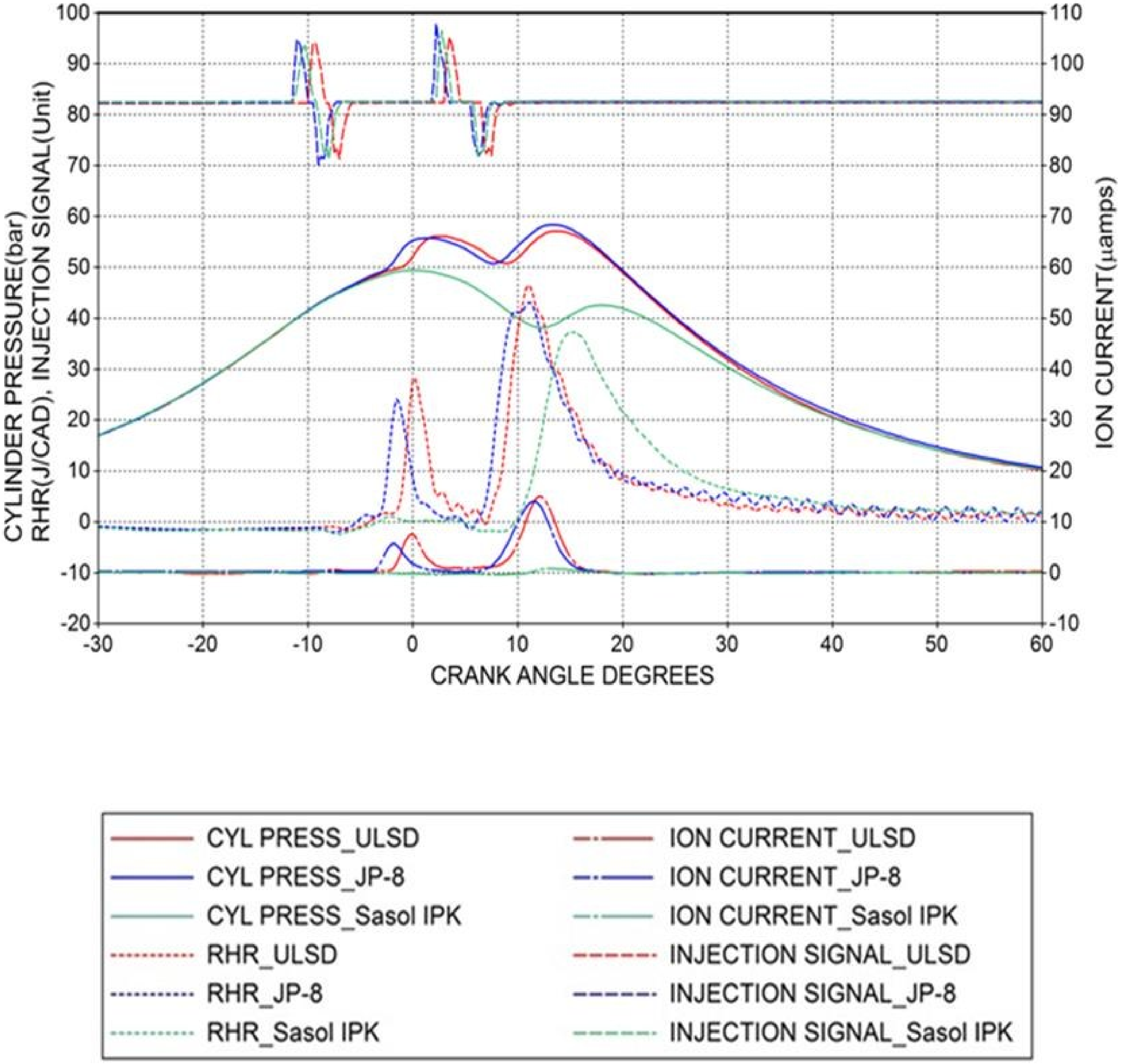

Figure 7-4. Cylinder pressure, RHR, ion current, needle lift traces for engine operation at 40Nm load, 1800rpm speed for ULSD, JP-8, and Sasol IPK fuels.

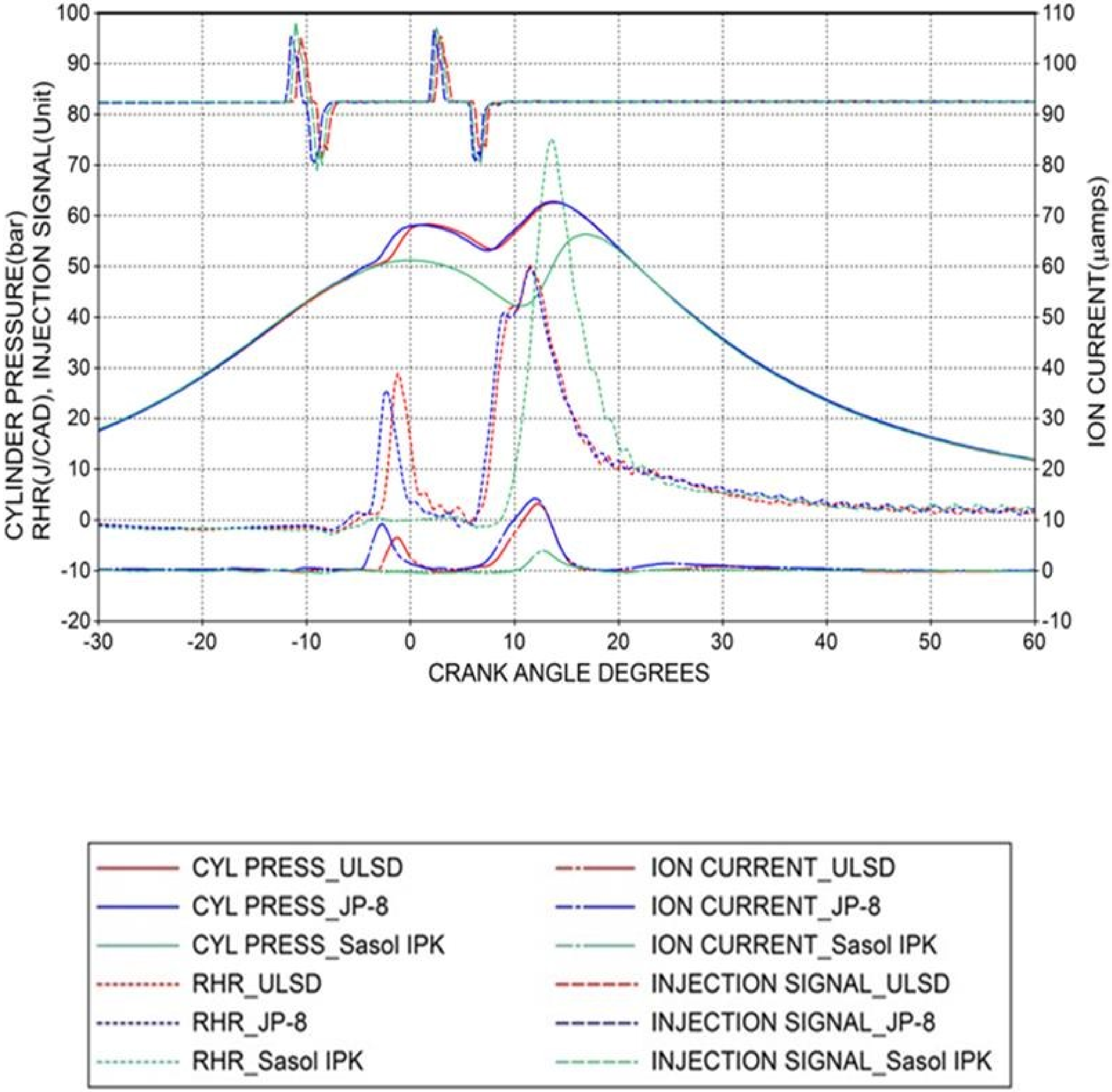

Figure 7-5. Cylinder pressure, RHR, ion current, needle lift traces for engine operation at 60Nm load, 1800rpm speed for ULSD, JP-8, and Sasol IPK fuels.

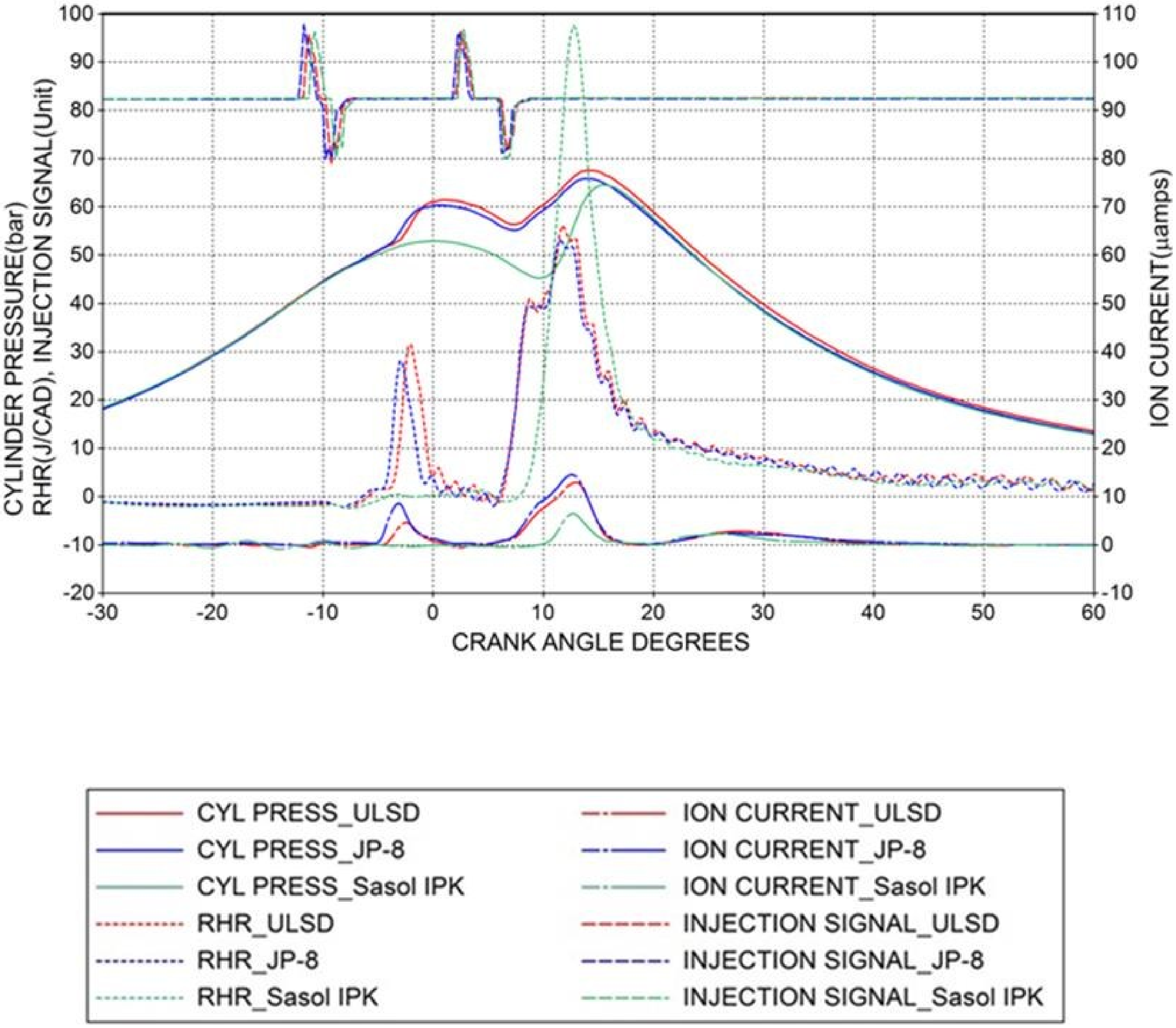

Figure 7-6. Cylinder pressure, RHR, ion current, needle lift traces for engine operation at 80Nm load, 1800rpm speed for ULSD, JP-8, and Sasol IPK fuels.

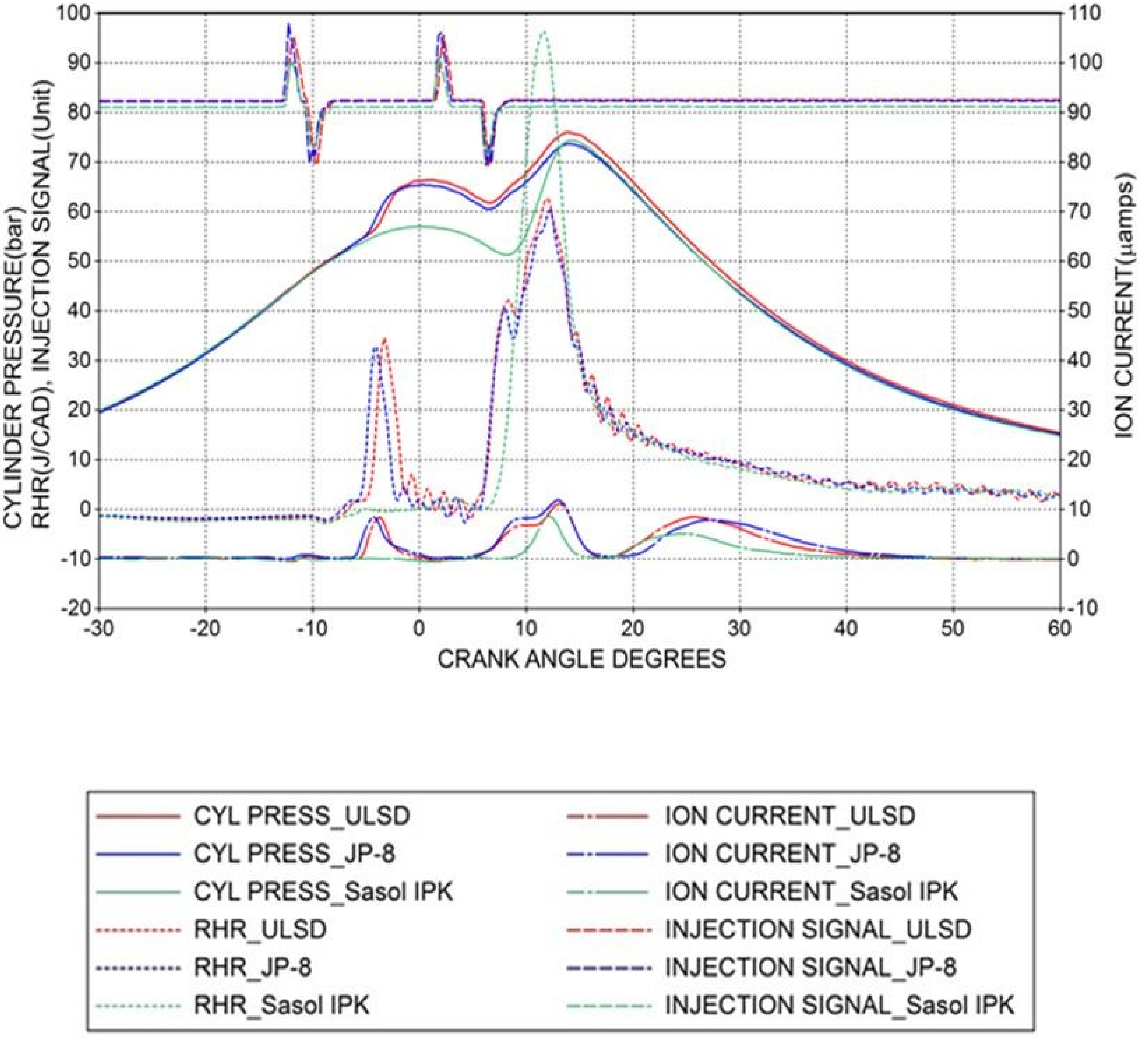

Figure 7-7. Cylinder pressure, RHR, ion current, needle lift traces for engine operation at 100Nm load, 1800rpm speed for ULSD, JP-8, and Sasol IPK fuels.

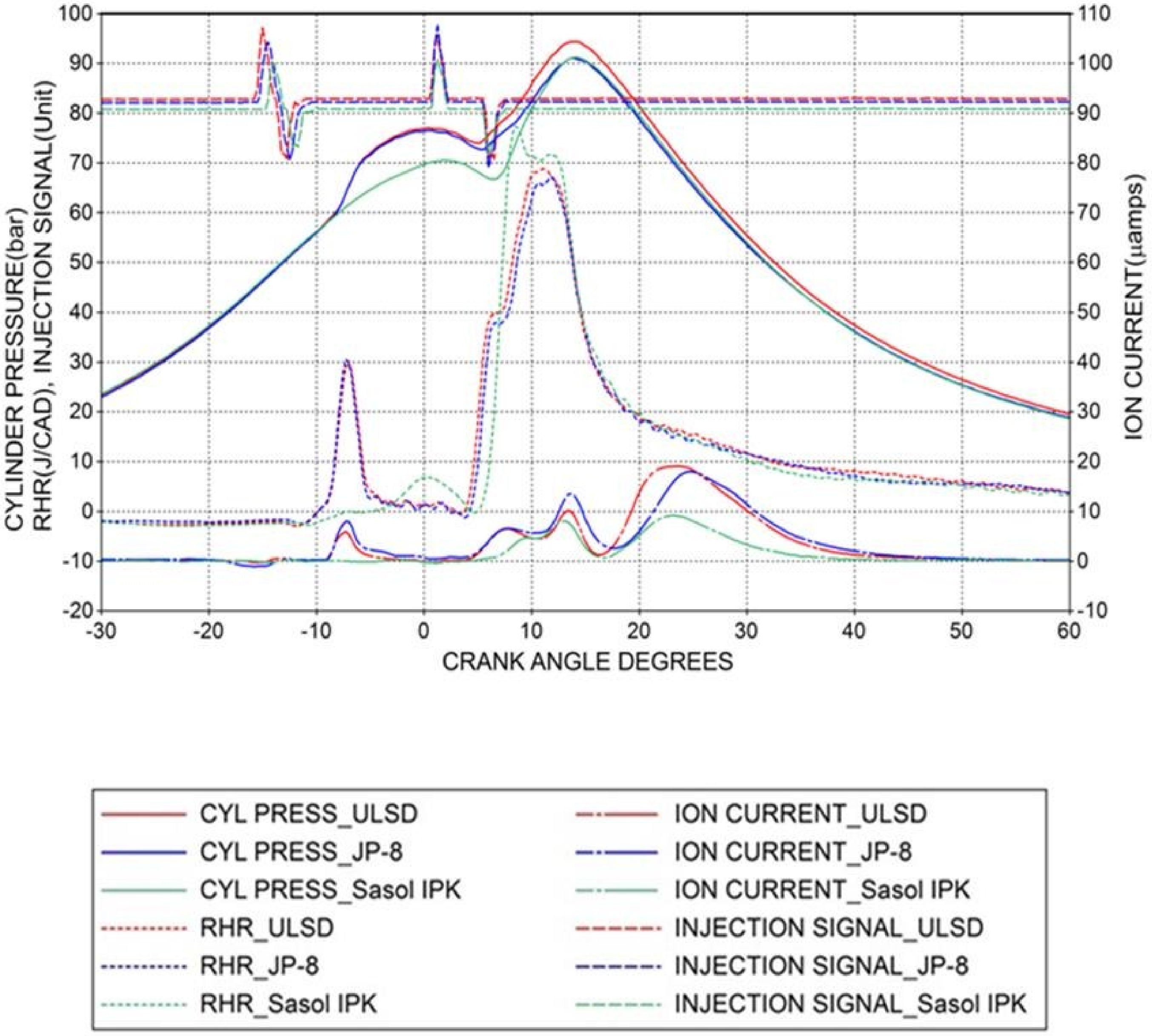

Figure 7-8. Cylinder pressure, RHR, ion current, needle lift traces for engine operation at 140Nm load, 1800rpm speed for ULSD, JP-8, and Sasol IPK fuels.

Engine operating at no load

Figure 7-2 shows over lapping plots for ULSD, JP-8 and Sasol-IPK with respect to in-cylinder pressure, RHR, ion current and injection signal during engine operation at no load. The start of injection command was captured using a current probe, where the start of the pilot pulse is represented by SOPP and the start of the main pulse is SOPM. The SOPP of JP-8 occurred at 10° bTDC followed by ULSD and Sasol-IPK at 9.25° bTDC. However, the JP-8 and ULSD had a pilot injection pulse duration of 4 and 4.25 CAD respectively, followed by Sasol-IPK with 5 CAD. The pilot injection event occurred early during compression which resulted into a short duration of premixed combustion at TDC; this improved the fuel mixing and auto-ignition development during the main combustion. The three tested fuels have distinct physical and chemical properties as shown in Table 7-1. It is worth noting that the fuel spray produced from the three fuels will be different in spray penetration, liquid break-up and atomization and therefore different fuel/ air mixing develops inside the combustion chamber. To better understand the auto-ignition and combustion process, the in-cylinder pressure, the ion current and the rate of the heat release (RHR) traces are used.

The first rise seen in the in-cylinder pressure near TDC was due to the auto-ignition of the pilot fuel ; this was observed for ULSD and JP-8. For ULSD, the fuel evaporation process started around 6° bTDC, which is seen as a dip in the RHR. As the exothermic reactions becomes more dominant, the RHR starts increasing. A slow rate of rise in the RHR denotes the low temperature combustion (LTC) regime. The start of high temperature combustion process was depicted by the sharp rise in the RHR at 0.5° aTDC due to the premixed combustion which then reaches a local maximum known as the peak of premixed combustion for pilot at 2° aTDC. JP-8 also developed a similar trend, where the fuel evaporation occurred around 7.5° bTDC which then produced LTC.

The high temperature combustion started at 1° bTDC and the location of peak premixed combustion of pilot (LPPCp) at 0.5° aTDC. The combustion process of Sasol-IPK was quite different from JP-8 and ULSD. Unlike ULSD and JP-8, Sasol-IPK could not produce any pressure rise but a change in the slope of the pressure trace was noticed during the expansion stroke. The RHR of Sasol-IPK indicated that the fuel evaporation process started around 6.5°bTDC, after which the rate of the heat release gradually increased due to the low temperature combustion (LTC). The LTC was quenched by the main fuel injection event at 2.25° aTDC, where no high temperature combustion is produced.

The ion current signal for ULSD is usually characterized by two to four peaks depending on the engine load [1]. The signal can be considered as the representation of the local combustion process which takes place in the vicinity of the probe location [11]. Analyzing shows that ion signal for ULSD detected combustion produced by the pilot event and started to rise at around 0.75° bTDC, which reached maximum amplitude of 11.5 μamps at 1.25°aTDC. The ion current signal for JP-8 followed a similar trend as ULDS. The ion current signal started to rise at 2° bTDC and reached a maximum of 11.2 μamps at 0.25° aTDC. Since Sasol-IPK produced only low temperature combustion due to the pilot injection, no ion current signal was detected compared to ULSD and JP-8. This is due to the low ignition quality of Sasol-IPK (CN=25.4) which exhibits very long ignition delay. It was observed that the ion current was formed explicitly during the high temperature combustion.

The following covers the analysis for the combustion of the main injection. The start of pulse of main injection (SOPM) of ULSD occurred at 3.75°aTDC. The injection pulse SOPM of Sasol-IPK and JP-8 were at 2.25°aTDC and 3°aTDC respectively. While ULSD and JP-8 had almost the same injection duration of 5.25 and 5.5 CAD respectively, Sasol-IPK had a higher duration of 6.5 CAD. The main injection event occurred late after TDC during the expansion stroke which resulted into a low peak pressure and temperature.

Both ULSD and JP-8 have a start of combustion due to the main injection at 8° aTDC, producing same peak combustion pressure at 13° aTDC. Although ULSD has a CN= 42.3 and JP-8 has a CN=49, ULSD has the shortest ignition delay of 4.75 CAD and JP-8 has ignition delay of 5 CAD. The main ignition delay was affected by the combustion produced by the pilot injection. Therefore, the pressure and temperature at the main injection for ULSD was higher than JP-8, which resulted in shorter ignition delay. Since a small amount of fuel was injected during the main injection at no load , the main combustion was dominantly premixed combustion fraction. The premixed combustion started at 9° aTDC, and it reached its maximum peak (LPPCm) at 12.5° aTDC and gradually the rate decreased as the piston moves down in the expansion stroke. The main combustion process of Sasol-IPK started very late at 13° aTDC. The RHR indicated a very slow burning rate for the Sasol-IPK mainly due to the late combustion timing. The RHR reached the maximum amplitude of 11.44 J/CAD with LPPC at 19.25° aTDC, where combustion continue to take place up to 50° aTDC. Due to the low peak of heat release for Sasol-IPK, the peak pressure developed during the expansion stroke is very low.

The ion current signal produced due to the main combustion is shown in Figure 7.5. The ion current signal decayed to zero after the completion of pilot combustion as seen for both ULSD and JP-8. Similar to the RHR, The ion current started to rise again at 9.5° aTDC and reached its maximum amplitude of 10.55 and 13.2µamps at 13.5° aTDC for ULSD and JP-8 respectively. At no load , only one peak of the ion current is observed, after which it dropped and decayed at 19° aTDC. While analyzing the location of peaks of ion current for pilot and main events, it can be observed that it coincides with the corresponding peaks of heat release. The ion current signal started to rise at 2° bTDC and reached a maximum of 11.2 µamps at 0.25° aTDC. Sasol-IPK produced a very slow burning rate which results in slow pressure and temperature development inside the combustion chamber. The amplitude of the ion current signal due to combustion is insignificant.

Engine operating at 60Nm

Figure 7-5 shows over lapping plots for ULSD, JP-8 and Sasol-IPK with respect to in-cylinder pressure, RHR, ion current and injection signal during engine operation at 60 Nm. The start of injection command for the three fuels occurred very closely, where SOPP of JP-8 and Sasol-IPK occurred at 11.75° bTDC followed by ULSD at 11° bTDC. ULSD had pilot injection pulse duration of 4 whereas, JP-8 and Sasol-IPK had an injection duration of 4.25 CAD.

The first rise seen in the in-cylinder pressure before TDC was caused due to the auto-ignition of the pilot fuel injected which was observed for ULSD as well as JP-8. For ULSD, the fuel evaporation process started around 8.25° bTDC, which is seen as the first dip in the RHR. A gradual rise in RHR trace marked the LTC regime, which was also observed during no load condition. The high temperature combustion process started at 2.75° bTDC and formed peak of premixed combustion due to pilot injection at (LPPCp) 1.25° bTDC. For JP-8, the fuel evaporation occurred around 9° bTDC which then produced LTC. It is worth noting that the RHR trace created a small dip during the LTC regime, which is indicative of the negative temperature coefficient (NTC) region. This phenomena was not seen during the combustion process of ULSD. The high temperature combustion started at 3.75° bTDC which then reached the peak of premixed combustion for pilot at 2.25° bTDC. On the other hand, Sasol-IPK could not produce any noticeable pressure rise from the pilot injection event. The RHR of Sasol-IPK indicates that the fuel evaporation process started around 8.75° bTDC followed by the low temperature combustion process. Sasol-IPK failed to produce any high temperature combustion.

Ion current signal for ULSD detected pilot combustion, where the ion current started to rise at 3° bTDC. It then reached maximum amplitude of 6.57µamps at 1.25° bTDC. Similarly, the ion current signal for JP-8 started to rise at 4.5° bTDC and reached a maximum of 9.27 µamps at 2.75° bTDC. No ion current signal was detected for Sasol-IPK since no high temperature combustion occurred due to the pilot injection.

Analysis for the combustion of the main injection during the engine operation at 60Nm is discussed in the following section. ULSD, JP-8 and Sasol-IPK had the same start of pulse of main injection (SOPM) at 2° aTDC. ULSD, JP-8 and Sasol-IPK had injection durations of 5.5, 5.75 and 6 CAD respectively. ULSD and JP-8 had same start of combustion due to the main injection at 6.25° aTDC, producing same peak combustion pressure at 13.75° aTDC. Since a higher amount of fuel was injected during the main injection at 60Nm load, the combustion consisted of premixed as well as diffusion/mixing controlled combustion fractions. The premixed combustion for ULSD and JP-8 started at 6.25° aTDC, but JP-8 reached its first peak (LPPCm) at 8.75° aTDC followed by ULSD at 9.75° aTDC. After LPPCm, rate of heat release for ULSD and JP-8 slowed down and rose again to reach their peak of diffusion combustion with an amplitude of 50.1J/CAD at 11.5° aTDC. For Sasol-IPK, the main combustion event of Sasol-IPK started at 8° aTDC. LPPCm was located at 13.5° aTDC with maximum amplitude of 75.07 J/CAD. Unlike ULSD and JP-8, combustion of Sasol-IPK comprised mainly of premixed charge which was due to the very long ID.

The ion current signal produced due to the main combustion at 60Nm is shown in Figure 6. After the ion current was formed due to the pilot combustion, it started to rise again at 8° aTDC and 7° aTDC for ULSD and JP-8 respectively due to the main combustion. It then reached a peak amplitude of 13.23 and 14.23 µamps at 12° aTDC for ULSD and JP-8 respectively. It is worth noting that the ion current peak closely followed RHR and corresponded to LPPCm. The ion current signal developed change in slope around 12.5° aTDC corresponding to the diffusion combustion indicated by the RHR. At 24° aTDC, the ion current observed to develop a new hump, which was more noticeable for JP-8. For Sasol-IPK, the ion current signal started to rise at 10.5° aTDC after a long ion current delay (ICD) and reached a peak of 3.9µamps at 12.75° aTDC. It was observed that the amplitude of the ion current signal due to combustion of Sasol-IPK was lower in comparison to the other two fuels ULSD and JP-8.

Engine operating at 140Nm

Figure 7-8 shows over lapping plots for ULSD, JP-8 and Sasol-IPK with respect to in-cylinder pressure, RHR, ion current and injection signal during engine operation at 140Nm load condition. SOPP of ULSD and JP-8 occurred at 15.25° bTDC followed by Sasol-IPK at 14.75° bTDC. All of them had the same injection duration of 4 CAD.

The following covers the analysis for the combustion of the pilot injection. The auto ignition of the pilot fuel injection caused the in-cylinder pressure of ULSD and JP-8 to rise before TDC whereas no significant pressure rise was observed from combustion of Sasol-IPK. Fuel evaporation process for ULSD and JP-8 started around 13.25° bTDC as observed from RHR. No LTC regime was observed at 140Nm in contrast to the combustion trends at lower loads. The high temperature combustion for ULSD and JP-8 started at 9° bTDC and reached LPPCp at 7° bTDC with an amplitude of 30 J/CAD. However, fuel evaporation process started for Sasol-IPK around 12° bTDC corresponding to the later injection timing then followed by low temperature combustion. Even though the high temperature process started at 3.75° bTDC, it was quenched due to the main fuel injection at 0.25° aTDC.

The ion current signal produced during the pilot combustion of ULSD and JP-8 started to rise at 9° bTDC and reached a peak at 7.25°bTDC with an amplitude of 7.96 and 5.85 µamps respectively. No ion current signal was detected during the LTC produced by Sasol-IPK.

For the main combustion event, three fuels produced the same SOPM at 0.75°aTDC and injection duration of 6.75 CAD. It can be observed that as the load increased to 140Nm, the injection timing advanced closer to TDC.

The analysis of the main combustion process shows the following. It was observed that ULSD and JP-8 had same start of combustion due to the main injection at 3.75° aTDC. LPPCm of ULSD and JP-8 was located at 6.25° aTDC and 6.5° aTDC respectively. Since a higher amount of fuel was injected during the main injection at 140Nm, the main combustion was dominantly diffusion/mixing controlled combustion. Sasol-IPK, with a longer ID, recorded its LPPCm at 8.5° aTDC. It is worth noting that Sasol-IPK produced higher premixed combustion fraction than ULSD and JP-8. After LPPCm, the rate slowed down and produced another peak which was mainly due to the diffusion combustion process. Location of peak of diffusion combustion (LPDC) for ULSD, JP-8 and Sasol-IPK was located at 11.25°, 11.75°, 11.75° aTDC with an amplitude of 68.83, 67.21, 71.68 J/CAD respectively. It is observed that the location of peak pressure was same for the three fuels at 140 Nm.

During the main combustion event; ULSD, JP-8 and Sasol-IPK produced ion current signal with three distinctive peaks. After the completion of the pilot combustion process, ion current signal gradually decayed to zero while operating with ULSD and JP-8. Ion current signal followed the rate of heat release trace and started to rise again at 9.5° aTDC and reached its first peak amplitude of 6.5 µamps at 7.75° aTDC for ULSD and JP-8. Sasol-IPK reached its first ion current peak at 9.5° aTDC with an amplitude of 4.6 µamps. After the first peak, amplitude of ion current signal dropped to a minimum and rose again to produce the second peak with an amplitude of 10.16, 13.5 and 8.12µamps at 13.5°, 13.75° and 13° aTDC for ULSD, JP-8 and Sasol-IPK respectively. The second peak of ion current was produced from the diffusion/mixing controlled combustion flames. A third ion current peak was observed with a maximum amplitude of 19.09, 17.98, 9.16 µamps at 19.06°, 24.75°, 23.0° aTDC for ULSD, JP-8 and Sasol-IPK respectively. The source of third peak can be associated with the diffusion combustion produced from the closest spray reaching the probe location [9].

Analysis of engine performance and emissions

In order to study the engine performance operating with the three fuels, various engine parameters such as manifold absolute pressure, fuel injection pressure, exhaust lambda, peak combustion pressure, indicated specific fuel consumption, ignition delay, ion current delay, and engine-out emissions, were compared.

Engine Performance:

The intake manifold pressure (MAP) was measured and plotted versus engine torque with engine operation on the three different fuels, as shown in Figure 7-9. It can be observed that intake pressure remained almost constant during each steady state operating point. Since the engine is equipped with a turbocharger, the manifold absolute pressure increased with increase in load.

The common rail injection pressure was measured during the engine operation for each fuel and plotted versus torque as shown in Figure 7-10. Considering ULSD as the baseline fuel, engine operation using jet fuels is compared with the operation using ULSD. JP-8 showed very little variation from the ULSD fuel operation at all loads tested. On the other hand during the operation with Sasol-IPK, it was observed that the ECU shifted to a higher injection pressure at no load and low engine loads. Sasol-IPK recorded injection pressure higher than ULSD with difference of 365, and 213 at no load and 20Nm respectively. It is worth noting that the ECU increased the injection pressure to deliver more fuel to keep the same torque. This is quite evident from the ISFC which is three times higher than that for ULSD. All the other steady state operating points higher than 40 Nm showed closer rail pressure values to that of the ULSD fuel.

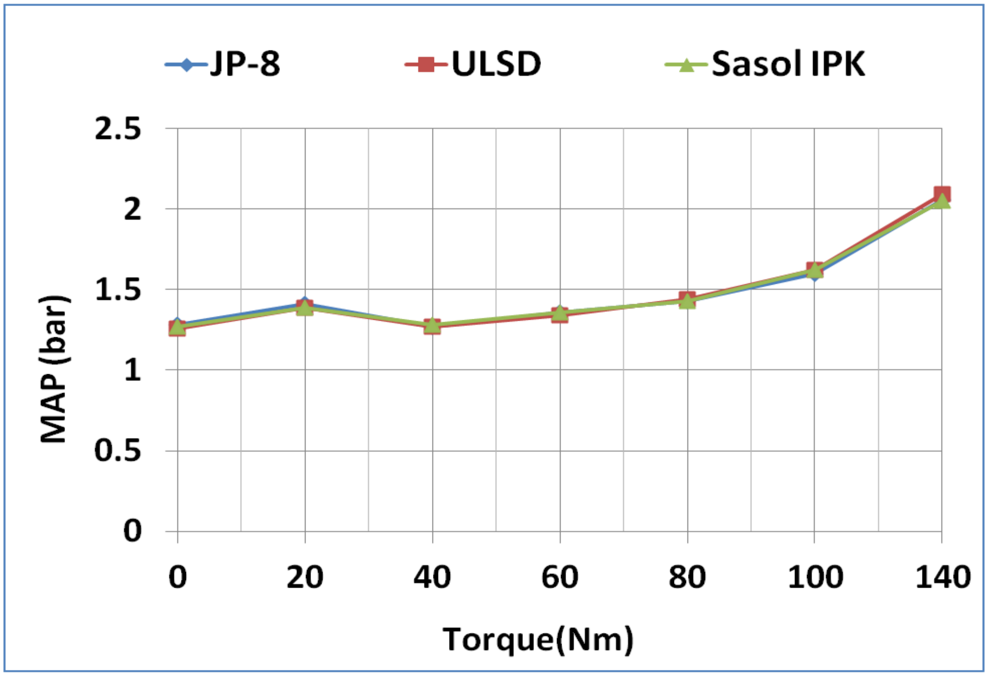

Figure 7-9. Intake manifold pressure vs. Torque, for engine operating under ULSD, JP-8 and Sasol-IPK fuel modes, at 1800rpm

Figure 7-11 shows the comparison of exhaust lambda versus engine torque using different fuels. The lambda value (ƛ) is used to indicate the overall level of air to fuel ratio developed inside the combustion chamber. Now considering the variation of jet fuel from ULSD, both JP-8 and Sasol-IPK showed more differences during no load and low load operating points. Sasol-IPK recorded lower values of ƛ, when compared to other two fuels, during no load and low load, which indicates that the combustion process was richer.

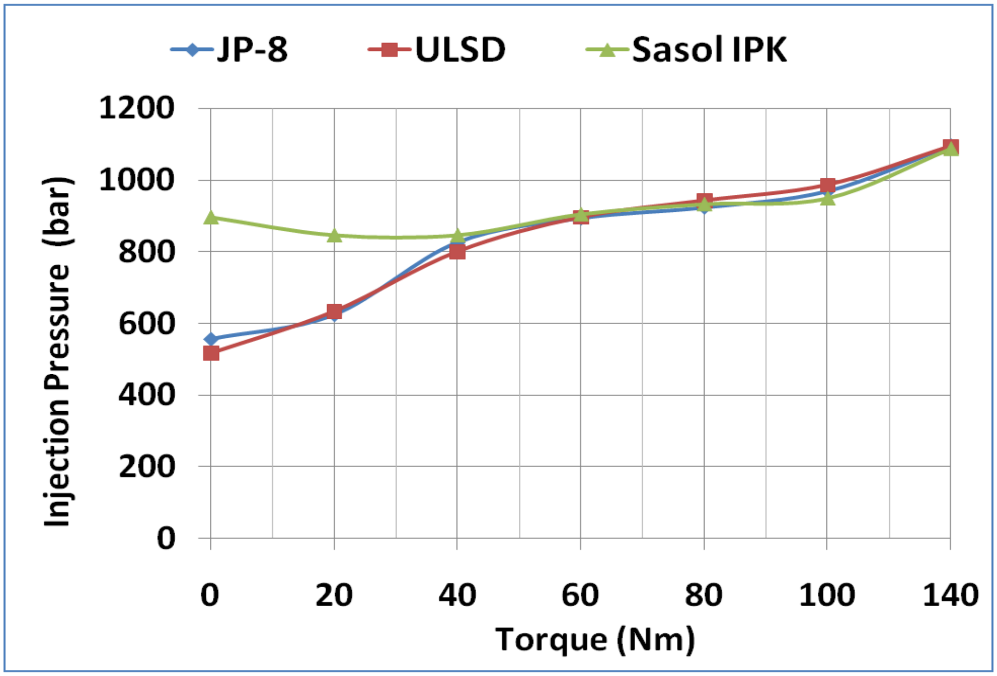

Figure 7-10. Fuel Injection Pressure vs. Torque, for engine operating under ULSD, JP-8 and Sasol-IPK fuel modes, at 1800rpm.

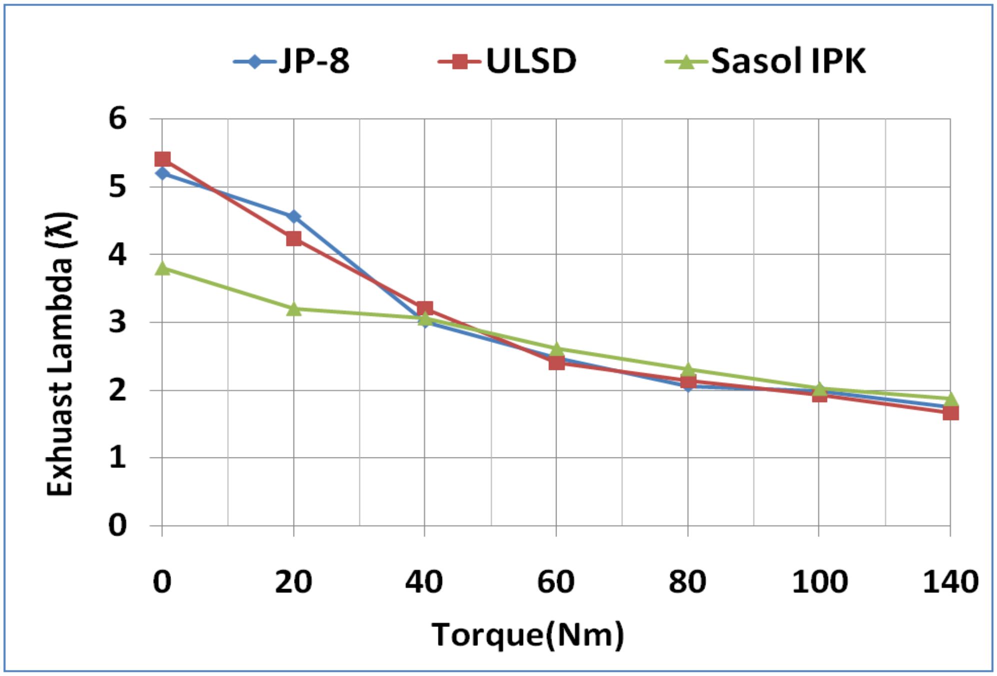

Figure 7-11. Exhaust Lambda vs. Torque, for engine operating under ULSD, JP-8 and Sasol-IPK fuel modes, at 1800rpm.

The peak combustion pressure was measured and represented as shown in Figure 7-12. Peak pressure inside the chamber was observed to increase with increase in engine load and the rate of pressure rise was greater at higher loads. JP-8 when compared to ULSD, shows almost no variation in peak pressure from no load to 60Nm. However, as the load increased further, the JP-8 produced a slightly lower peak pressure. On the other hand, Sasol-IPK produced lower peak pressures in comparison to the other two fuels and variation with respect to ULSD operation seems to be high at no load and lower loads. The variation decreased as engine load increased. Sasol-IPK produced a variation of about 15% at 40Nm and 4% at 140 Nm.

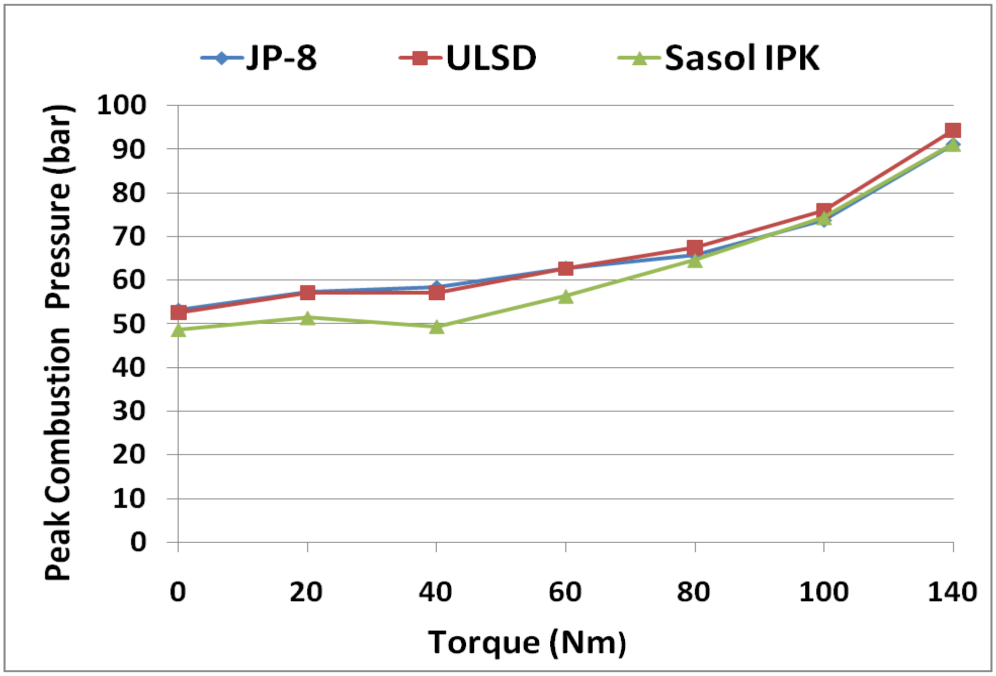

Figure 7-12. Peak combustion pressure vs. engine load, for engine operating under ULSD, JP-8, and Sasol-IPK fuel mode, at 1800 rpm

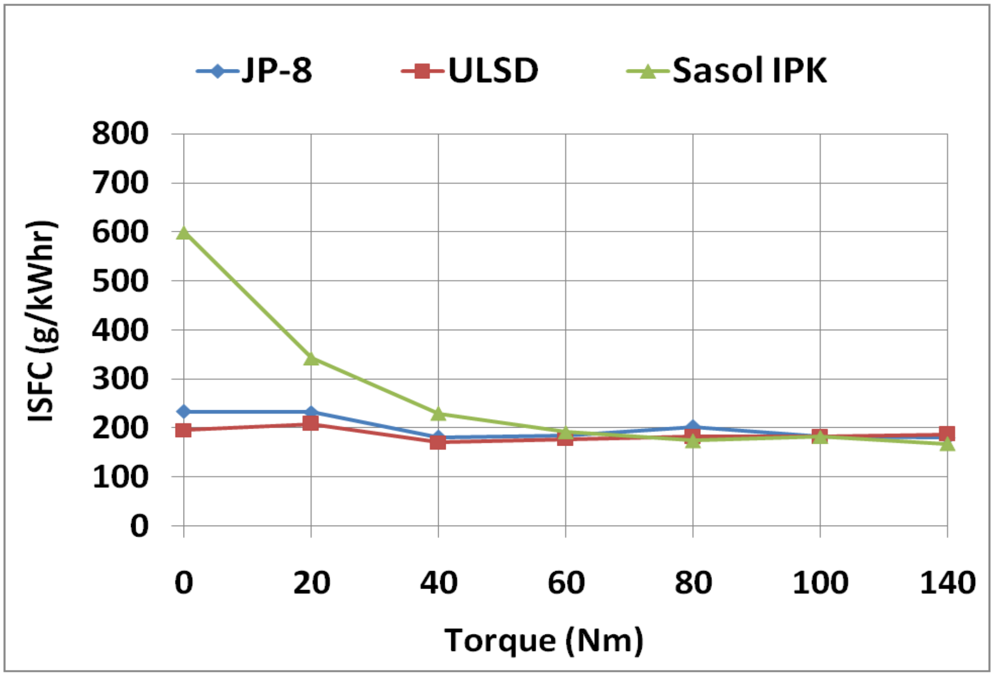

Figure 7-13. Indicated specific fuel consumption vs. engine load, for engine operating under ULSD, JP-8, and Sasol-IPK fuel mode, at 1800 rpm

The indicated specific fuel consumption (ISFC) was calculated to account for the variation in the fuel economy of the jet fuels from baseline ULSD operation. Figure 7-13 shows the indicated specific fuel consumption variation with increase in engine torque operating with the three fuels. JP-8 shows relatively higher fuel consumption in comparison with ULSD. However, the variation decreases as the load increases at high loads. On the other hand, Sasol-IPK showed serious penalty in fuel economy at no load with ISFC of 600 g/kWh compared to 196.32 and 233.79 g/kWh for ULSD and JP-8 respectively. This indicates poor combustion efficiency at no load and low loads operation for Sasol-IPK. The ISFC decreased to 343g/kWh and 230g/kWh at 20Nm and 40Nm respectively. At 60Nm and higher loads, Sasol-IPK shows very close ISFC compared to ULSD and JP-8.

Ignition Delay:

The ignition delay (ID) and ion current delay (ICD) were calculated and plotted in separate figures for pilot and main combustion events. The ID is defined as the period in CAD from the start of injection to the start of high temperature combustion in the RHR. The ICD is defined as the period in CAD from the start of injection to the start of rise in the ion current signal. Figure 7-14 shows variation in ID and ICD for pilot combustion of JP-8 and ULSD. Operation under Sasol-IPK did not produce any pilot combustion and hence no delay was recorded. The effect of the CN was evident in the ignition delay analysis. JP-8 with a higher CN had a shorter ignition delay than ULSD, as expected. A similar trend was followed by the ICD as seen in the figure. The variation in the ID of the JP-8 in comparison to ULSD, was found to be less than 1 CAD.

Figure 7-15 shows variation in ID and ICD for main combustion event of JP-8, ULSD, and Sasol-IPK. ULSD and JP-8 indicate a similar ID and ICD at all engine loads. Both ULSD and

JP-8 show that the ID and ICD decrease with increase in engine load. Sasol-IPK produced a higher ID at all engine loads in comparison to ULSD and JP-8. Sasol-IPK had an ID of 23.5 and 20.5 CAD at no load and 140Nm in contrast to ULSD which had an ID of 5.5 and 3.5 CAD respectively. Sasol-IPK recorded no ion current signal from no load to 40 Nm since no ion current was detected during these engine loads. No ion current signal was observed during this period due to the late combustion phasing and low in cylinder temperatures produced as a result of poor combustion. ICD was detected from 60 to 140 Nm, where a similar trend to ID was observed.

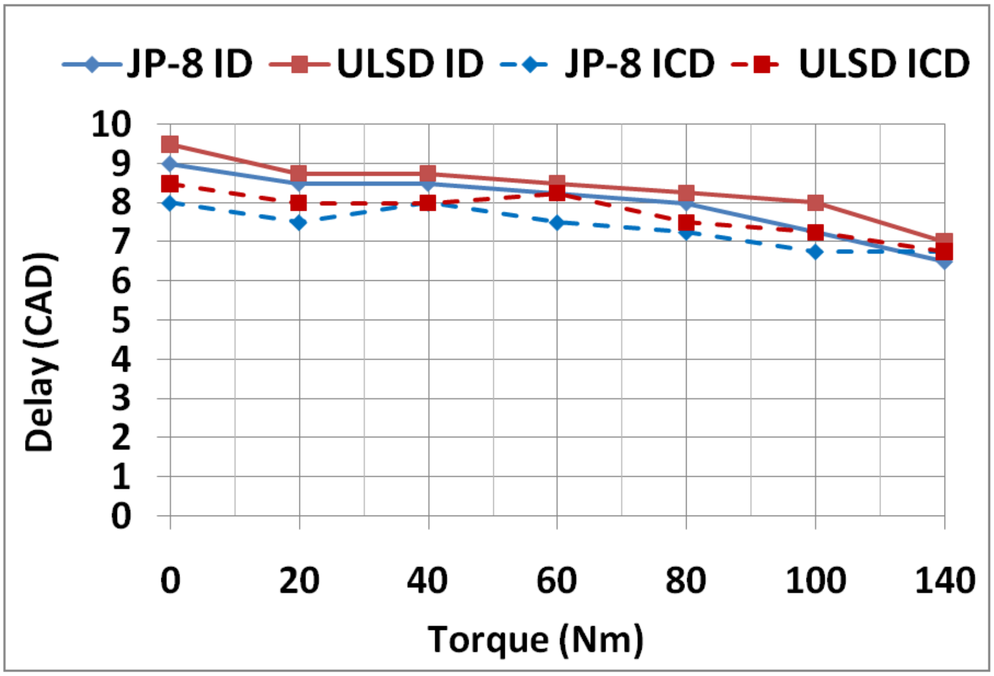

Figure 7-14. Data analysis showing the pilot ignition delay period for JP-8 and ULSD mode engine operation at varying load & 1800rpm

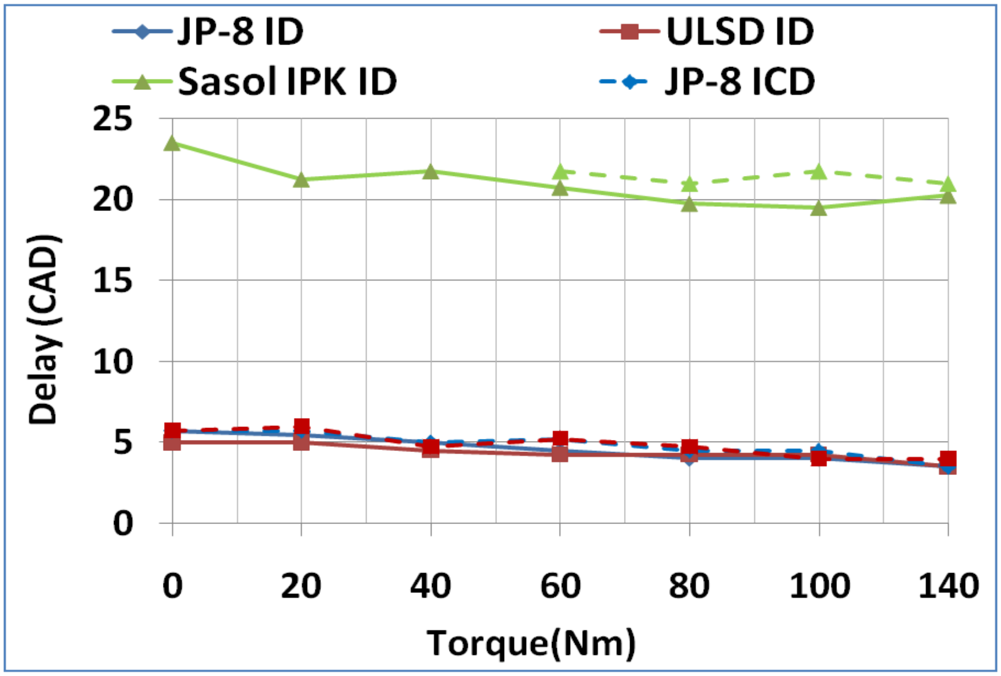

Figure 7-15. Data analysis showing the main ignition delay period for JP-8, ULSD & Sasol-IPK mode engine operation at varying load @ 1800rpm

Engine-Out Emissions:

A comparison of Nitric oxide (NO) concentration between the three fuels at different loads is shown in Figure 7-16. The NO concentration shows an increasing trend with increase in engine load. At all loads, ULSD produced higher NO concentration in comparison to jet fuels. Sasol-IPK on the other hand, consistently produced lowest NO emissions compared to ULSD and JP-8, except at 140Nm. The late combustion phasing and hence lower peak pressure and temperatures caused to the engine operation with Sasol IPK to produce lower NO emissions.

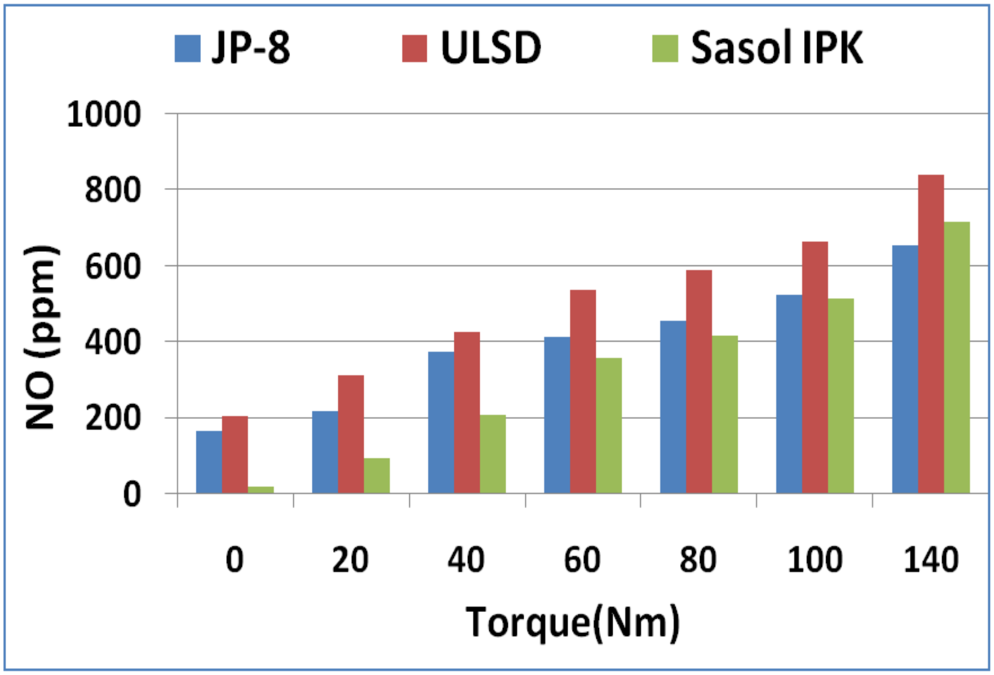

Figure 7-16. NO concentration versus engine load @ 1800rpm for engine operation with JP-8, ULSD, Sasol-IPK fuel.

Soot emission was recorded using opacity meter for the three fuels and compared in Figure 7-17. The opacity percentage values was plotted versus engine load for the operation with the three fuels. The opacity percentage for the jet fuels, in general shows lower values in comparison with ULSD fuel. The aromatic content of the fuel plays a key role in the soot formation and the one with higher aromatics tend to form higher values of soot. Sasol-IPK has negligible aromatics content of 0.2%. Also, JP-8 has lower aromatic content of 16.3% compared to ULSD with 27.8% as shown in Table 7-1.

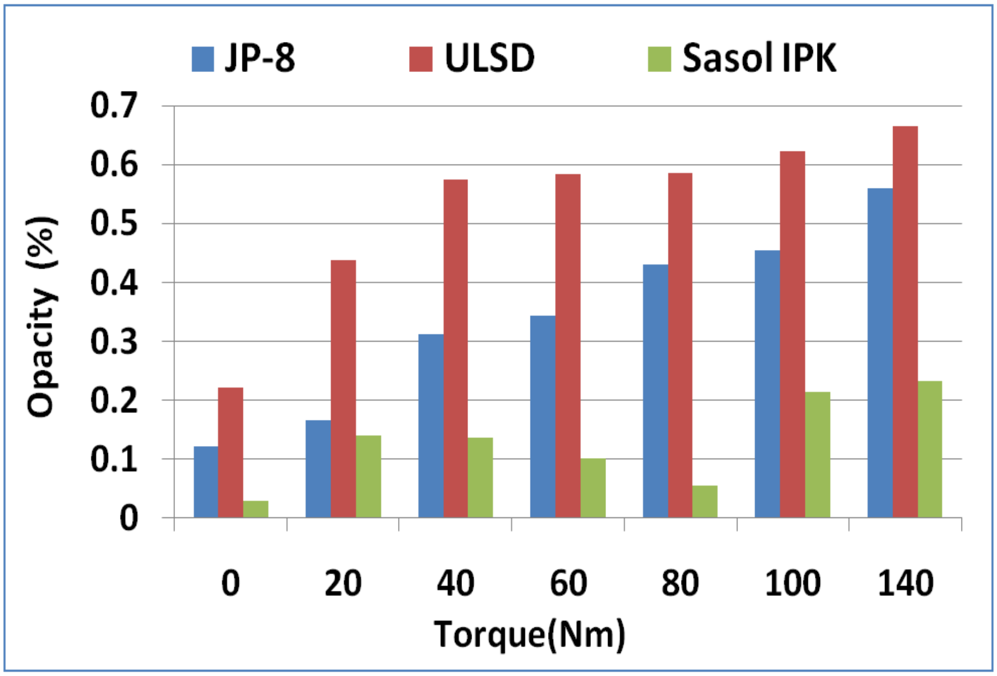

Figure 7-17. Opacity percentage versus engine load @ 1800rpm for engine operation with JP-8, ULSD, Sasol-IPK fuel

7.4 *Summary*

The impacts of using fuels with different physical and chemical properties in a modern automotive diesel engine has been investigated and compared with the ULSD fuel operation. In order to quantify the effects of using JP-8 and Sasol-IPK as replacement fuel in the diesel engine, experiments were conducted without any change in the original engine ECU. Tests were done at a series of engine loads and at a constant speed of 1800 rpm. The ion current sensor has the capability of detecting the ionization produced due the premixed and diffusion combustion under different loads using different fuels ULSD, JP-8, and Sasol-IPK. No combustion was developed from the pilot injection for Sasol-IPK at all engine loads due to its long ignition delay. Sasol-IPK showed very high ISFC at no load and low loads indicating a very poor combustion efficiency, where ISFC improved after 40 Nm. The Sasol-IPK showed the longest ID and ICD compared to

ULSD and JP-8. The ID and ICD for ULSD and JP-8 are similar due to the main combustion. Sasol-IPK produced the lowest concentrations of NO emissions at all engine loads, followed by JP-8, where ULSD produced the highest concentration of NO emissions. Sasol-IPK produced the lowest soot emissions at all loads, followed by JP-8, where ULSD showed high soot emissions with increasing loads.

CHAPTER 8

DISCUSSIONS AND CONCLUSIONS

In this thesis, tests were conducted on a 2.0 L VW, four-cylinder, turbocharged diesel engine under constant speeds of 1600, 1800, 2000 rpm and different loads to investigate ion current signal. The engine is equipped with a common rail injection system and piezo operated injectors. The main objective is to determine the signal characteristics over a wide range of engine speeds and loads. Furthermore, this study investigates the impact of using different alternate fuels such as JP-8 and Sasol-IPK on a modern automotive diesel engine, without making any adjustments or changes in its control strategies. So, the engine operation was under the control of the production ECU. Comparisons between the three fuels are presented in terms of performance, fuel consumption, auto ignition and emissions considering ULSD as a baseline fuel. This work was also aimed to identify the possibility of using jet fuels in a modern automotive diesel engine without any modifications.

The conclusions are for the ion current characteristics in a modern production high speed diesel engine operating at different loads and speeds, using conventional ULSD and alternate fuels. The engine is equipped with a common rail fuel injection system and piezo operated injectors. The first part of the conclusions deals with the operation on ULSD. The second part is for the impact of using two alternate fuels without any adjustments in the production ECU, considering ULSD as a base fuel.

A. Operation on the base ULSD fuel

- The Ion current signal detected the combustion of the pilot as well the main injections and their timings at different speeds and loads.
- The ion current signal has peaks indicative of the different modes of combustion. The ion current signal produced by the combustion of the pilot injection has one peak produced by the premixed combustion.
- The ion current signal produced by the main injection has three peaks. The first is for the premixed combustion. The second is for the mixing-diffusion controlled combustion. The third is for the oxidation of the incomplete combustion products later in the expansion stroke.
- The ignition delay of the ion current has a linear relationship with the ignition delay measured from the rate of heat release for the pilot and main injections at different loads.
- The start of ion current as well as the first peak of ion current are related to the peak location of premixed combustion. Although both ion current parameters were found to have a linear relationship with LPPC, the first peak of ion current was observed to have more consistent correlation during both pilot and main combustion process.

B. Impact of the use of JP-8 and Sasol-IPK

- The ion current probe detected the different combustion modes of JP-8, and Sasol-IPK as well as for ULSD.
- The Sasol-IPK showed the longest ID and ICD compared to ULSD and JP-8. The ID and ICD for ULSD and JP-8 are similar due to the main combustion.
- As expected the ion current did not show any signal as the pilot injection of Sasol-IPK fails to burn at all engine loads covered in this investigation. Sasol-IPK produced the lowest

concentrations of NO emissions at all engine loads, followed by JP-8, where ULSD produced the highest concentration of NO emissions.

- Sasol-IPK produced the lowest soot emissions at different engine loads, followed by JP-8, where ULSD showed high soot emissions with increasing loads.

In conclusion the ion current has the potential of use as a feedback signal to the ECU for the control of advanced high speed diesel engines to achieve their production goals.

APPENDIX

DEFINITIONS/ABBREVIATIONS

ECU: Electronic Control Unit

aTDC: After Top Dead Center

bTDC:Before Top Dead Center

CAD: Crank angle degree

ULSD:Ultra low sulfur diesel

CN: Cetane number

RHR: Rate of heat release

SOPP: Start of injection pulse - pilot

SOPM: Start of injection pulse - main

LTC: Low temperature combustion

LPPCp: Location of peak premixed combustion - pilot

LPPCm: Location of peak premixed combustion - main

PICp: Peak of ion current – pilot

PIC1: 1st Peak of ion cuurent

PIC2: 2nd Peak of ion cuurent

PIC3: 3rd Peak of ion cuurent

NTC: Negative temperature coefficient

ID: Ignition delay

ICD: Ion current delay

MAP: Manifold absolute pressure

ISFC: Indicated specific fuel consumption

REFERENCES

1. Henein, N., Bryzik, W., Abdel-Rehim, A., and Gupta, A., "Characteristics of Ion Current Signals in Compression Ignition and Spark Ignition Engines," *SAE Int. J. Engines* 3(1):260-281, 2010.

2. S. Yoshiyama, E. Tomita, N. Tabuchi, K. Matsumoto and K. Matsuki. "Combustion Diagnostics of a Spark Ignition Engine by Using Gasket Ion sensor," SAE Technical paper No. 2003-01-1801, 2003

3. Rivara, N., Dickinson, P., and Shenton, A., "Peak Pressure Position Control of Four Cylinders through the Ion Current Method," SAE Technical Paper 2009-01-0235, 2009

4. Reinmann, R., Saitzkoff, A., and Mauss, F., "Local Air-Fuel Ratio Measurements Using the Spark Plug as an Ionization Sensor," SAE Technical Paper 970856, 1997.

5. Yoshiyama, S., Tomita, E., Kitawaki, S., and Kamada, K., "Ion Current During the Exhaust Process Under the Idling Condition in a Spark Ignition Engine," SAE Technical Paper 2005-01-3872, 2005.

6. Zhu, G.G.; Haskara, I.; Winkelman, J., "Closed-Loop Ignition Timing Control for SI Engines Using Ionization Current Feedback," *Control Systems Technology, IEEE Transactions on*, vol.15, no.3, pp.416,427, May 2007.

7. Abdel-Rehim, A., Henein, N., and VanDyne, E., "Ion Current in a Spark Ignition Engine using Negative Polarity on Center Electrode," SAE Technical Paper 2007-01-0646, 2007.

8. Henein, N. A., Badawy, T., Rai, N., and Bryzik, W., "Ion Current, Combustion and Emission Characteristics in an Automotive Common Rail Diesel Engine," Journal of Engineering for Gas Turbines and Power, 134(4), pp. 042801-042807, 2012.

9. Rai, N. D., “Measurement and Analysis of Ion Current Signal in an Automotive Common Rail Diesel Engine.” Master of Science Thesis, Wayne State University, 2010.
10. Badawy, T., Rai, N., Singh, J., Bryzik, W., and Henein, N., "Effect of design and operating parameters on the ion current in a single-cylinder diesel engine," International Journal of Engine Research, 2011.
11. Badawy, T., “Investigation Of The Ion Current Signal In Gen-Set Turbocharged Diesel Engine.” Master of Science Thesis, Wayne State University, 2009
12. Badawy, T., Henein, N., and Bryzik, W., "Closed Loop Control Using Ion Current Signal in a Diesel Engine," SAE Technical Paper 2011-01-2433, 2012.
13. Badawy, T., "Ionization in Diesel Combustion for On-Board Diagnostics and Engine Control." PhD Dissertation, Wayne State University, 2013.
14. Kubach, H., Velji, A., Spicher, U., and Fischer, W., "Ion Current Measurement in Diesel Engines," SAE Technical Paper 2004-01-2922, 2004.
15. "Specifications for Volkswagen Industrial Engine." Volkswagen AG Engine Manual, 2009.
16. "2.0L TDI Engine with common rail fuel injection system - design and function." Self-Study Program 403, service training Volkswagen of America, Inc., 2008.
17. Min, Lee, J., Min, K., Kang, K., and Bae, C., "Hydraulic Simulation and Experimental Analysis of Needle Response and Controlled Injection Rate Shape Characteristics in a Piezo-driven Diesel Injector," SAE Technical Paper 2006-01-1119, 2006.
18. Oki, M., Matsumoto, S., Toyoshima, Y., Ishisaka, K. et al., "180MPa Piezo Common Rail System," SAE Technical Paper 2006-01-0274, 2006.

19. Oh, B., Oh, S., Lee, K., and Sunwoo, M., "Development of an Injector Driver for Piezo Actuated Common Rail Injectors," SAE Technical Paper 2007-01-3537, 2007.
20. "Kistler M5 – Sensors, Type 6052 A," Instruction Manual
21. Kistler Piezo-resistive High Pressure Sensor Specification Sheet (No. 03.4067).
22. Max Machinery, Inc. Model 710 Wall Mount Fuel Measurement System Manual.
23. Bittle, J., Zheng, J., Xue, X., and Jacobs, T. "Cylinder to cylinder variation sources in diesel low temperature combustion and the influence they have on emissions." International Journal of Engine Research January, 15: 112-122, 2014.
24. Schihl, P. and Hoogterp-Decker, L., "On the Ignition Behavior of JP-8 in Military Relevant Diesel Engines," *SAE Int. J. Engines* 4(1):1-13, 2011.
25. Papagiannakis, R., Kotsiopoulos, P., Hountalas, D., and Yfantis, E., "Single Fuel Research Program Comparative Results of the Use of JP-8 Aviation Fuel versus Diesel Fuel on a Direct Injection and Indirect Injection Diesel Engine," SAE Technical Paper 2006-01-1673, 2006.
26. Nargunde, J., Jayakumar, C., Sinha, A., Acharya, K. et al., "Comparison between Combustion, Performance and Emission Characteristics of JP-8 and Ultra Low Sulfur Diesel Fuel in a Single Cylinder Diesel Engine," SAE Technical Paper 2010-01-1123, 2010.
27. Pickett, L. and Hoogterp, L., "Fundamental Spray and Combustion Measurements of JP-8 at Diesel Conditions," *SAE Int. J. Commer. Veh.*1(1):108-118, 2009.
28. A M Ickes., S V Bohac., and D N Assanis., "Effect of fuel cetane number on a premixed diesel combustion mode," International Journal of Engine Research, 10:251-263, 2009.

29. Schihl, P., Decker-hoogterp, L., Pence, K., and Leonard, K., "On the Premixed Phase Combustion Behavior of JP-8 in a Military Relevant Single Cylinder Diesel Engine," *SAE Int. J. Engines* 4(1):27-37, 2011.

ABSTRACT

INVESTIGATION OF ION CURRENT SIGNAL IN A MODERN AUTOMOTIVE DIESEL ENGINE

by

Rojan Mathew George

May 2014

Advisor: Dr. Naeim Henein
Major: Mechanical Engineering
Degree: Master of Science

Research is driven towards finding an alternative or extender to the conventional diesel fuel for compression ignition engines. Such alternative fuels have wide ranges of physical and chemical properties which is not suitable for CI engines. Therefore, experimental investigation to understand the effects of different fuels on engine performance, combustion, and emissions are necessary. A complete understanding of ion current signal during heterogeneous diesel combustion has not yet been made. Implementation of ion current signal as a feedback in diesel engines, during all operating conditions needs further research and understanding.

This thesis covers the investigation of ion current signal characteristics as well as combustion, auto-ignition and engine out emission characteristics during the operation of modern high speed diesel engine using ULSD. Furthermore, the study covers the effect of using different fuels such as JP-8 and Sasol-IPK on a multi cylinder, direct injection diesel engine. Comparative results of three fuels are presented considering ULSD as a baseline fuel. This work aims to identify the possibility of using jet fuels in a modern automotive diesel engine without any modifications. Ion current signal characteristics during the operation with the three fuels and its correlations with combustion parameters and emissions are presented.

AUTOBIOGRAPHICAL STATEMENT

I was born in Trivandrum, India on April 26th, 1989. My fascination towards the automobile and its operation urged me to delve deeper into their functions and features. This passion made me take up the decision of my undergraduate studies in Mechanical Automobile Engineering at Sree Chitra Thirunal College of Engineering under the Kerala University, India. I have gained a lot of theoretical as well as application-oriented knowledge through comprehensive curriculum at the undergraduate level. Consequent to my Bachelor's graduation in May 2011, I felt the urge explore more in the realm of internal combustion engines. Chasing my dreams and passion led me to Wayne State University, Detroit, Michigan in August 2011 to purse my Master's in mechanical engineering. My coursework specialization was thermal combustion, which gave me an in-depth knowledge of the latest nuances of developments in this realm of Engineering. I was fortunate enough to get an opportunity to work in Centre for Automotive Research as a Graduate Research Assistant under the guidance of Prof. Naeim Henein. My primary assignment was to set up and fully instrument a multi cylinder diesel engine. The main focus of my research comprised of the study of ion current characteristics during heterogeneous diesel combustion. I conducted extensive testing and research on multi-cylinder diesel engine operated ULSD (Ultra low Sulfur Diesel) as well as alternative fuels such as JP-8 and Sasol IPK to investigate the ion current signal and combustion characteristics. I believe in exploring new arenas and attaining knowledge as I continue to work as Gasoline Engine Mapping & Development Engineer with Ford Motor Company since September 2013.